Dissertation
submitted to the
Combined Faculty of Natural Sciences and Mathematics
of the Ruperto Carola University Heidelberg, Germany
for the degree of
Doctor of Natural Sciences

presented by:
M. Sc. Chiara Di Ponzio

born in: Taranto, Italy

Oral examination date: 12.07.2021

# Optimization of strategies for overcoming therapy resistance in pancreatic cancer chemotherapy by mathematical modelling

Referees:

Prof. Dr. Roland Eils

Prof. Dr. Andreas Trumpp

Ai miei genitori, Ghituccis ed Egidio.

A nonno Silvio e agli inguaribili curiosi.

# Acknowledgement

Once upon a time there was a young and naive lady who left her not-so-far-away country to get to the magic land of Heidelberg. Her goal was to find something that some people said existed and some others denied, the pot under the rainbow: a doctorate.
Little did she know of what awaited her and what an adventure it would be.
But somehow, she made it.

Now, you may well wonder how she made it.
Of course, my dear reader, with a lot of energy, smiles, and tears, but above all with the support of the incredible people she had in her life. And here is who helped her pull through.

First, she met Dr. Dr. Kallenberger, a brilliant researcher, full of ideas who never gave up.
Thank you, Stefan, for sharing your knowledge with me, for your support and your never-ending will to discuss unsuccessful experiments with me.

Along came Prof. Dr. Eils, with his wisdom and advice.
Roland, thank you for giving me the opportunity of a lifetime and the freedom to grow as a scientist and as a person.

The young lady found new collaborators who made her life more interesting.
Here is a thank you to Manuel, Ornella, Martin, Kai Hu and Dr. Giese for the many brainstorming sessions and the contributions to this thesis.
My gratitude also goes to Prof. Dr. Trumpp and Prof. Dr. Kummer for the insight provided to me during these years in our limited yet fundamental TAC sessions.

Academia does not facilitate friendships, everyone comes and goes, but this lady found new friends somehow.
Thank you to everyone who came in the picture, even just for short time (or a short coffice), especially to Anna, Tim and Farzaneh.

Ai miei amici di Taranto, a voi che mi avete visto poco e sentito meno, ma non siete mai mancati.
Una menzione speciale a Ciccio che ha sempre creduto in me.

Always far but always close: Fra and Gaia.
Fra, sei la mia spalla, la mia persona, da sempre e per sempre. 15 anni, migliaia di km, ma non sentirli.
Gaia, abbiamo condiviso questo scempio dal giorno 1 e abbiamo costruito sempre di più. Sorelle nella scienza e nelle bestemmie.

In every story there is a magical helper, and this lady had two: Fede and Ale.
Fede, la compagna di (dis)avventure che in tre anni mi ha insegnato cosa fosse una piastra per le cellule e come si facesse il casatiello (tra un pianto e una risata).
Ale, amico di una vita e fonte inesauribile di energia positiva e strumenti musicali.
And with Ale the Werderstr. people with their energy, their positive souls, and their creativity. And now also the last (but not least) addition and graceful soul, Kaie.
You all made Heidelberg a better place.

Finally, the two things this lady loves the most in her life.
I cinque Di Ponzio-Stasi senza cui non sarei qui. Tutto questo lo dedico a voi.
E Mario. L'altalena emotiva della mia vita e il punto fisso all'orizzonte che mi spinge sempre avanti.

So, my dear reader, this journey was long and crazy, but it was worth the time and energy, worth the frustration and the joy.
The lady found her doctorate. No, not a title. A life-changing experience.

# Abstract

Pancreatic ductal adenocarcinoma (PDAC) is the fourth leading cause of cancer-related death worldwide, and often chemotherapy fails due to post-treatment cell survival and patient relapse. Although extensive qualitative research has been performed on drug resistance, the combination of experimental and computational methods offers the perspective of a quantitative prediction for tumour-specific therapeutic approaches. In this context, it is important to study molecular mechanisms involved in drug resistance in PDAC on a systems level and integrate knowledge about involved signal transduction pathways. The aim of this thesis is to investigate two of these mechanisms and quantitatively analyse their role in drug resistance.

In the first sub-project of the thesis, the ubiquitin ligase Casitas B-lineage lymphoma c (CBLc) was characterised as a subtype biomarker for drug resistance in PDAC cells by a combination of mathematical modelling and experiments. It was observed that CBLc confers drug resistance to PDAC cells by amplifying the activation of downstream effectors of the MAPK and PI3K/Akt pathways, which stands in contrast to the well-established role of CBL ubiquitin ligases as negative regulators of membrane receptor tyrosine kinases (RTKs). The observed effect of an increased Erk and Akt activation in presence of Erlotinib could be explained by mathematical modelling assuming a novel function of CBLc as a scaffold for mediators of downstream phosphorylation reactions, responsible for tuning cell response to external stimuli.

The second sub-project of the thesis addressed the spatio-temporal dynamics of drug delivery in PDAC tumour tissue depending on the heterogeneous expression of a drug-metabolizing enzyme, CYP3A5, a member of the cytochrome P450 enzyme family. Recently, it was observed that patient-derived model cell lines of the exocrine-like PDAC subtype express this enzyme, which resulted in drug resistance in cell culture experiments. Accordingly, it can be predicted for tumour tissues that CYP3A5 expression results in local drug gradients and survival of cancer cells. To quantitatively simulate this effect, an agent-based reaction-diffusion model of 3D cell cultures was created. Based on experimental data, the formation of resistant tumour niches due to CYP3A5-expressing cells was simulated. The model was used to create predictions about the selection of resistant cell populations upon treatment with oncological drugs such as erlotinib and paclitaxel.

In conclusion, quantitative descriptions of two distinct cellular mechanisms of drug resistance in the complex landscape of PDAC were established. On the one hand, a new functional role of the potentially oncogenic protein CBLc was mechanistically characterized; on the other, the effect of heterogeneously expressed drug-degrading enzymes resulting in tumour niches protected from cytotoxic drugs was characterised via mathematical modelling. In future, the integration of the developed models could be applied to optimize experimental strategies for *in vitro* testing of targeted cancer inhibitors and combinations of chemotherapy agents on PDAC and other tumours.

# Zusammenfassung

Das duktale Pankreas-Adenokarzinom (PDAC) ist die vierthäufigste krebsbedingte Todesursache weltweit. Oft scheitert die Chemotherapie aufgrund therapieresistenter Tumorzellen, durch welche Rezidive entstehen.

Im Gegensatz zur qualitativen Erforschung von Medikamentenresistenz, bietet die Kombination von Experimenten mit computergestützten Ansätzen die Perspektive einer quantitativen Vorhersage tumorspezifischer Therapieansätze. In diesem Zusammenhang ist es wichtig, molekulare Mechanismen, die an der Medikamentenresistenz bei PDACs beteiligt sind, auf systemischer Ebene zu untersuchen und das Wissen über beteiligte Signaltransduktionswege in mathematischen Modellen zu kombinieren. Das Ziel dieser Arbeit ist es, zwei dieser Mechanismen zu untersuchen und ihre Rolle bei der Medikamentenresistenz quantitativ zu analysieren. Im ersten Teilprojekt der Dissertation wurde die Ubiquitin-Ligase Casitas B-lineage Lymphoma c (CBLc) als Subtyp-Biomarker für Medikamentenresistenz in PDAC-Zellen durch eine Kombination aus mathematischer Modellierung und Experimenten charakterisiert. Es wurde beobachtet, dass CBLc zur Resistenz von PDAC-Zellen gegenüber chemotherapeutischen Medikamenten führt, indem es die Aktivierung nachgeschalteter Effektoren der MAPK- und PI3K/Akt-Signalwege verstärkt. Diese Funktion steht im Gegensatz zur etablierten Rolle von CBL Ubiquitin-Ligasen als negativen Regulatoren von Membran-Rezeptor-Tyrosinkinasen (RTKs). Der beobachtete Effekt einer erhöhten Erk- und Akt-Aktivierung unter Behandlung mit Erlotinib konnte durch mathematische Modellierung erklärt werden. Die Funktion von CBLc als Adapter für Mediatoren nachgeschalteter Phosphorylierungsreaktionen wurde durch das Modell vorhergesagt und konnte experimentell bestätigt werden. Im Rahmen des zweiten Teilprojekts der Arbeit wurde die räumlich-zeitlichen Dynamik der Effekte chemotherapeutischer Medikamente im PDAC-Tumorgewebe, beeinflusst durch die heterogene Expression von CYP3A5, einem Mitglied der Cytochrom-P450-Enzymfamilie, durch welches Medikamente abgebaut werden, charakterisiert. Kürzlich wurde beobachtet, dass aus Tumoren abgeleitete Modellzelllinien des exokrinen PDAC-Subtyps dieses Enzym exprimieren, was in Zellkulturexperimenten zu einer Medikamentenresistenz führte. Dementsprechend kann für Tumorgewebe vorhergesagt werden, dass die CYP3A5-Expression zu lokalen Wirkstoffgradienten und zum Überleben der Krebszellen beiträgt. Um diesen Effekt quantitativ zu simulieren, wurde ein agentenbasiertes Reaktions-Diffusions-Modell von 3D-Zellkulturen entwickelt. Basierend auf experimentellen Daten wurde die Ausbildung von resistenten Tumornischen durch CYP3A5-exprimierende Zellen simuliert. Das Modell wurde verwendet, um Vorhersagen über die Selektion resistenter Zellpopulationen bei der Behandlung mit onkologischen Medikamenten wie Erlotinib oder Paclitaxel zu erstellen.

Zusammenfassend wurden quantitative Modelle von zwei unterschiedlichen zellulären Mechanismen der Chemotherapieresistenz in PDACs etabliert. Zum einen wurde eine neue

funktionelle Rolle des potentiell bei der Krebsentstehung involvierten Proteins CBLc mechanistisch charakterisiert, zum anderen der Effekt von heterogen exprimierten medikamentenabbauenden Enzymen, durch welche resistente Tumornischen entstehen können, basierend auf mathematischen Modellen charakterisiert. Die entwickelten Modelle könnten in Zukunft zur Optimierung experimenteller Strategien für die In-vitro-Testung zielgerichteter onkologischer Wirkstoffe und Kombinationen von Chemotherapeutika an PDACs und anderen Tumoren eingesetzt werden.

# Contents

# Contributions

Unless otherwise explicitly stated in figure descriptions and related paragraphs, all data were obtained by me under the supervision of Dr. Dr. Stefan Kallenberger and Prof. Dr. Roland Eils. This also includes the design of experimental strategies, conductance of experiments, development of mathematical models, data analysis and presentation.

Several datasets presented in this thesis were obtained in collaboration with my colleagues. I am grateful for the hard work everyone put into these two projects and the support I received from my collaboration partners.

# 1. Introduction

## *1.1 Preface*

Pancreatic ductal adenocarcinoma (PDAC) is the most common type of pancreatic cancer and the fourth most frequent cause of cancer-related deaths globally, with a 5-year survival of less than 8% [1]. Almost 200.000 people die from PDAC every year worldwide, and numbers are still increasing, with overall survival of typically six months from diagnosis.
It usually affects the elderly, with most cases occurring between the age of 60 and 80 [2]. Due to the ageing of the world population, understanding and fighting this tumour is of uppermost importance. The complexity of pancreatic cancer makes the development of effective therapies quite challenging, primarily due to resistance mechanisms. Many molecular aspects of drug resistance have been studied in different solid tumours. However, little is still known about PDAC, and the scarcity of data from PDAC patients and the lack of quantitative knowledge about the dynamics underlying these resistance phenomena create an additional limitation in the advancements of clinical studies.

In this work, the analysis of two critical aspects of drug resistance in PDAC combining experimental and computational approaches will be presented in order to elucidate the temporal and spatial evolution of mechanisms that have not been characterised yet. The molecular mechanisms here investigated involve enzymes in signalling pathways and xenobiotics metabolism pathways due to their role in drug failure. This quantitative study will contribute to a better understanding of the impact of these enzymes in pre-treatment and drug-induced resistance and will in the future support the development of novel therapies.

## *1.2 Pancreatic ductal adenocarcinoma*

### *1.2.1 Tumour characteristics*

The pancreas is a complex organ divided into four parts - head, neck, body, and tail – each containing one or more types of cells (endocrine, exocrine or acinar, and epithelial cells). Most of this organ is made of exocrine tissue, i.e. cells that provide exocrine juice to the digestive tract, necessary during digestion. The exocrine juice is released into the common bile duct via the pancreatic duct, a long channel that runs along the pancreas.
Pancreatic ductal adenocarcinoma (PDAC) originates from the ductal epithelium and develops in pre-malignant lesions before fully degenerating into invasive cancer.
Usually, PDAC tissue is differentiated into subtypes with different characteristics, and the malignant tissue is histologically divided into three grades based on the degree of tissue differentiation - well,

moderately, and poorly differentiated - which are used to categorize the tissue clinically and are usually correlated with patient outcome [3].

Moreover, the tumour microenvironment does not only include cancer tissue, but it is diverse and consists of extracellular matrix, immune and inflammatory cells, blood vessels and fibroblast - a heterogenous microenvironment that plays a crucial role in PDAC treatment.

For instance, PDAC histological samples often show dense stroma formed due to pancreatic stellate cells that deposit significant amounts of extracellular matrix. The stroma tissue is involved in the formation, progression, and invasion of cancer tissue (stroma cells usually express high levels of growth factor receptors - such as PDGF or vascular endothelial growth factor receptors), but also causes poor vascularization and hypoxia of the tumour tissue which impair drug delivery [4].

At the same time, cancer stem cells compose 1-5% of tumour tissue [4]. Cells in this compartment can self-renew unlimitedly and can divide asymmetrically, giving birth to more differentiated cells. In fact, cancer stem cells are usually more resistant to chemotherapy and radiotherapy and targeting cancer stem cells might be the key to overcome poor prognosis and improve patient survival [5].

Although PDAC is highly malignant and extensively studied, much is still unknown about the complexity of this tumour and understanding the dynamics of drug response of PDAC will be fundamental to define optimal treatment strategies for patients.

### *1.2.2 PDAC tumour profiling*

Subtyping of tumours is commonly used for the clinical identification of the most efficient therapeutic agents and the prediction of patient outcome. PDAC is highly heterogeneous and presents a complex mutational landscape, so several attempts have been made during the last decade to define a standard set of PDAC subtypes. However, the identification of PDAC subtypes has been limited by the scarcity of tumour specimens available, especially from the early stages of tumour development since patients usually present symptoms in the advanced stages of the disease.

PDAC is characterised by some common oncogenic events, namely activation of the GTPase KRAS and inactivation of the tumour suppressor protein 53 (TP53), the tumour suppressor mothers against decapentaplegic homologue 4 (SMAD4) and the cyclin-dependent kinase inhibitor 2A (CDKN2A). By investigating precursor lesions [6], [7] the timing of the genetic mutations in tumorigenesis was outlined: KRAS and CDKN2A mutations are present in most low-grade pancreatic neoplasias. At the same time, loss of SMAD4 and alterations in TP53 are late events occurring in grade 3 and invasive PDAC. Nonetheless, these mutations are characteristic of most PDAC cells and not sufficient to predict subtype-specific chemotherapy response.

In this perspective, the application of next-generation sequencing has represented a turning point. For instance, Connor et al. [8] investigated the mutational landscape of PDAC and performed a

retrospective cohort study of resected tumours. Based on sequencing data, they clustered resectable PDACs into four major subtypes - age-related, double-strand break repair, mismatch repair, and one with unknown aetiology – which were further matched in metastatic tissue.

Collisson et al. [9] combined analysis of transcriptional profiles of primary PDAC samples from several studies with human and mouse PDAC cell lines. They defined three PDAC subtypes: classical, quasi-mesenchymal (QM-PDAC) and exocrine-like and analysed therapeutic response differences. The classical subtype is characterised by high expression of adhesion-associated and epithelial genes. In contrast, the QM-PDAC subtype presents an increased expression of mesenchyme-associated genes, and the exocrine-like subtype shows relatively high expression of tumour-derived digestive enzyme genes. By testing established chemotherapeutic drugs used in clinical treatments of PDAC, such as gemcitabine and erlotinib (described in detail in the following paragraph), they observed that QM-PDAC cell lines are, on average, more sensitive to gemcitabine than the classical subtype. In contrast, erlotinib is more effective on classical subtype cell lines.

Moffitt et al. [10] applied blind source separation on PDAC gene expression microarray data and obtained a stroma-specific subtype and two tumour-specific subtypes, specifically basal-like and classical-like subtype. To confirm the stratification, the authors also analysed patient-derived xenografts via RNA-sequencing expression and confirmed the presence of classical or basal-like subtypes. Interestingly, the basal subtype showed a better response to adjuvant therapy. When cross-referencing the subtyping with Collisson et al. [9], the two classical subtypes overlapped, while the quasi-mesenchymal tissue was a mixture of basal-like and stromal subtypes.

Later, Bailey et al. [11] proposed a novel classification. They applied a combination of whole-genome and deep-exome sequencing to determine mutational mechanisms and genomic events important in PDAC carcinogenesis. This study highlighted four subtypes with different histopathological characteristics: squamous, pancreatic progenitor, immunogenic and aberrantly differentiated endocrine exocrine (ADEX).

The results obtained by the authors partially overlap with [8] and [10]. Interestingly, the Collisson quasi-mesenchymal subtype corresponds to the squamous tissue, the classical tissue was comparable to the pancreatic progenitor, and the exocrine-like could overlap with the ADEX. Some of the Bailey squamous subtype tumours were characterised as the basal subgroup of [10], while others were composed of a mixture of other Bailey/Collisson subtypes.

Finally, Muckenhuber et al. [12] tested drug response in the two subtypes presented in all the previous publications: the classical and QM subtypes. These two subtypes present distinct immunohistochemistry features and can be recognised using two biomarkers: KRT81 is specific to QM/squamous/basal-like PDAC, while HNF1A characterises non-QM/exocrine/ADEX PDAC. The study highlighted that the non-QM subtype shows a better prognosis than the QM one when treated with established chemotherapy drugs, such as gemcitabine.

This highlights that subtyping PDAC is not straightforward, especially concerning drug response due to the variability of the tumour samples used to establish a subtype set. In fact, no consensus classification exists so far, as all these studies present different sets of subtypes and prove that the complexity of this tumour needs to be further dissected. In this thesis, the classification proposed by Collisson et al. [9] was followed to test drug resistance in the exocrine-like and classical subtypes due to the expression of drug-metabolizing enzymes. In future, a standard classification will facilitate the development of subtype-specific treatments and the prediction of tissue outcome, although upon chemotherapy intervention, a more dynamic stratification might be necessary due to tumour cell plasticity.

### *1.2.3 Treatment strategies for pancreatic ductal adenocarcinoma*

Patients affected by pancreatic ductal adenocarcinoma are usually treated with surgery, chemotherapy, radiotherapy, or palliative care, depending on the stage of the disease. Clinically, pancreatic cancer causes obstructive cholestasis, characterised by abdominal discomfort and nausea, asthenia and weight loss, often combined with venous thrombosis and liver function abnormalities [4]. Since these symptoms develop at later stages, most patients are diagnosed with locally advanced or metastatic PDAC and the only treatment strategy, in this case, is palliative chemotherapy. Nonetheless, surgical resection of PDAC malignant tissue is considered the only curative treatment to guarantee more prolonged patient survival [2], but only 15-20% of patients are usually eligible for it [13].

Adjuvant therapy is applied as pre- or post-surgery, but the chance of delivering the entire dose is higher before surgical intervention because surgery can cause a lack of oxygenation in the tissue, thereby impairing drug delivery. Many neoadjuvant treatments of PDAC are at present still experimental, and a list of compounds currently investigated in clinical trials in surgically treated patients is available in the publication by Seufferlein et al. [14].

Patients with inoperable and metastatic cancer are usually treated with systemic chemotherapy in monotherapy or combinations of drugs. The current standard for pancreatic patients is upfront resection and adjuvant chemotherapy either with gemcitabine alone or in combination with chemotherapy agents described in the following, which is the standard chemotherapy for PDAC patients since 1997, after the publication of a hallmark clinical study [15]. Gemcitabine is a prodrug, meaning that it exerts its activity after an intracellular conversion. This molecule is a nucleoside analogue used as chemotherapy, as it replaces cytidine, one of the building blocks of nucleic acids, during DNA replication in the S phase. This process arrests tumour growth because a new thymidine nucleotide cannot be attached to the faulty nucleoside, resulting in apoptosis.

## 1.2 Pancreatic ductal adenocarcinoma

Recently, the *FOLFIRINOX* protocol (a combination of oxaliplatin, irinotecan, fluorouracil and leucovorin) has demonstrated high efficacy in the adjuvant setting compared to gemcitabine alone [14]. Also, the combination treatment of PDAC with gemcitabine and erlotinib improves progression-free patient survival [16]. Erlotinib interferes with the activation of the epidermal growth factor receptor (EGFR) tyrosine kinase and is clinically used for different kinds of cancer where EGFR is highly expressed. This compound reversibly binds to tyrosine kinase at the adenosine triphosphate (ATP) binding site of the receptor. By avoiding the binding of ATP to EGFR, erlotinib inhibits the activation of intracellular signalling cascades related to cell proliferation. However, the specificity of erlotinib to other receptors is not fully characterised yet, and side effects can be pretty strong due to the ubiquitous expression of EGFR in many cell types.

Another conventional treatment for a variety of solid tumours, among which also PDAC, is paclitaxel. Paclitaxel was extracted in the '60s from a plant called Taxus Brevifolia and is a drug that promotes microtubule polymerization and stabilization in living cells, thereby inducing mitotic arrest [17]. Thus, chromosomes are unable to achieve the correct spindle configuration during metaphase, and the prolonged activation of the mitotic checkpoint leads cells to apoptosis.
Although paclitaxel is recognised as one of the most effective chemotherapy agents, it causes many side effects as it is solved in oil-based solvents to increase its distribution. Its poor aqueous solubility causes low intra-tumoral concentrations – often too low to cause mitotic arrest, resulting in multipolar cell divisions instead. Therefore, higher drug concentrations are required to affect the tumour [17]. Consequently, nab-paclitaxel was developed to avoid the excessive toxicity of paclitaxel in patients. Nab-paclitaxel is a 130-nm, albumin-bound formulation of paclitaxel with a more extensive distribution volume and a faster clearance than paclitaxel [18]. In 2011, a phase I/II trial identified advantages in using a nab-paclitaxel plus gemcitabine regimen, such as tolerable adverse effects and substantial anti-tumour activity [19].

Finally, thanks to genomic profiling, some key mutations in signalling pathways were identified in PDAC tissue, so several proteins involved in these pathways are established chemotherapeutic targets. Currently, the PI3K/Akt pathway includes several targets for widely used drugs, such as rapamycin (inhibitor of mTOR), trastuzumab (membrane receptor inhibitor), panPI3K inhibitors (targeting all isoforms of PI3K). At the same time, inhibitors of proteins in the MAPK pathway offer promising perspectives, as in the case of drugs targeting BRAF and Erk. Although targeting EGFR alone with compounds as erlotinib is often not effective, multi-target strategies on the MAPK and PI3K pathways have given convincing performances in pre-clinical studies [1].

In the context of PDAC chemotherapy, the frequency and dose of drug administered to patients can significantly impact the efficacy of the treatment. In clinical studies, dose and frequency depend on

the maximum tolerated dose to guarantee an acceptable level of safety to patients, but the target engagement is often insufficient. Nonetheless, recent findings suggest that treating patients with high doses and intermittent therapy might achieve a better effect and enhance patient outcome [20], and this highlights the importance of understanding the evolution of tumour response during treatment to optimize these strategies.
Current studies do not consider the dynamic aspects of drug resistance developing in PDAC tissue, so the purpose of this thesis is to elucidate the response of PDAC cells to clinically relevant drugs, such as erlotinib and paclitaxel, considering mechanisms of drug resistance that impair drug efficacy.

## *1.3 Drug resistance in PDAC*

One of the most critical aspects of pancreatic cancer, among other tumours, is the inefficacy of drug treatments due to cell resistance. Several molecular phenomena causing drug resistance in PDAC have already been investigated [21], but the dynamics behind the onset of these mechanisms are not clear yet. In this context, it is necessary to distinguish between intrinsic and acquired resistance (**fig. 1**) and their impact on chemotherapy failure. Intrinsic resistance refers to molecular factors that exist before chemotherapy treatment and often give tumour tissue an evolutionary advantage over other cells. By contrast, acquired resistance develops after drug exposure and is usually due to changes arising in the cells as a response to chemotherapy, e.g. mutations of drug targets, alterations in drug metabolism, or selection of resistant subpopulations [22].

Drug resistance is further increased by poor drug delivery, for instance, due to the hypo-vascularization and high density of stroma cells that impair the diffusion of chemotherapy to the desired targets.
Also, drug delivery is affected by enzymes that interact with drug molecules and reduce their toxicity. The activity of chemotherapeutic compounds is limited by the induced over-expression of drug-metabolizing proteins [23], as well as by the presence of drug-efflux proteins, such as ATP-binding cassette (ABC) proteins, which export drug molecules out of cells. In fact, cancer stem cells that highly express proteins from these two families are less affected by targeted therapies such as imatinib and erlotinib, or dasatinib [22], [23].

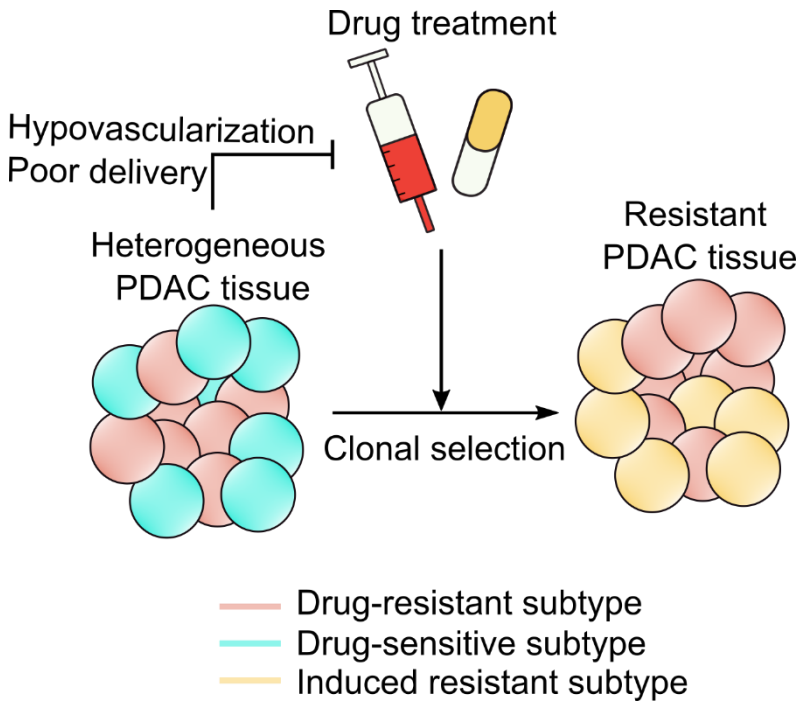


***Figure 1:*** *Intrinsic and acquired drug resistance. Heterogeneous cancer tissue can present pre-treatment resistance mechanisms specific to some subtypes, such as activating mutations in signalling proteins (HRAS, BRAF), adaptor proteins and membrane receptors (EGFR). Drug delivery is limited by the presence of dense stroma, which causes hypovascularization and impairs drug diffusion. After drug treatment, cells can acquire drug-induced resistance mechanisms that reduce chemotherapy's efficacy, such as mutations on drug targets or the over-expression of drug metabolizers and drug exporters.*

The development of drug resistance depends on the mechanism of action and activation of the chemotherapeutic agent. For instance, metabolism alterations reduce the activation of pro-drugs, such as gemcitabine, which release the active drug after a chemical transformation in vivo to exert the desired pharmacological effect [24]. This activation is mainly based on intra-cellular reductive or oxidative processes after drug uptake. When genetic mutations alter the metabolism, the conversion of pro-drugs into active drugs cannot occur, thus reducing the cytotoxic effect on cells.

PDAC is often characterised by activating mutations that reduce the efficacy of drug treatment as in the case of anti-apoptotic proteins: malignancies are often characterised by amplification of genes encoding anti-apoptotic proteins, such as the ones controlling the transcription factor NF-κB. Increasing levels of anti-apoptotic proteins enable cell survival by escaping drug-induced death [25].

Similarly, higher expression of drug targets decreases the effect of inhibitors since the ratio of target to inhibitor molecules increases. Often oncogenic kinases undergo amplification upon drug exposure, as in the case of EGFR, targeted by erlotinib, gefitinib and other compounds. Consequently, patients who initially respond to these treatments sometimes develop activating mutations or chromosomal rearrangements - therefore resistance - within few months from the beginning of the cure [26].

Other activating mutations develop in signalling proteins along proliferation pathways, such as the MAPK/Erk and PI3K/Akt pathways, where proteins adapt to the inhibitory effects of targeted therapies and activate oncogenic bypasses. For instance, EGFR blockade is bypassed by activating downstream effectors, such as BRAF or KRAS, typically kept in an active conformation in pancreatic cancer [22]. Moreover, pathways create an intricate network of proteins, interacting via regulation and feedback loops, so a limiting factor for drug treatments is the mutual compensatory behaviour of targeted and non-targeted pathways. These aspects are discussed more in detail in the following paragraph.

Overall, the range and complexity of drug resistance mechanisms seem to be daunting, but current treatment strategies have already achieved considerable improvements in patient survival. To better assess drug resistance, studies *in vitro* and *in vivo* should in future be combined with quantitative analysis of molecular mechanisms that impair drug efficacy.

## *1.3.1 Dysregulation of signalling pathways*

Drug resistance is a common characteristic of cancer cells and is often related to the dysregulation of signalling pathways responsible for cell growth and proliferation. In tumour cells, the activation of such pathways is often independent of external signals due to mutations that leave proteins, especially kinases, in an active state and give tumour cells a higher chance to survive under stress.

This section will focus on two pathways, the RAS-MAPK/Erk and the PI3K/Akt pathways, to characterise their role in pancreatic cancer and drug resistance.

### *1.3.1.1 Membrane receptors and signalling pathways activation*

Biochemical events in signalling pathways start at the membrane level, where an external signal is converted into an intracellular message by membrane receptors. Cells receive external stimuli in the form of growth factors, small proteic molecules that bind to specific receptors, most of which belong to the family of receptor tyrosine kinases (RTKs). All RTKs have similar architecture: a ligand-binding domain in the extracellular area, a single transmembrane helix and a cytoplasmic part containing one or more protein tyrosine kinase domains, a carboxyl C-terminal and a juxtamembrane regulatory region. The human epidermal growth factor receptor (EGFR) family consists of four members that belong to the Erbb lineage of proteins (ErbB1–4) and can bind to several ligands, including the epidermal growth factor (EGF). Membrane receptors undergo conformational changes upon growth factor binding, i.e. activation of the transmembrane glycoproteins and exposure of previously occluded dimerization sites to create dimers or oligomers with other receptors [27].

This way, the external information is transmitted to the intra-cellular area with strength and duration depending on negative regulatory mechanisms, such as RTK internalization.

Internalization happens via two types of endocytosis, clathrin-mediated (CME) and non-clathrin mediated (NCE) endocytosis. According to a recent study [28], the path along which an EGFR is internalized depends on the concentration of EGF: while CME is present at any concentration of EGF and leads the receptor to recycling, NCE is only active in case of high EGF concentration in a threshold-controlled process that leads EGFR towards degradation. The whole process is directed by the attachment of ubiquitin molecules to the receptor, also called ubiquitination - which will be further described in the following section. As a consequence, changes in the ubiquitination of the receptors influence the dynamics of EGFR inhibition by leading it towards anomalous recycling or degradation.

Moreover, cancer cells often compensate for the negative regulation of EGFR through amplification, point mutations at the genomic level or transcriptional upregulation in order to increase proliferation and survive drug treatment [26]. In the treatment of pancreatic cancer, EGFR is a common target; in fact, most chemotherapeutic strategies in clinical practice employ erlotinib and other EGFR inhibitors combined with gemcitabine. Nonetheless, Miyabayashi et al. [29] investigated how the treatment of pancreatic cancer mouse models with gemcitabine strongly induces the overexpression of EGFR and activates the MAPK pathway due to heterodimerization of Erbb2/EGFR. Overexpression of EGFR is, in fact, a common biomarker for resistance, as it often undergoes secondary mutations under drug pressure and is further activated by autocrine ligand production that can occur after exposure to cytotoxic drugs [30].

Over the years, research has focused on this family of receptors since EGFR is ubiquitously expressed in epithelial cells and drugs targeting EGFR are highly efficient in treating solid tumours, although side effects limit dosing of such treatments.

Further attention will be given in the following paragraphs to the signalling pathways activated downstream of EGFR, their structure, and their crosstalk.

#### *1.3.1.5 CBL ubiquitin ligases regulate receptor activity*

Receptor signalling is influenced by the assembly of supramolecular-protein complexes called signalosomes, which are essential for regulating and propagating signals from the membrane to different compartments of the cell. An essential protein in signalosomes is the Growth factor receptor-bound protein 2 (GRB2), an adaptor protein that participates in several complexes to facilitate the activation of signalling pathways. GRB2 binding to EGFR is involved in transferring EGFR signal to downstream cascades, but also in the internalization of EGFR mediated by ubiquitination.

Ubiquitination is the process of attaching a ubiquitin molecule to a protein through a covalent bond and is the first step towards EGFR (and other receptors) internalization and degradation. Generally, ubiquitin is bound to lysine residues on the substrate, and the transfer of the ubiquitin molecule is

catalysed by a family of proteins called ubiquitin ligases. EGFR ubiquitination is mainly mediated by Casitas B-lineage Lymphoma (CBL) proteins (**fig. 2**).

Different isoforms characterise the CBL family of proteins (in humans CBL or c-CBL; CBL-b; and CBLc, CBL-3 or CBL-SL) able to act as E3 enzymes, i.e. ubiquitin ligases. CBL proteins contain a tyrosine-kinase binding domain (TKB) at the N-terminal region, a proline-rich domain, and a Really Interesting New Gene (RING) finger domain that acts as a platform for the interaction with ubiquitin-conjugating enzymes (E2) [31]. The isoforms differ for their C-terminal domain because c-CBL and CBL-b contain additional C-terminal motifs, namely a ubiquitin-associated (UBA) domain and leucine zipper (LZ) motif, which are truncated in CBLc.

CBL proteins interact with GRB2 through their proline-rich domain and lead to the monoubiquitylation and endocytosis of EGFR; GRB2 mediates the interaction of EGFR with coated pit proteins which contain ubiquitin-interaction motifs. It has been shown that GRB2 is indispensable for this process since knockdown of GRB2 leads to a loss of EGFR endocytosis, even in presence of CBL overexpression [32]. Upon ubiquitination, receptors are internalized and recycled or delivered to early endosomes, which then mature into late endosomes and lead the proteins to lysosomes for degradation [33].

The presence of tyrosines and serines typifies CBL proteins as adaptor molecules, in fact they act as scaffolds for several proteins in EGFR signalosomes. For instance, c-CBL and CBL-b recruit the adaptor protein CBL-interacting protein of 85 kDa (CIN85), which triggers signalling cascades to start early phase endocytosis, while CBLc does not interact with CIN85 due to the truncated proline-arginine motif in the distal C-terminal [34].

c-CBL and CBL-b isoforms have been extensively studied and are responsible for different signal transduction pathways: CBL-b is involved in cytoskeleton remodelling, while c-CBL is involved in the negative regulation of the Src-family kinase in thymocytes [34]. CBLc is known to exert similar functions, and according to a recent study [35], it is the most important regulator of the oncoprotein c-Src (short for Sarcoma), encoded by the v-Src gene. While CBL binds to phosphorylated Src through the RING finger and proline-rich domains, CBLc binds to it through the TKB domain, and it exerts a stronger role in the ubiquitination of Src compared to other isoforms. c-Src is involved in several mitogenic signalling pathways, and it is inhibited by CBLc, which promotes ubiquitination of Src and leads it to lysosomal degradation, thus reducing its oncogenic activity [35].

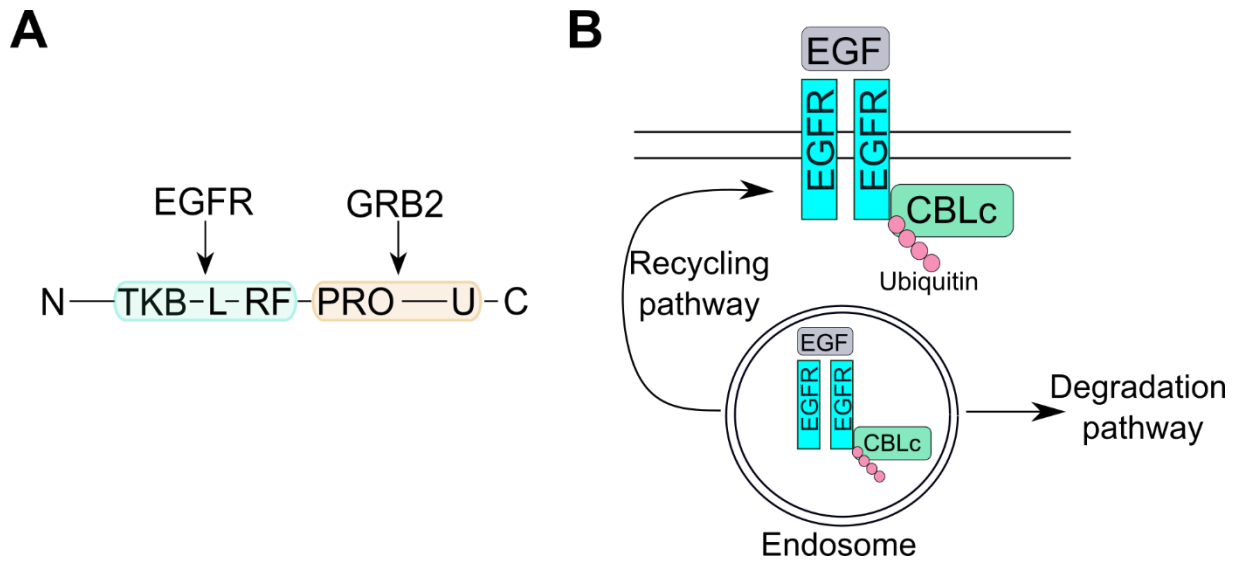


***Figure 2:*** *CBLc ubiquitin ligases.* ***A.*** *Protein domains of CBL ubiquitin ligases. In light blue, the N-terminal domains, common to all isoforms, include the tyrosine binding domain (TKB) – through which CBL proteins interact with EGFR. In orange, the proline-rich domain (PRO) and ubiquitin-associated domain (U) in the C-terminal, truncated in the CBLc isoform.* ***B.*** *CBLc leads to receptor internalization by ubiquitinating active EGF receptors. Internalized receptors are either embedded in endosomes and carried to lysosomes, where they undergo degradation, or recycled and carried back to the cell membrane.*

CBL proteins are also involved in pathways dysregulation in cancer, as it has been shown that CBL mRNA is decreased in 60% of tumours. Interestingly, c-CBL and CBL-b are ubiquitously expressed while CBLc is restricted to epithelial cells, and this suggests different roles of the isoforms in cancer development. In presence of low CBL, for instance, EGFR activation is higher in PDAC (PANC-1) cell lines. When treated with gemcitabine, low CBL leads to autoactivation of EGFR, but a combination of gemcitabine and erlotinib restores chemosensitivity in CBL-low tumours [30]. By contrast, CBLc is upregulated in non-small lung cancer (NSCLC) cells after exposure to chemotherapy, while expression levels do not change for other isoforms, and knock-down of CBLc renders NSCLC sensitive to TKI treatment. Studies in lung adenocarcinoma have proved that the half-life of Erk after EGF stimulation is increased in CBLc overexpressing cells. CBLc is therefore thought to stabilize active EGFR through binding competition with CBL. This indicates that upregulation of CBLc might reduce ubiquitination and degradation of active EGFR and be a mechanism of resistance in cancer cells [36].

These examples show that the expression of CBL proteins impacts the dynamics of active EGFR in signalosomes and influences the activation of downstream pathways in cancer, partially increasing tumour survival.

### *1.3.1.2 The Ras/MAPK pathway*

The Ras/MAPK signalling cascade is one of the many intra-cellular transduction cascades, consisting of enzymes, adaptors and signalling molecules that integrate the extra-cellular information and propagate it to the transcription factors required for cell growth (**fig. 3**).

Signalling in the MAPK pathway is started by the interaction of one or more growth factors with a specific receptor, mainly an epidermal growth factor receptor (EGFR), which initiates a series of biochemical events after amplifying the external signal [33]. To propagate the signal from the membrane level to the intracellular compartments, adaptor proteins translocate to the membrane level, and link activated receptors to signalling pathways.

One of the most critical adaptor proteins for the MAPK pathway is GRB2 which presents a cytosolic distribution in resting state; however, upon growth factor binding to the membrane, GRB2 is relocated to the plasma membrane within a few minutes [37]. This protein contains one Src-homology-2 and two Src-homology-3 (SH3) domains. The SH2 domain binds tyrosine phosphorylated sequences, for example on EGFR, while one of the SH3 domains directs complex formation with proline-rich regions of other proteins, for example with the Ras-guanine exchange factor Son-of-sevenless (SOS). Finally, the presence of the second SH3 domain allows the recruitment of a docking protein, the GRB2-associated binder (GAB1), to the GRB2-SOS complex. Docking proteins typically contain a membrane targeting side at their N-terminus and a tyrosine phosphorylation site to bind signalling proteins [27].

Downstream of GAB1, a cascade of phosphorylation messages converges in the amplification of the membrane signal to sustain cell proliferation, growth, and survival. This signalling cascade is fine-tuned, and every step is activated in a switch-like fashion: phosphorylation and dephosphorylation of proteins, via kinases and phosphatases respectively, are universal motifs for cell signalling where the phosphorylated state is typically associated with active signalling molecules.

The MAPK pathway starts with the Rat sarcoma (Ras) superfamily of GTPases, comprising over 150 small G-proteins, such as HRAS, KRAS, NRAS [38]. Ras GTPases convert GTP to GDP and activate an initial GTPase-regulated kinase, i.e. Rapidly Accelerated Fibrosarcoma (Raf), also called MAPK kinase kinase (MAPKKK). The Raf protein family contains several isoforms, such as ARAF, BRAF, CRAF.

In turn, Raf phosphorylates and activates an intermediate kinase, the MAPK/Erk kinase (MEK). MEK then phosphorylates the final effector kinase, the mitogen-activated protein kinase (MAPK), also called extracellular signal-regulated kinase (Erk), which targets transcriptional factors inducing expression of early genes, such as c-Myc [39].

Many proteins in the pathway are also involved in feedback loops (see paragraph 1.3.1.4) that compensate for inactivating effects of chemotherapy and therefore become therapy targets, for example MEK1/2. It has been proved that MEK inhibition has potent anti-tumour activity against human and mouse PDAC cell lines and orthotopically implanted tumours, causing a cytostatic

response [40]. Several mutations at each step along the pathway have been connected to oncogenesis and tumour development: for instance, almost 30% of solid tumours exhibit mutations in the RAS gene [38]. Pancreatic cancer is commonly characterised by an activating KRAS mutation, which keeps KRAS in the phosphorylated form, thereby activating the pathway in absence of an external stimulus. This anomalous behaviour reduces the effect of cytostatic chemotherapy on cancer cells; therefore, the targeted inactivation of proteins in the signalling pathways might be an effective approach to improve patient outcome and contrast the development of PDAC.

#### *1.3.1.3 The PI3K/mTOR/Akt pathway*

Another critical signalling pathway that controls cell division and survival is the phosphatidylinositol 3-kinase (PI3K)-mammalian target of rapamycin (mTOR) pathway (**fig.3**). Growth factor receptors activate PI3K, a lipid kinase directly recruited to the membrane level and evolutionarily conserved as a mechanism to respond to external growth signals.

PI3K binds directly to the receptors or the adaptor protein GAB1 and generates phosphatidylinositol 3,4,5 triphosphate ($PIP_3$), also regulated by the well-studied PTEN protein. PTEN is a phosphatase, which has been widely characterised for its role as an oncosuppressor since its phosphatase action regulates the cell cycle and survival. It was shown that the loss of PTEN, in combination with KRAS activating mutations, leads to the sustained activity of the transcription factor NF-κB in PDAC primary tissues [41].

Active $PIP_3$, in turn, recruits the protein Akt. Akt recruitment to $PIP_3$ facilitates the phosphorylation of Akt, mediated by its upstream activating kinase, PDK1. Akt is key for cell survival, as it acts on different substrates from functional classes including kinases, transcription factors, metabolic enzymes, E3 ubiquitin ligases, cell cycle regulators, and many others. The phosphorylation activity of Akt on one or more substrates highly depends on the protein localization, the cellular conditions, and the duration of Akt activation [42].

It is worth mentioning that Akt is not the only effector of PI3K, which also acts on the mTOR proteins in their two complex forms, mTORC1 and mTORC2. mTORC1 consists of the kinase mTOR, a scaffolding protein associated with mTOR, RAPTOR, and the mammalian lethal with Sec13 protein8 (mLST8). This complex is involved in events promoting ribosome biogenesis and translation of cell growth proteins. In contrast, the complex mTORC2 contains mTOR, RICTOR, mLST8 and a stress-activated protein kinase interacting protein (mSIN1), and it phosphorylates Akt and regulates cytoskeleton organization, lipid metabolism and cell survival [39]. In this dissertation, the role of PI3K in mTOR activation in PDAC was not investigated and will not be further discussed.

Treatment of cancer with PI3K inhibitors seems a reasonable choice due to its involvement in many processes favouring tumour progression. Nonetheless, the PI3K pathway also plays a key role in

glucose metabolism, and prolonged inhibition of this pathway can lead to hyperglycaemia. Therefore, targeted inhibitors might cause a systemic metabolic effect and reduce the efficacy of chemotherapy treatment in the long term. Also, the PI3K pathway is activated by many receptors with high plasticity, so compensatory mechanisms are frequent in presence of inhibitory drugs to maintain the signal transmission along the cascade within hours from drug exposure. Consequently, dose induced toxicity is a limiting factor for targeted chemotherapy because the desired cytostatic effect can only be obtained with a high dosage [20]. Nonetheless, oncogenic mutations in the PI3K-mTOR-Akt pathway appear to be more subclone specific than in the MAPK/Erk pathway, which tends to be more ubiquitous in the tumour. Thus, targeting PI3K in combination with other signalling proteins represents a valuable option in the context of personalized chemotherapeutic approaches based on the mutational landscape of tumour subtypes.

#### *1.3.1.4 The Ras/MAPK and PI3K/Akt pathways: crosstalk and mutual regulation*

The MAPK/Erk and PI3K/Akt pathways interact via positive and negative feedback loops in mutual communication (**fig. 3**). This interaction is key for cancer cells as one of the hallmarks of cancer is escaping apoptosis and keeping signalling cascades active through compensatory mechanisms. Therefore, reciprocal activation and inhibition of proteins in the MAPK and PI3K/Akt pathways have been extensively investigated, and a complex network of regulatory mechanisms has been discovered. Mendoza et al. [39] summed up different interaction mechanisms between the two pathways, some of which will be presented in this paragraph.

Feedback loops regulate the intensity and duration of pathways activation and cause network oscillations and switch-like transitions.

Within each pathway, protein activity is controlled via negative and positive loops, whereas the mutual regulation between MAPK and PI3K/Akt pathways is based on cross-inhibition, cross-activation that influence the system's stability. Negative loops generally decrease the activity of a target and usually start from a downstream protein in the cascade inhibiting an upstream member, while positive feedforward loops amplify protein signals by increasing the activity of the target.

Several downstream effectors of Akt, such as mTORC1, act as negative regulators of Akt itself directly or through other mediator proteins. For instance, Akt is inhibited by S6K1, which inhibits PI3K activity at different levels, whereas Akt self-regulates by inhibiting FOXO-mediated receptor tyrosine kinases expression, thus reducing the activation of the pathway – FOXO is one of the transcription factors regulated by Akt [43]. In the MAPK pathway, the most significant negative feedback loops start from the Erk protein. Erk phosphorylates and inhibits SOS, Raf and MEK, thus influencing its activation. Although it sounds counterintuitive, such mechanisms of indirect self-regulation are quite common in signalling pathways. For instance, Erk induces the transcription of genes that encode MAPK phosphatases and proteins interfering with the Raf-mediated MEK activation, and in turn, inhibit the pathway activation and reduce Erk activity [39].

Positive loops are less present but equally essential to amplify the external signal correctly and lead the cell to the appropriate response. The most significant positive loop in the MAPK-PI3K interaction is related to GAB1, a protein that is involved in the activation of the MAPK pathway and interacts with PI3K and $PIP_3$. GAB1 recruits PI3K to the membrane level, increasing the local level of $PIP_3$, leading to additional GAB1 recruitment to the membrane and, in turn, to an increase of signal transmission in the pathway [39].

The integration of the pathways comes from cross-inhibition mechanisms, such as the ones connecting MEK and Akt or GAB1 and PI3K: MEK inhibitors enhance EGF-induced Akt activation, while phosphorylation of GAB1 by Erk inhibits GAB1 itself and consequently GAB1-dependent recruitment of PI3K to EGFR. By contrast, examples of cross-activations are related to the activity of Ras-GTP, which binds and activates PI3K and, in turn, mTORC1 [39], which suggests that Ras could be a significant therapeutic target. However, Ras is also a suppressor of PTEN that inhibits PI3K, so inhibition of Ras could increase signalling on the PI3K pathway, developing a resistance mechanism against targeted inhibitors[38].

These interactions create new challenges in developing treatment strategies for many kinds of cancer, as they are commonly activated during oncogenesis and drug exposure. The plasticity of these pathways creates a limitation in drug development, but combinations of inhibitors of signalling enzymes show the best response in several kinds of solid tumours. Inhibitors cocktails kill resistant melanoma cell lines, reduce tumour tissue in prostate and lung cancer mouse models with the best outcome obtained by targeting both pathways with MEK and PI3K inhibitors [39] and this opens new perspectives for the treatment of pancreatic cancer.

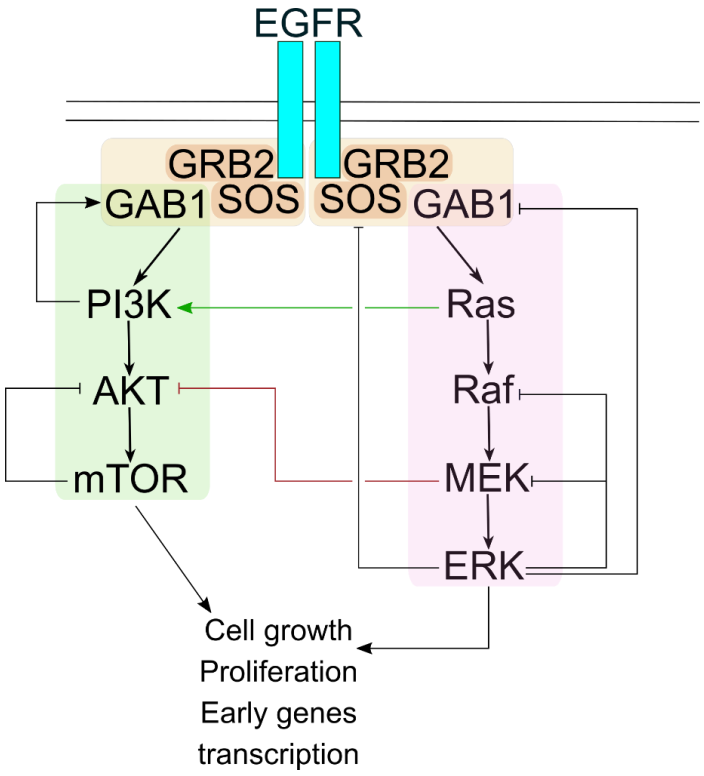


***Figure 3:*** *Ras/MAPK and PI3K/AKT pathways. Schematic representation of the MAPK and PI3K/Akt pathways and main proteins along the signalling cascades. These pathways regulate several mechanisms in the cell, such as cell proliferation and gene transcription, and are often activated by EGF, which binds to EGF receptors (EGFR). EGFR dimerizes and forms signalosomes at the membrane levels, i.e., protein complexes of receptors and adaptor proteins, such as GAB1. Along the pathways, proteins transmit the membrane signal towards the nucleus by phosphorylating and dephosphorylating downstream targets. Proteins can also regulate each other via cross-inhibitions (red arrows) and cross-activations (green arrows) or feedback loops (upward black lines) which control the stability of the system.*

### *1.3.2 Xenobiotic metabolism pathways and CYP3A5*

Dysregulation of cell pathways is a hallmark of cancer which involves not only signalling pathways but also metabolic ones, such as xenobiotic metabolism pathways that modify the chemical structure of xenobiotics such as drugs.

In humans, xenobiotic sensors are mainly proteins from the family of Cytochrome P450 (CYP), with approximately 60 proteins classified in 18 families [44]. The cytochrome P450 proteins are monooxygenases that catalyse many reactions involved in drug metabolism and the synthesis of cholesterol, steroids, and other lipids. These cell detoxifiers are designated by the letters CYP and a number denoting the CYP family, followed by a letter indicating the subfamily and another number representing the individual gene or isoform (e.g. CYP3A5). Under physiologic circumstances, these enzymes are expressed in liver cells, but CYP proteins have variable activity in different solid tumours [45] since several factors influence the expression of CYP proteins, such as anomalous hormone levels and genetic polymorphisms. [46]. Due to the strong DNA instability in cancer cells, poorly expressed CYP enzymes are often induced in specific tumour subclones [47]. CYP induction

is mostly transcriptional, and genes belonging to CYP families 1–4 can be transcriptionally activated by the presence of xenobiotics. Recently, it was found that nuclear receptors Constitutively Activated Receptor (CAR) and Pregnane X receptor (PXR) act as xenobiotic sensors and transactivate the CYP3A5 promoter, thus leading to CYP3A5 induction [48]. Although many isoforms share similar functions in the metabolism of exogenic or endogenic xenobiotics, CYP3A4 and CYP3A5 are highly relevant in oncology as they metabolise a large set of substrates (most of which are shared targets), including many cancer inhibitors. Therefore, the aberrant expression of these two isoforms has a substantial impact on drug delivery and targeting them could increase drug sensitivity [49].

Noll et al. [23] newly described a potential mechanism of chemotherapy resistance in some PDAC subtypes. Patient-derived model cell lines of the exocrine-like PDAC subtype heterogeneously express CYP3A5 (**fig. 4A**), but not the isoform CYP3A4, and immunohistochemical staining of tumour cross-section are characterised by cells strongly overexpressing CYP3A5 interspersed with cells without detectable CYP3A5 expression. In this project, pre-treating cells with a pan-CYP inhibitor resulted in an increased sensitivity of PDAC cells to the chemotherapeutic drugs paclitaxel and TKIs erlotinib or dasatinib showing that CYP3A5 contributes to drug resistance in exocrine-like PDACs. The same publication also highlighted the importance of the drug-induced expression of CYP3A5 in PDAC tissue. Treating the classical subtype with paclitaxel for two rounds led to an initial inhibition of tumour growth during the first round, followed by the development of paclitaxel resistance during the second (**fig. 4B**) which confirms that CYP3A5 upregulation is one of the mechanisms responsible for acquired resistance in PDAC. This suggests that CYP3A5 expression should be considered when testing novel PDAC treatments since adverse drug effects due to therapy might be alleviated by developing new compounds that can selectively modulate the expression of CYP3A5 [49].

Although the investigation of CYP enzymes has been in focus for the last 20 years, a quantitative description of the dynamics of CYP3A5-related drug resistance at the tissue level is not available, especially in pancreatic cancer. In this perspective, studying the systemic action of drug-metabolizing proteins in tumour tissue could be a turning point in understanding the role of these enzymes in drug resistance.

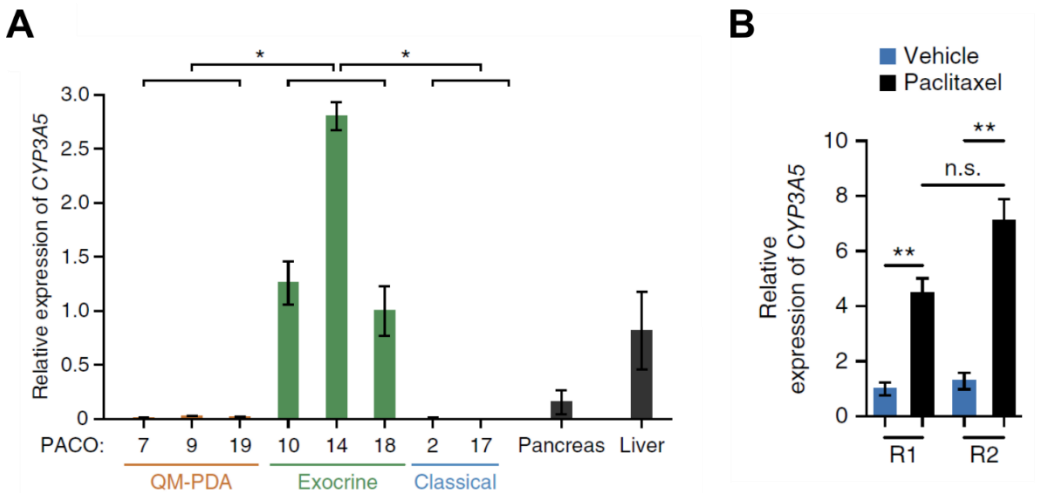


***Figure 4:*** *CYP3A5 contributes to drug resistance in PDAC.* ***A.*** *Patient-derived cancer stem cells heterogeneously express CYP3A5. Exocrine-like subtype (in green) expresses CYP3A5 at high levels while Quasi-mesenchymal and Classical cell lines exhibit low CYP3A5 expression.* ***B.*** *CYP3A5 is induced in cells from the classical subtype after one and two rounds of chemotherapy treatment with paclitaxel. Data by Noll et al.*[23]

## *1.4 New experimental strategies to test drug resistance in cancer*

Most chemotherapeutic agents target intra-cellular mechanisms, but the systemic response on the tissue level is often neglected or directly tested in pre-clinical trials on animal models. Nonetheless, animal models are expensive in terms of cost and time, so lab-based cell culture still plays an important role in cancer research, and the development of three-dimensional methods to create tissue-like structures has revolutionized the field of drug discovery [50]. In fact, the 3D cell environment can be manipulated to mimic the *in vivo* behaviour of cells and create an improved picture of cell-to-cell interactions in oncology and other diseases. It is known that the heterogeneity of cancer due to the presence of different cell subtypes leads to different dynamics in 3D compared to classical 2D cell cultures. 3D cell culture can accurately resemble heterogeneous populations, quite close to animal models, with dramatically lower costs. Pluripotent stem cells and cancer stem cells are capable of self-organizing into structures resembling early stages of developing tissues, leading 3D cultures to the next stage of complexity.

In the last decade, many techniques were developed to grow 3D structures from cancer cells, mainly divided into scaffold-based and scaffold-free methods.

Scaffold-based techniques provide cells with ECM-like support, such as hydrogel, Matrigel and other synthetic materials, where organoids can develop from mixtures of cells [51]. In this case, soluble factors such as cytokines and growth factors can diffuse in the gel and lead to realistic gradients of nutrients. Also, using scaffolds allows scaling experiments to tissue-like cultures as cells do not undergo necrosis due to a lack of nutrients or cell-to-cell contact.

On the other hand, scaffold-free techniques rely on the ability of cells to aggregate. Methods like hanging drop microplates, magnetic levitation, and spheroid microplates with ultra-low attachment

coating have gained consensus in the last few years as they are easy to handle. Since most scaffold-free methods make use of microplates produced with high manufacturing precision, they allow better experimental replicability than scaffold-based methods, especially when co-culturing multiple cell lines. Evenly distributing cells in gel scaffold is challenging even for experienced researchers and can create a bias in the aggregation of cancer clones or cells of different nature.
Recently it was shown that cells cultured in 2D show different behaviours than in 3D due to different aggregation, proliferation, and differentiation rates [52]. For instance, cells grown in 2D are more sensitive to drugs targeting membrane receptors than in 3D because of the protein arrangement along the cell surface and the binding efficacy of drugs to receptors [50]. Also, cells in tissue usually co-exist in various cell stages and proliferation activities: proliferating cells are usually located along the external surface of the tissue where they have more space to duplicate, and this can only be reproduced in 3D cell cultures [50]. Finally, cells have different shapes in 2D than 3D causing changes in local pH levels and metabolic profiles within cells, contributing to drug resistance [53].
Independent of the technique, 3D cell cultures represent a promising evolution for cancer research to observe cell response to drugs in a system that resembles mice and human models. Albeit being in the early development stage, these methods are replacing 2D cell cultures and were therefore employed in this dissertation to test mechanisms of drug resistance in heterogeneous populations of PDAC cancer.

## *1.5 Open questions in drug resistance*

Cancer cell populations can evolve to resist stress caused by chemotherapeutic drugs. Mechanisms of drug resistance were mentioned in the previous paragraphs and range from alterations in drug targets to the development of alternative pathways for growth activation to increased drug efflux and drug inactivation through regulatory changes [54]. Although with the development of new experimental approaches, many resistance mechanisms have been investigated, novel cell behaviours still develop as a reaction of cancer cells to new chemotherapy agents. The mechanism of action of the chemotherapy agent influences how cells develop resistance, for instance, by increasing the expression of selected proteins or creating alternative pathways to circumvent cytotoxicity. Moreover, cancer tissues are complex and often stratified in subtypes that respond to drugs in diverse ways, limiting the efficacy of a single agent. In this perspective, the combination of chemotherapy drugs targeting multiple aspects of cancer is more effective but is rarely considered in clinical trials due to the high level of toxicity for patients. Thus, testing chemosensitivity in organoids might be beneficial to understand how cells adapt under treatment and optimize chemotherapeutic strategies.

Since tumour sequencing has become part of the clinical tests run on patients to predict drug response, it has created many opportunities for personalized treatments based on pre-treatment

tumour characteristics. The limitation of this approach is inevitably related to the onset of drug resistance caused by the plastic response of cells during treatment. Therefore, three are the main questions that cancer research needs to elucidate further to contrast drug resistance in patients. These three topics are to be considered as a whole, although they represent different layers in the tumour environment. First, it is necessary to identify the full range of intracellular mechanisms that create an evolutionary advantage for cancer before drug treatment and target the intricate network of compensation mechanisms that cells activate in response to drug exposure. Second, with the support of *in silico* modelling, it is crucial to understand the temporal and spatial evolution of drug resistance phenomena in cancer tissues, considering the systemic response of the cancer ecosystem. Finally, it is fundamental to create standardized subtyping methods for cancer tissue to predict the response of different subtypes to chemotherapy.

This thesis contributes to answering these questions by combining computational and experimental methods to investigate two mechanisms that contribute to pre- and post-treatment resistance, their evolution on the systemic level, and their potential role as cancer biomarkers.

## *1.6 Systems biology approach to investigate drug resistance*

Resistance to chemotherapy is one of the major obstacles in cancer treatment because the development of resistance phenomena impairs the efficacy of drugs. The behaviour of cancer cells has been extensively investigated from a qualitative point of view, but little knowledge has been collected on the dynamics of such mechanisms. Intra-cellular modifications, from the genetic to the protein level, and systemic processes such as hypo-vascularization impact the delivery and efficacy of chemotherapy.

In this perspective, mathematical modelling has been of great support during the last decades, and technological evolutions now allow more in-depth knowledge of the processes behind drug resistance. Although complex systems as the biological ones require many simplifications for a model to work in a reasonable time, applying mathematical models to the study of drug resistance is highly valuable. Ranging from more straightforward but fast and reliable mathematical approaches to more advanced but computationally demanding algorithms, modelling is the cheapest and most flexible way to test hypotheses and predict new cellular behaviours.

Though pancreatic cancer is extensively studied, the discovery of some PDAC resistance mechanisms is relatively new to the scientific community, and further efforts are still needed to gain a detailed quantitative description.

The following paragraphs present an overview of systems biology approaches applied to oncogenesis and drug response mechanisms that highlight the importance of combining computational and experimental methods to characterise the behaviour of cancer cells.

### *1.6.1 Mathematical models of biological systems*

Modelling of biological systems can have different aims: it can be used to explain new experimental evidence based on known mechanisms, with the mechanistic or bottom-up approach, or it can infer new cell features by analysing data without prior knowledge, through top-down methods - generally used on big data such as genomics data.

Mechanism-based models are kinetic descriptions of biochemical events in which a state variable is assigned to every entity in the model, e.g. to proteins in a network. The state variable can be discrete and continuous: in the first case, it can only be assigned a discrete number of states (e.g., On/Off state as in Boolean or logical models) and usually represents long-term behaviours of molecules; in the second, the variable can have continuous distributions and describe temporary events [55]. The interactions among entities are usually characterised by kinetic parameters that typify the biological context of interest. The goal of such models is to extract these parameters to gain insight into the dynamics of the system. The model parameters can be estimated by fitting experimental data, i.e. by minimizing the distance between estimated variable trajectories and experimental evidence, but generally, even a simplified model requires a set of parameters and variables that exceeds the experimental data. This is often due to the costs and complexity of the experimental methods used to get reliable evidence from biological systems. Consequently, the model parameters are non-identifiable, i.e. there is no unique set of parameters that give a complete picture of system dynamics.

Kinetic models are usually based on differential equations, used to describe temporal and spatial distributions of proteins or other molecules in the cellular context. A state variable, in this case, can represent the abundance of a molecular species, which is dynamically controlled by a combination of processes that increase and decrease its level [56]. Ordinary differential equation (ODE) models describe cell population dynamics in time through laws of mass action. Generally, enzyme-catalysed reactions are described through Michaelis–Menten kinetics. Population growth is described with logistic kinetics, whereas all other reactions are represented by mass–action kinetics (see **table 1**) - most of these kinetics were applied in this dissertation in different contexts. When considering differential equations for both temporal and spatial dynamics – for instance, to describe drug delivery patterns as in the second sub-project of this dissertation – the model generally is extended to partial differential equation (PDE).

| Model | Reaction | Equations |
|---|---|---|
| *Mass action kinetics* | Chemical reaction<br>$A + B \xrightarrow{k} C$<br>k, reaction constant | $\frac{dA}{dt} = -k\,[A][B]$<br>$\frac{dB}{dt} = -k\,[A][B]$<br>$\frac{dC}{dt} = k\,[A][B]$ |
| *Michaelis-Menten kinetics* | Enzymatic reaction<br>$E + S \underset{k_1, k_{-1}}{\longleftrightarrow} ES \xrightarrow{k_2} E + P$<br>$k_1$, $k_{-1}$, $k_2$, reaction constants<br>$K_M = \frac{k_{-1} + k_2}{k_1}$ | $V = -\frac{d[ES]}{dt} = \frac{V_{max}[S]}{K_M + [S]}$<br>$V_{max} = k_2\,[E]_0$ |
| *Logistic growth* | Population (P) growth<br>K, carrying capacity<br>k, growth speed | $\frac{dP}{dt} = kP\left(1 - \frac{P}{K}\right)$ |
| *Reaction-diffusion* | Drug diffusion and degradation<br>c, drug concentration<br>D, diffusion constant<br>$k_{deg}$, degradation rate | $\partial_t c = D\nabla^2 c - k_{deg} c$ |

***Table 1*** *Parts of mechanistic models commonly used in systems biology. ODE models are used to describe concentrations in a well-mixed system or numbers (e.g., of cells or species) over time. Reactions are described by mass action kinetics (used to represent simple conversion reactions), Michaelis-Menten kinetics (used to represent enzyme-catalysed reactions) or logistic growth (used to represent population growth). PDE models are used to describe reactions in the biological system depending on time and space. A common example is a reaction-diffusion model that results in concentration gradients.*

Mechanistic models can quantitatively describe known mechanisms but fall short in discovering novel molecules, such as new cancer-specific biomarkers and gene signatures. Data-driven models are generally applied in this context, as they do not rely on assumptions about the biological system but are based only on the analysis of data and often reveal new biological insights [57]. Nonetheless, complex data-driven models often require a more significant computational burden than mechanistic models due to the extent of the data analysed. The application of -omics technologies, from high-throughput sequencing to automated screenings, has generated large-scale data, and many data-driven techniques have been developed to analyse high-dimensional datasets. However, these methods were not applied in this study and therefore will not be further discussed.

Overall, mechanistic models are extensively used to quantitatively describe the dynamic behaviour of cellular processes associated with cancer. In this dissertation, mechanistic approaches based on ODEs and PDEs were employed to describe resistance mechanisms in PDAC and cervical cancer and support the design of experiments to elucidate the response of cells to chemotherapy.

### *1.6.2 Multi-scale modelling*

Mathematical models are simplified descriptions of complex systems but represent a valuable resource to analyse cells in a complex microenvironment, such as cancer tissue. Including cell-specific rules in a more comprehensive model of the tissue level is the new frontier of systems biology, known as multi-scale modelling.

In oncology, a major challenge for mathematical modelling is the heterogeneity of the tumour environment. Through multi-scale cell-based models, also called agent-based models, cancer tissues can be described as a collection of autonomous agents that contribute to the overall behaviour of the tissue. These agents are generally characterised by individual sets of parameters specific, for instance, for their subtype. These models can be pretty detailed and computationally demanding by their nature, so a common approach to reducing the complexity of these methods is to place cells along a predefined and regular lattice. Lattice-based models are usually fast and allow the quick testing of new ideas but often do not resemble realistic biomechanical features. On the other hand, off-lattice models are ideal for representing the stochastic growth of cells in the tumour environment but necessitate time-consuming simulations and more computational power to test several parameters sets, which means several biological conditions.

The goal of these models is to describe phenomena in 2-dimensional (as in 2D cell culture) or 3-dimensional cancer environments (as in 3D cell organoids or xenograft) and gain insight into the systemic behaviour of the tissues.

Multi-scale models are usually hybrid, i.e. they contain discrete and continuous rules. The diversity of cells in a tissue can be represented with discrete rules specified for single agents or ODE models to describe intra-cellular molecular processes. At the same time, phenomena such as nutrients or drug diffusion in the micro-environment are continuous and usually based on partial differential equations (PDEs). Deterministic models made of ODEs and PDEs are pretty common to integrate data and estimate parameters from different sources, such as protein measurements and transcriptome sequencing combined with microscopy data. Recently, stochastic models were proposed to include processes on a smaller scale [58], but the computational burden they require for parameter estimation and prediction of confidence bounds limits the applicability in many cellular contexts. A general approach used in this case to reduce the required computational power is to create a single-scale model first and subsequently couple them while trying to ensure consistency in parameter estimation. Nonetheless, an optimal method for multi-scale modelling does not exist yet, but many computational packages have been developed to solve multi-scale models, and a good summary of the most popular ones can be found in [59] and [60].

In the context of solid tumours, the development of cell-based models will facilitate the optimization of drug delivery strategies. For instance, in the case of pancreatic ductal adenocarcinoma, it is known that the formation of resistant niches is an adaptation mechanism of the tumour to drug

exposure [61]. 3D computational models can simulate nutrients concentrations, the proliferation of cells, or necrosis in 3D tissues and can be applied to study the dynamics of niche adaptation to new drug treatments *in silico*. Cell-based methods are, in fact, suitable to track changes of single-cell traits during treatment to understand how the response of single cells or cells subtypes combines into the general response of the whole tissue [62]. So far, algorithm-specific biases make no single method ideal for all contexts, but technological advancements open the way to numerous approaches to understand new cell mechanisms and optimize cancer treatments.

### *1.6.3 Mechanistic modelling of intracellular networks*

Although simplistic, computational modelling of intracellular pathways is an established method to explain complex molecular interactions and understand the role of signalling proteins in the development of diseases.

The anomalous activation of MAPK and PI3K/Akt pathways in cancer has been extensively studied both experimentally and computationally, but the complexity of the system is a challenge for two reasons: first, the more extensive and accurate models require massive computational power, so the simplification of the biochemical reactions is necessary; second, molecular interactions in cancer cells are often context-specific, related to the type of cancer or the mutational status of the patient, therefore a global model that portrays the plasticity of cancer is complicated to define. Many theoretical models have been proposed for a quantitative description of the behaviour of these pathways, but no unified model has been created yet.

#### *1.6.3.1 Modelling the signalling cascades: the MAPK and PI3K pathways*

Signalling pathways are usually described as networks of nodes and edges, where nodes represent biological entities, such as proteins, and edges are the interactions among them. In these models, the temporal and spatial organization of cellular reactions is defined by dynamic functions to explain how signalling cascades integrate internal and external inputs and lead to different cell response.

During the last decades, most studies have proposed compartment-specific models of pathways activation: an example is represented by the extensive literature on the activation of membrane receptors. It is known that RTKs over-expression increases the oncogenic activation of the MAPK and PI3K pathways, generally dependent on ligand concentration and RTK expression [63]. Ligand-induced internalization of EGFR happens in a stepwise fashion: first, different phosphorylation stages of the receptor and conformational changes occur, then signalosomes form thanks to adaptor proteins and negative regulators of membrane receptors, and finally, the membrane undergoes modifications leading to endocytosis. A systems biological analysis of this process can elucidate

temporal and spatial dynamics of the phenomena involved, as attempted by Schmidt-Glenewinkel et al. [64]. By combining mechanistic modelling and experimental data from quantitative imaging and flow-cytometry, they investigated the temporal evolution of EGFR endocytosis and assessed the role of the internalization machinery. This method could be essential to understand the change in EGFR dynamics based on EGFR abundance, which is often altered in cancer cells.
As previously mentioned, post-translational modifications, such as ubiquitination, are fundamental when modelling the dynamics of RTKs signalling. Capuani et al. [65] described a threshold effect of EGFR ubiquitination determined by EGF concentration and GRB2-CBL complexes. Through *in silico* modelling, they investigated how GRB2, although not directly involved in ubiquitination, influences the binding of CBL to EGFR. The absence of GRB2 abruptly reduces CBL-related ubiquitination of EGFR, thus showing that cooperativity between the two molecules determines the dynamic of EGFR internalization. This computational analysis has highlighted the importance of EGFR, GRB2 and CBL protein expression ratios to guarantee the correct interaction. Another study investigating by computational modelling the components of signalosomes - such as GRB2 and GAB1 - and the intricate network of feedback loops regulating them [66] has shown that the spatial localization of adaptor proteins influences the speed of activation of downstream cascades.

Describing compartment-specific dynamics is not sufficient to portray the complexity of the cell system since downstream of the membrane level, an intricate network of reactions characterises the cellular signalling systems; in fact, several models include the effect of feedback loops on the formation of membrane complexes.
For instance, Kholodenko et al. [67] simulated signal transduction from EGFR to SOS and applied the model to predict the impact of EGFR binding dynamics on Erk activation. Later, Schoeberl et al. [68] created one of the most detailed ODE models of the binding of EGF receptors to EGF and consequent activation of the Erk pathway, consisting of 101 reactions and 94 species.
Further applications of these modelling strategies in oncology focused on disease-specific models of the activation of signalling pathways. Orton et al. [69] modelled the MAPK pathway considering EGFR overexpression and specific cancer-related mutations, such as RAS, BRAF and EGFR. After the discovery of random mutagenesis in cancer signalling pathways, Stites et al. [70] included random mutations in a model of the Ras/Erk pathway and found cooperation between mutations in signalling proteins and oncosuppressor genes. An interesting perspective was then proposed by Sturm et al. [71] who compared MAPK signalling to a negative feedback amplifier (NFA). Basing the model parameters on Schoeberl et al. [68], they simulated and then proved experimentally that the NFA-like nature of the MAPK pathway is due to feedback loops originating from Erk. This NFA pattern confers stability to the whole system against perturbation, so disruption of this feedback via chemotherapy inhibitors of proteins inside the NFA module is less efficient than inhibiting external targets.

## 1.6 Systems biology approach to investigate drug resistance

Two studies [72], [73] analysed the effect of ErbB receptors on the PI3K pathway by modelling the membrane compartment, where ligand binding occurs, and the downstream activation of PI3K and Akt. Based on these publications, a later model by Schoeberl et al. [74] focused on the PI3K pathway and predictions identified ErbB3 as the key node in response to ligands that can bind either ErbB3 or EGFR. Based on this, the group proceeded with the development of a new therapeutic agent, a monoclonal anti-ErbB3 antibody called seribantumab (MM-121, Merrimack), currently undergoing clinical trials. This example values the application of the principles of systems biology in the discovery of new treatment strategies for cancer.

Nonetheless, all these studies focused mainly on single pathways and feedback loops within them, while it is known that the crosstalk of pathways is a common feature in normal and cancer cells. The integration of different pathways in computational approaches is fundamental to have a complete overview of intra-cellular events due to feedback loops that cause compensatory behaviours and affect cell response in normal and pathological conditions.

In this perspective, several integrated models have been proposed in the last decade to portray the complexity of signalling pathways. Suresh Babu et al. [75] created one of the first integrated models in 2008 and were among the first to quantitatively describe time trajectories of the activation of proteins along the pathways. By simulating the activation of the MAPK and PI3K pathways via EGFR or NGFR with Gepasi [76], they could prove that EGF solicits transient signalling in the cell and that EGFR-dependent activation of Erk reaches maximal activation at 5 minutes, decreasing after around 20 minutes, while Akt shows a peak at 1 minute, to reach the baseline again after 5 minutes. Moreover, they showed that Akt activation induces Erk phosphorylation, thus confirming that the pathways proceed independently, but communication is necessary for the correct cell functioning.

Arkun et al. [77] investigated the temporal evolution of feedback loops by using dynamic modelling on previously published parameter values. This analysis revealed the presence of four fundamental inter-pathway feedback loops, which work in tandem with one negative loop within the MAPK pathway and two loops within the PI3K pathway. Among these, the Erk-Akt mutual inhibitory pathways via mTOR and GAB1-PI3K resulted to be the most significant loops in cells stability due to the high sensitivity of the pathways to their disruption.

All studies described in this section share a common goal: they use computational models to increase our understanding of the dynamics of cellular responses to external stimuli in different contexts. Nonetheless, several limitations in the applicability of these models in clinical practice derive from data quality, the complexity of the biological systems and other factors presented in the following paragraph.

### *1.6.3.2 Challenges in modelling of intracellular mechanisms*

Mathematical models are by their very nature simplifications, and, especially in the field of biology, there is a critical trade-off between accuracy and simplicity. The major limitation of the models presented in the previous paragraph stands in the computational power they require and the impossibility to identify a unique set of parameters due to lack of data; in fact, most methods are specific for the physiological functions and the cell context under investigation to reproduce the available experimental data.

To characterise a model reliably, the number of observations should be at least equal to the number of components of the model, and this requirement is hardly met in most studies due to the cost and complexity of thorough experimental analyses. Depending on the available data, the reconstruction of a biological system can have different levels of resolution, i.e. can be more or less detailed, and often simplifications are compensated by statistical and regression methods. Especially in the case of signal transduction networks, where the number of proteins in the model is relatively high to have a complete overview of the system, these methods can help gain more evidence from incomplete datasets [78]. Although the limiting factor is the paucity and quality of data, many studies might benefit from applying mathematical methods to disambiguate noisy information, especially when dealing with patient-derived data [79].

Patient-derived data pose a further challenge for systems biology studies in oncology due to intra-tumour heterogeneity that derive from drug treatment and leads to varying drug response based on cell-specific features. Translating models into clinical approaches still presents patient-specific challenges, such as diverse mutational landscapes. Therefore, drug response in stratified tumours can only be described with detailed and computationally demanding models that can be adjusted to subtype-specific pharmacokinetic features. *In silico* models might predict tumour behaviours by considering network rearrangements due to pre-existing or drug-induced mutations and structural modifications, thus facilitating the development of new clinical strategies.

Despite the extensive qualitative research on cancer, no comprehensive quantitative description of most cellular processes involved in cell response is available yet, as the biological approach has relied for a long time only on experimental evidence more than theoretical approaches. An optimal trade-off between an in-depth description of biological mechanisms and the low amount of experimental evidence, as in the case of PDAC, could lay in a minimalistic modelling approach that will facilitate the analysis of currently available data.

## *1.6.4 Modelling drug resistance in oncology*

Precision medicine approaches are changing chemotherapy. Oncologists identify specific drug treatments depending on patient-specific mutational landscape or the presence of molecular cancer markers. Nonetheless, chemotherapy response is often variable and affected by drug-induced

resistance, so modelling the effect of chemotherapy can help to predict long-term patient response with limited costs. This paragraph is a collection of some of the many models developed to describe drug resistance in cancer to give an overview of mathematical approaches used so far in this field.

Thanks to the introduction of tyrosine kinase inhibitors (TKIs) for cancer treatment, modelling of signalling pathways has gained consensus in the clinical context because dynamics of TKIs directly affect established drugs currently in use for cancer patients. The *in-silico* analysis of signalling pathways in relation to drugs efficacy has been crucial to determining weaker points in protein cascades and predicting tumour outcome based on the mutational status.

For instance, Chmielecki et al. [80] created a mechanistic approach to study optimal dosing of TKIs in non-small cell lung cancer (NSCLC) and showed that TKI doses used in clinical regimen are not optimized for EGFR mutants. This study predicted alternative therapeutic strategies that could optimize and prolong the clinical benefit of TKIs against EGFR-mutations by delaying the development of resistance. Gómez Tejeda Zañudo et al. [55], instead, tested combinatorial drug interventions on a breast cancer network model based on pre-existing literature. According to this analysis, many molecular nodes in the network, most of which are signalling proteins, are important markers to predict drug response and could be targets for inhibitors in the clinical context.

Another interesting study [81] investigated the complex mechanism of drug resistance related to a common mutation in melanoma, the activating BRAF mutation. By simulating with COPASI [82] a generic growth factor stimulation, in the presence or absence of BRAF activating mutations, the authors created a quantitative model of how the activating BRAF mutations might lead to higher Erk activation levels, and in turn to higher proliferation. Consequently, this model is a platform to test if established drugs affect BRAF-mutated melanoma as expected or if compensatory mechanisms reduce their efficacy. The model predictions suggest that treating patients with BRAF inhibitor might decrease Erk levels and reduce cancer survival. Finally, a study in lung cancer by Kim et al. [83] investigated the heterogeneity of MAPK and PI3K networks response to kinase inhibitors in the presence and absence of HGF treatment. The model presented in this study suggests that a combination of Akt and MEK inhibitors reduces the activity of compensation loops and strongly reduces cancer cell viability.

The flexibility of mathematical models is also crucial to integrate data from different cell contexts. For instance, it was recently shown by Shi et al.[84] that the abundance of most core proteins in the MAPK pathway is conserved over normal and breast cancer cell lines, while EGFR and feedback regulators are differentially expressed in the two conditions, which show diverse cell responses to EGF stimulation. Bouhaddou et al.[85] defined a pan-cancer mechanistic model based on multi-omics data and predicted that Erk, and not Akt, drives cell-to-cell proliferation variability in mammary cancer, so targeting Erk might be valuable to increase drug efficacy. On the other hand, by using the same model on glioma cells, they obtained realistic predictions on increased cell death

by treating cells with Akt inhibitors. Therefore, their pan-cancer model could help discriminate between cancer-specific dynamics that impair drug treatment.
In the context of PDAC, few studies have addressed drug resistance with computational models compared to other kinds of tumours, such as breast cancer [86]. Detecting the tumour in the initial stages is complicated, and the lack of data limits the applicability of systems biology to PDAC in the clinical context to facilitate early diagnosis [87]. Therefore, some studies have described the kinetics of more advanced stages of cancer, as for metastatic cancer [88], but mostly lack clinical validation. In this thesis, the study of drug resistance in PDAC was based on experimental data collected from patient-derived cells to reduce the gap between established cell lines and patient characteristics that are often hard to reconstruct. Combining such evidence with computational modelling gives insight into the behaviour of the tumour in a context that partially resembles the complexity of human tissue.

Although the variety of applications here presented shows that our knowledge of pan-cancer and tumour-specific drug response is still limited, the evolution of comprehensive computational methods combined with established experimental techniques is opening new possibilities to understand resistance mechanisms. Multidisciplinary approaches as the ones presented in this dissertation will in future facilitate the prediction of drug resistance and the optimization of treatment strategies based on cancer subtyping, mutational landscape, and cancer biomarkers.

# 2. Optimization of PDAC treatment with erlotinib dependent on CBLc expression

## *Contributions*

In this project, I performed experiments in PDAC (SU.86.86) and cervical cancer (HeLa) cell lines and worked on mathematical modelling. An initial dataset obtained in SU.86.86 cells, two clones of CBLc-overexpressing SU.86.86 cells and survival data in patients were provided by collaboration partners from the Department of Surgery at Heidelberg University (Dr. Kai Hu, group of N. Giese).

## *2.1 Aim of the study*

This sub-project aims to investigate the role of the ubiquitin ligase CBLc in the activation of signalling pathways in drug-resistant PDAC cells via experimental and computational analysis.

Dysregulation of signalling pathways regulating cell growth and survival is known as a major cause of oncogenic transformation. Biochemical pathways activated by EGF receptors (EGFR), such as the MAPK and PI3K/Akt pathways, are the most intensively studied signal transduction systems due to their essential role in cell growth, differentiation, migration, and apoptosis and are often mutated in cancers [89]. For this reason, therapeutic MAPK pathway inhibitors were developed that act at the receptor level, as in the case of erlotinib, or downstream along the pathways [90]. It is well-established that these two signalling pathways exhibit several cross-talks and regulate each other at the transcriptional level. Moreover, casitas B-lineage lymphoma (CBL) ubiquitin ligases negatively regulate active receptor tyrosine kinases (RTKs) by targeting phosphorylated RTKs for degradation or accelerating their removal from the cell surface.

Our partners at the Department for Surgery of Heidelberg University found that patients with PDACs expressing the CBL species CBLc have improved survival over three years. Surprisingly, molecular biological experiments conducted in PDAC cell lines expressing or not expressing CBLc showed a paradoxical amplification of MAPK and PI3K/Akt signalling activities in PDAC cell lines overexpressing CBLc treated with the tyrosine kinase inhibitor (TKI) erlotinib compared to PDAC cells not expressing CBLc over a short timeframe. CBLc-expressing cells exhibited residual activation of signalling proteins, such as Erk and Akt, in presence of chemotherapy and higher amplitude in absence of chemotherapy compared to non-expressing cells. Although erlotinib was effective on EGFR activity, no effect of CBLc-overexpression was visible on EGF receptor expression, suggesting that the enzyme acts downstream of the membrane level.

As part of this thesis, a computational ODE model of the MAPK pathway and its crosstalk with the PI3K/Akt pathway was developed to explain these experimental observations and confirmed that the increased activity of Akt and Erk is due to the role of CBLc as scaffold for downstream proteins.

Further experimental validation confirmed that CBLc increases the recruitment of adaptor proteins to membrane complexes, thus enhancing the signal transmission downstream of the membrane level.

In conclusion, the analysis presented in this project highlights the relevance of CBLc in the short-term activation of signalling pathways in PDAC cells and the transcriptional regulation of early genes and oncogenes fine-tuned by Akt and Erk. Therefore, CBLc over-expression represents an innate resistance mechanism and could in future become a potential biomarker used to predict drug response in pancreatic cancer.

# *2.2 Materials and methods*

## *2.2.1 Experimental analysis*

### *2.2.1.1 Cell lines*

Human pancreatic ductal adenocarcinoma cell lines (SU.86.86) in the wild-type (wt) form and stably expressing CBLc (SU.86.86) were maintained in RPMI1640 medium supplemented with 10% foetal calf serum, 2 mM L-glutamine and 100 U/ml penicillin and 100 µg/ml streptomycin. HeLa cells were maintained in Dulbecco's Modified Eagle Medium (DMEM) supplemented with 10% foetal calf serum (brand), 2 mM L-glutamine (Invitrogen/Gibco), 100 U/ml penicillin and 100 µg/ml streptomycin (Invitrogen/Gibco). The medium for SU.86.86 and HeLa transfected cells was additionally supplemented with 500 µg/mL Geneticin (G418 sulphate, Gibco). All cell lines were cultivated at 37 °C and 5% CO2 in a humidified tissue culture incubator and were passaged when reaching ~70-90% confluency.

### *2.2.1.2 Stable transfection of HeLa cells for CBLc characterization*

HeLa cells were seeded in large Petri dishes (150x21, ThermoFisher) at a concentration of $10^5$ cells per dish. After one day, transfection was performed using Lipofectamine 2000 (Invitrogen) according to the manufacturer's instructions. A total amount of 2 µg DNA (pCMV6-AC-GFP-CBLC construct, Origene) per Petri dish was used for the transfection. Cells were incubated with selection medium (1 mg/ml G418 in DMEM) for 2 to 3 weeks and medium was replaced every 3 days. Afterwards, resistant colonies were marked based on the fluorescence level and isolated by using metal cloning cylinders. Colonies were then detached from the Petri dish using 0.05% Trypsin-EDTA and re-seeded in 6-well plates (CytoOne). Finally, CBLc positive clones were seeded and maintained in culture flasks (Greiner Bio One). The transfection of CBLc was confirmed via immunoblotting.

### *2.2.1.3 Erlotinib dose-response analysis in wild-type and CBLc-expressing cells*

a. Human cervix carcinoma cells - HeLa

   Wild-type and CBLc-expressing cells were seeded in 6-well plates (CytoOne) two days prior to EGF exposure at a concentration of 0.5 x $10^6$ cells per well. After one day, maintenance medium was exchanged with starvation medium (phenol red-free, glutamine-free, serum-free DMEM) for 24 hrs. One hour prior to EGF exposure, cells were treated with erlotinib (LC Laboratories). Erlotinib stocks (10 mM in DMSO) were serially diluted in starvation medium at different concentrations (10 µM, 1 µM, 300 nM, 100 nM, 10 nM). The medium was exchanged with fresh starvation medium in untreated control samples. EGF stocks (R&D systems, 20 µg/ml in PBS) were freshly diluted in starvation medium to a

concentration of 10 ng/ml and cells were treated for either 5 or 10 minutes, then harvested and analysed via Immunoblotting.

b. Human pancreatic ductal adenocarcinoma cell lines - SU.86.86

Wild-type SU.86.86 cells were seeded in 6-well plates (CytoOne) two days prior to EGF exposure at a concentration of 0.3 x $10^6$ cells per well. After one day, cells were transfected with pCMV6-AC-GFP-CBLC or pCMV6-AC-GFP constructs. X-treme Gene 9 (Roche) was used as transfection reagent according to the manufacturer's protocol. After 24 hours, maintenance medium was exchanged with starvation medium (glutamine-free, serum-free RPMI1640) for 6 hrs. One hour prior to EGF exposure, cells were treated with erlotinib (LC laboratories). Erlotinib stocks (10 mM in DMSO) were serially diluted in starvation medium at different concentrations (10 µM, 1 µM, 300 nM, 100 nM, 10 nM). The medium was exchanged with fresh starvation medium in the untreated control sample. EGF stocks (R&D systems, 20 µg/ml in PBS) were freshly diluted in the starvation medium at a concentration of 10 ng/ml and cells were treated for 5 minutes, then harvested and analysed via immunoblotting.

#### *2.2.1.4 EGF treatment in wild-type and CBLc-expressing cells*

a. Human cervix carcinoma cells - HeLa

Wild-type and CBLc-expressing cells were seeded in 6-well plates (CytoOne) two days prior to EGF exposure at a concentration of 0.5 x $10^6$ cells per well. After one day, maintenance medium was exchanged with starvation medium (phenol red-free, glutamine-free, serum-free DMEM) for 24 hrs. One hour prior to EGF exposure, cells were treated with erlotinib. Erlotinib stocks (10 mM in DMSO) were serially diluted in starvation medium at different concentrations (10 µM, 1 µM, 300 nM, 100 nM, 10 nM). Medium was exchanged with fresh starvation medium in untreated control samples. EGF stocks (R&D systems, 20 µg/ml in PBS) were freshly diluted in starvation medium at a concentration of 10 ng/ml. Cells were treated with EGF, then harvested at different time points (0, 5, 10, 20 minutes) and analysed via immunoblotting.

b. Human pancreatic ductal adenocarcinoma cell lines - SU.86.86

Wild-type SU.86.86 cells were seeded in 6-well plates (CytoOne) two days prior to EGF exposure at a concentration of 0.3 x $10^6$ cells per well. After one day, cells were transfected with pCMV6-AC-GFP-CBLC or pCMV6-AC-GFP constructs. X-treme Gene 9 (Roche) was used as transfection reagent according to the manufacturer's protocol. After 24 hours, maintenance medium was exchanged with starvation medium (glutamine-free, serum-free RPMI1640) for 6 hrs. One hour prior to EGF exposure, cells were treated with erlotinib.

Erlotinib stocks (10 mM in DMSO) were serially diluted in starvation medium at different concentrations (10 µM, 1 µM, 300 nM, 100 nM, 10 nM). The medium was exchanged with fresh starvation medium in the untreated control sample. EGF stocks (R&D systems, 20 µg/ml in PBS) were freshly diluted in starvation medium at a concentration of 10 ng/ml. Cells were treated with EGF and harvested at different time points (0, 10, 20, 60 minutes) and analysed via immunoblotting.

### *2.2.1.5 Immunoblotting analysis*

Cells were harvested with ice-cold lysis buffer (150 mM NaCl (58,44 g/mol), 10 mM Tris base (121.14 g/mol), 1 mM EDTA (292,24 g/mol), 0.5% NP-40, Protease Inhibitor (cOmplete – Roche)), mixed with sample buffer (BioRad) and cooked at 95°C, followed by protein separation by SDS-PAGE. Proteins were then transferred onto a Polyvinylidenfluorid (PVDF) membrane (transfer buffer: 10% ethanol, 25mM Tris, 192 mM Glycine, 2lt, 1x) and the membrane was blocked using 2% BSA (Sigma) in TBS-T.

Seven proteins in the phosphorylated or non-phosphorylated form (pErk, Erk, pAkt, Akt, pEGFR, EGFR, and pSrc, Src and CBLc) were quantified in four time points (0, 5, 10, 20 minutes) in SU.86.86 cells. Four proteins (pErk, pAkt, pEGFR and pSrc) were quantified in four time points (0, 5, 10, 20 minutes) for treated and untreated HeLa (wt or stably expressing CBLc) cells. Four proteins (pErk, pAkt, pEGFR and pSrc) were quantified in four time points (0, 10, 20, 60 minutes) for treated and untreated SU.86.86 (wt or transiently expressing CBLc) cells.

Primary antibodies were diluted in 2% BSA in TBS-T and applied for one hour or overnight, followed by incubation with a secondary anti-mouse IgG or anti-rabbit IgG for one hour. A list of antibodies and corresponding dilutions is shown in **table 2**.

Chemiluminescence was detected using the SuperSignal® West Pico Chemiluminescent Substrate (Thermo Scientific) and the ChemoCam Imager (Intas) or Azure biosystems 400.

### *2.2.1.6 Immunoprecipitation of EGFR complexes in PDAC cells*

Wild-type HeLa cells were seeded in 100x17 Petri dishes (Nunc - ThermoFisher) two days prior to EGF exposure at a concentration of 1.5 x $10^6$ cells per dish. After one day, cells were co-transfected with pcDNA5-FRT-TO-GRB2-GFP plasmid (Addgene plasmid #86873) and pCMV6-AC-GFP-CBLC or pCMV6-AC-GFP constructs. Lipofectamine 2000 (ThermoFisher) was used as transfection reagent according to the manufacturer's protocol. After 24 hours, maintenance medium was exchanged with starvation medium (glutamine-free, serum-free DMEM) for six hours. EGF stocks (R&D systems, 20 µg/ml in PBS) were freshly diluted in starvation medium at a concentration of 10 ng/ml and cells were treated for 15 minutes, then harvested with lysis buffer (150 mM NaCl (58,44 g/mol), 10 mM Tris base (121.14 g/mol), 1 mM EDTA (292,24 g/mol), 0.05% NP-40, Protease Inhibitor (cOmplete

– Roche), phosphatase inhibitor (Halt - ThermoFisher). Lysates were incubated overnight with 2 µl of EGFR antibody. On the following day, lysate-antibody mixtures were incubated for 30 minutes with magnetic beads (ThermoFisher). After incubation, beads-antigen complexes were washed with ice-cold lysis buffer for three times, then mixed with 2x Laemmli sample buffer and cooked at 95°C. Immunoprecipitated complexes were then analysed via immunoblotting.

| Protein | Supplier | Order number | Concentration |
|---|---|---|---|
| pErk | Cell Signaling | 4377 | 1:2000 |
| Total Erk | Cell Signaling | 4695 | 1:2000 |
| pAkt | Cell Signaling | 4060 | 1:2000 |
| Total Akt | Cell Signaling | 4691 | 1:2000 |
| pEGFR | Abcam | Ab32430 | 1:2000 |
| Total EGFR | Abcam | Ab52894 | 1:2000 |
| pSrc | Cell Signaling | 6943 | 1:2000 |
| Total Src | Cell Signaling | 2102 | 1:2000 |
| Vinculin | Abcam | Ab129002 | 1:2000 |
| GAPDH | Abcam | Ab9484 | 1:2000 |
| GRB2 | Abcam | Ab111031 | 1:2000 |
| CBLc | Origene | TA505052 | 1:1000 |
| Anti-rabbit IgG | Cell Signaling | 7074 | 1:10000 |
| Anti-mouse IgG | Novex | A15975 | 1:10000 |
| VeriBlot for IP | Abcam | Ab131366 | 1:5000 |

***Table 2:*** *List of primary and secondary antibodies used in the immunoblotting analysis. VeriBlot for IP refers to a secondary antibody specific to detect immunoprecipitated target protein bands, without interference from denatured IgG.*

### *2.2.1.7 GRB2-GFP transient transfection for GRB2 recruitment analysis*

HeLa cells were seeded in 8-well borosilicate glass-bottom dishes (Nunc - ThermoFisher) at a concentration of $2x10^4$ cells per well. The following day, transfection was performed using Lipofectamine 2000 (Invitrogen) according to the manufacturer's instruction and 200 ng of total DNA (pcDNA5-FRT-TO-GRB2-GFP - Addgene) per well. After 24hrs transfection, microscopy imaging was performed.

### *2.2.1.8 Confocal laser scanning microscopy and GRB2 recruitment*

Confocal laser scanning microscopy was performed using a Nikon C2 Plus point scanning confocal microscope system, equipped with automated temperature (37°) and $CO_2$ (5%) control, 2 laser lines (488 and 640 nm) and a Nikon Apo λS 60x (NA 1.40) objective with oil immersion (working distance 0.14mm). Cells were focused using the bright-field channel to avoid premature bleaching of fluorescent signals. Rectangular ROIs were selected for each condition, based on cell density in wells. Prior to scanning, cells were starved for 4 hours. Selected ROIs were initially imaged before EGF treatment. Alexa Fluor 647 conjugated-EGF (ThermoFisher) was diluted to a concentration of 200 ng/ml in starvation medium and further diluted 1:2 in each well. ROIs were then imaged every 2 minutes for up to 20 minutes during EGF exposure. ROIs were sequentially scanned for GRB2 expression (488 nm laser beam, 527 nm W55 filter, 19% laser power intensity, 200 ms exposure) and EGF (640 nm laser beam, dual-pass filter 485/60 and 705/90, 30% laser power intensity, 500 ms exposure). The camera sensitivity was set to 50.

### *2.2.1.9 Dose-response viability assay in HeLa cells treated with paclitaxel*

HeLa cells (wt and stably CBLc-overexpressing) were seeded in 96-well plates at a density of $10^4$ cells per well and grown for 24 hours. On the following day, cells were treated in triplicates with serial dilutions of paclitaxel ($10^{-3}$, $10^{-2}$, $10^{-1}$, 1, 3.3, 10 and 100 μM). DMSO controls for each drug concentration and untreated controls were included. To test for drug response, CellTiter Glo3D (Promega) was used after 48 hrs of drug exposure according to the manufacturer's guidelines. Luminescence was recorded with an Infinite 200 plate reader with 500 ms exposure. Data were fitted with custom codes in Matlab, using Hill-type equation in the form:

$$f(C) = (1 - f_0)\frac{1 - C^h}{\left({K_D}^h + C^h\right)} + f_0$$

where C is the drug concentration, $f_0$ is the background viability, $K_D$ is the concentration related to half-maximal viability, and h is the Hill coefficient.

## *2.2.2 Computational analysis*

### *2.2.2.1 ODE model of MAPK and PI3K pathways*

An ordinary differential equations (ODE) model of the MAPK pathway, its crosstalk with the PI3K/Akt pathway and Src activation was created to describe the recorded experimental dataset for EGFR activation, formation of active EGFR complexes with CBLc, and GRB2-associated-binding protein 1 (GAB1), as well as pathways activation in presence or absence of EGF and erlotinib treatments.

Four model variants were tested to verify two main hypotheses. First, two model variants were created including or not CBLc as a scaffold in signalosomes and an activator of downstream proteins (Ras and PI3K). Then these two variants were extended to test the hypothesis by Hong et al. [36] that CBLc expression leads to reduced EGFR degradation.

Each model describes interactions of 33 species, consists of 49 reactions, and contains 120 parameters (**fig. 5**; **table 7** in the appendix). All ODE models were implemented and fitted using the Matlab toolbox PottersWheel [91]. Model equations are available in **table 6** in the appendix. Model selection was based on the $\chi^2$ goodness of fit test performed on the best fits out of 1500 fitting iterations.

The model was fitted simultaneously to three datasets, derived from different immunoblotting experiments on wild-type (wt) SU.86.86 PDAC cells and wt HeLa cells, three CBLc-overexpressing SU.86.86 cell clones and one CBLc-overexpressing HeLa clone. To consider cell-specific dynamics, different initial protein concentration for HeLa and SU.86.86 cells were defined. At the same time, the comparable dynamics of cell activation were assumed, i.e. the same parameter sets were considered for the three cell lines. In the investigation, experiments were performed on both stably and transiently transfected SU.86.86 cells. Since one can expect pathway dynamics to be similar in CBLc-expressing SU.86.86 originating from the same wild-type batch and transfected with the same protocol, the same error model was used for transiently and stably transfected SU.86.86 cells to overcome the lack of replicates of the dataset collected by our collaborators in presence of erlotinib. The equation for the error model reads

$$f(y) = m_1 * y + m_2 * \max(y)$$

Where y represents the protein concentration, and m1 and m2 are available in the **table 3**.

| **Protein** | **$m_1$** | **$m_2$** |
|---|---|---|
| EGFR | 0.22 | 0.09 |
| Src | 0.23 | 0.1 |
| Akt | 0.18 | 0.03 |
| Erk | 0.21 | 0.53 |

***Table 3:*** *Parameters of error model used for data collected from stably transfected SU.86.86 cells and estimated from transiently transfected SU.86.86 cells.*

### *2.2.2.2 Statistical analysis*

All data are shown as the mean ± standard deviation (SD) or standard error of the mean (SEM) of three independent experiments (4 experiments were performed only on time-course data extracted from SU.86.86 cells). IC50 values were obtained using Matlab by fitting dose-response data of SU.86.86 or HeLa cells with a Hill function in the form of

$$f(C) = A * \frac{{K_D}^h}{\left({K_D}^h + C^h\right)}$$

Where A is the amplitude of the function, C is the drug concentration, $K_D$ is the drug concentration causing half-maximal death rate and h is the Hill coefficient.

Statistical significance of dose-response data collected from HeLa cells treated with paclitaxel was analysed with a two-sample t-test (ttest2 function, Matlab) with a significance threshold of 0.05.

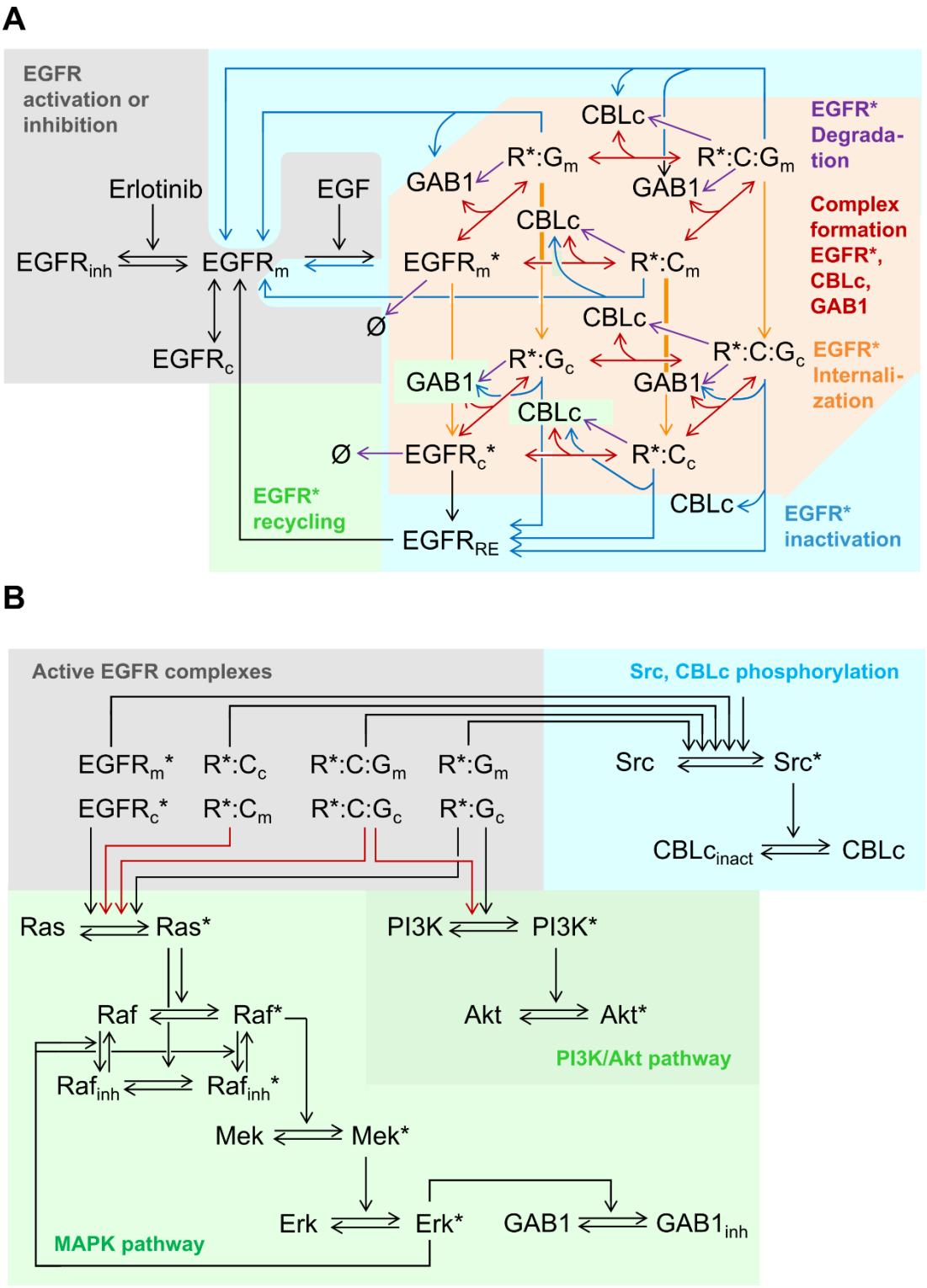


*Figure 5: ODE model of MAPK and PI3K signalling pathways. **A.** Reactions at the membrane level of the model describe the activation of EGFR, the inhibition of EGFR by erlotinib, the formation of protein complexes comprising EGFR, CBLc and adaptor protein GAB1, the internalization of EGFR, along with receptor inactivation, degradation, and recycling. **B.** Part of the model describing the MAPK and PI3K/Akt pathways and the propagation of the membrane signal to reach downstream effectors Erk and Akt.*

## 2.3 Results and discussion

### 2.3.1 CBLc expression is associated with longer survival of PDAC patients

CBLc was described as negative regulator of EGF receptors in membrane signalosomes due to its activity as an E3 ubiquitin ligase [92], [93], which leads to EGFR internalization and inactivation. This enzyme has clinical relevance as a potential tumour suppressor because it inhibits the activation of proliferation pathways. To test whether CBLc has an impact on tumour survival, a Kaplan-Meier analysis was performed at the Department of Surgery based on data collected from a pool of PDAC patients, after an initial selection of tumours expressing or not expressing CBLc. Survival was evaluated in a sample of 39 PDAC patients (26 CBLc positive, 13 CBLc negative) within 36 months. Significantly different survival distributions between CBLc-expressing and non-expressing samples were observed (log-rank test p-value = 0.033).

Consistent with the role of CBLc as a negative regulator of EGFR and inhibitor of the activation of proliferation pathways, the Kaplan-Meier analysis highlights improved prognosis in CBLc positive patients (dark grey in **Fig. 6**). Although the contribution of other isoforms cannot be ruled out, the prolonged survival of CBLc-positive patients suggests that CBLc might be a prognosis predictor for PDAC; therefore, detection of CBLc in patient tissues might be relevant in the selection of chemotherapy dosage. Also, CBLc might act as a subtype indicator because the Kaplan-Meier curve here presented suggests that heterogeneous tumours with a high fraction of CBLc expressing cells have higher chances of regression under chemotherapy treatment and improved patient survival.

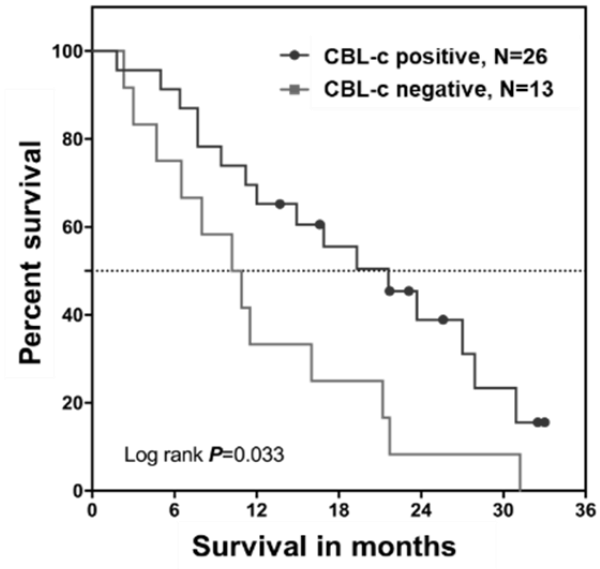


***Figure 6:*** *PDAC patients tissue expressing CBLc shows higher long-term survival. Kaplan-Meier analysis of CBLc positive and negative patients was performed on data recorded over a period of 36 months. Results show increased survival in CBLc-positive compared to CBLc-negative patients. Data provided by Dr. K. Hu.*

### *2.3.2 CBLc reduces erlotinib efficacy on the short-term activity of signalling pathways*

To further investigate the role of CBLc as a subtype marker in pancreatic cancer, the behaviour of two proliferative pathways – namely the MAPK and PI3K/Akt pathways – was tested in established PDAC cells (SU.86.86) exposed to EGF in vitro for 20 minutes (**fig. 7**).

Intuitively, one would assume an inhibition of Erk and Akt phosphorylation due to CBLc overexpression, as also indicated by the more prolonged survival of patients' tissue shown in the Kaplan-Meier analysis. Proteins from the CBL family are involved in tumour progression as inhibitors of EGFR [94], and CBLc as a ubiquitin ligase should induce degradation of active receptor tyrosine kinases and decrease EGFR levels upon stimulation with EGF. However, no changes in the activity of active EGFR were visible in the short time frame of 20 minutes, but rather an anomalous activity of proteins along the MAPK and PI3K/Akt signalling pathways.

Trajectories for EGFR were comparable for wild-type or CBLc-overexpressing SU.86.86 cells, and the expression of active EGFR was reduced by treatment with erlotinib independent of the presence of CBLc. Interestingly, the analysis highlighted that in the presence of erlotinib two downstream proteins, Erk and Akt, are active in CBLc over-expressing clones (in turquoise in **fig. 7**), whereas their expression was strongly reduced by chemotherapeutic treatment in wild-type SU.86.86 cells (in black in **fig. 7**). The residual activity of Erk and Akt seems to be transitory under drug treatment, with a peak between 5 and 10 minutes after EGF treatment followed by a steep decrease and further inactivation after 20 minutes. Untreated SU.86.86 cells instead exhibit a steady activation after 20 minutes in both CBLc-expressing and non-expressing cells, suggesting that erlotinib still acts as an inhibitor on the protein network but might be temporarily compensated by the activity of CBLc. This evidence seems in contrast to the Kaplan-Meier analysis and suggests an activating role for CBLc on the timescale of 20 minutes, causing an increase in the activity of proteins that control the growth and proliferation of cells. Interestingly, since CBLc does not affect the expression of EGFR and active EGFR, which was not significantly different in the CBLc-expressing clones and wild-type cells, the enhanced activation of the pathways might derive from the presence of CBLc in signalosomes downstream of EGFR.

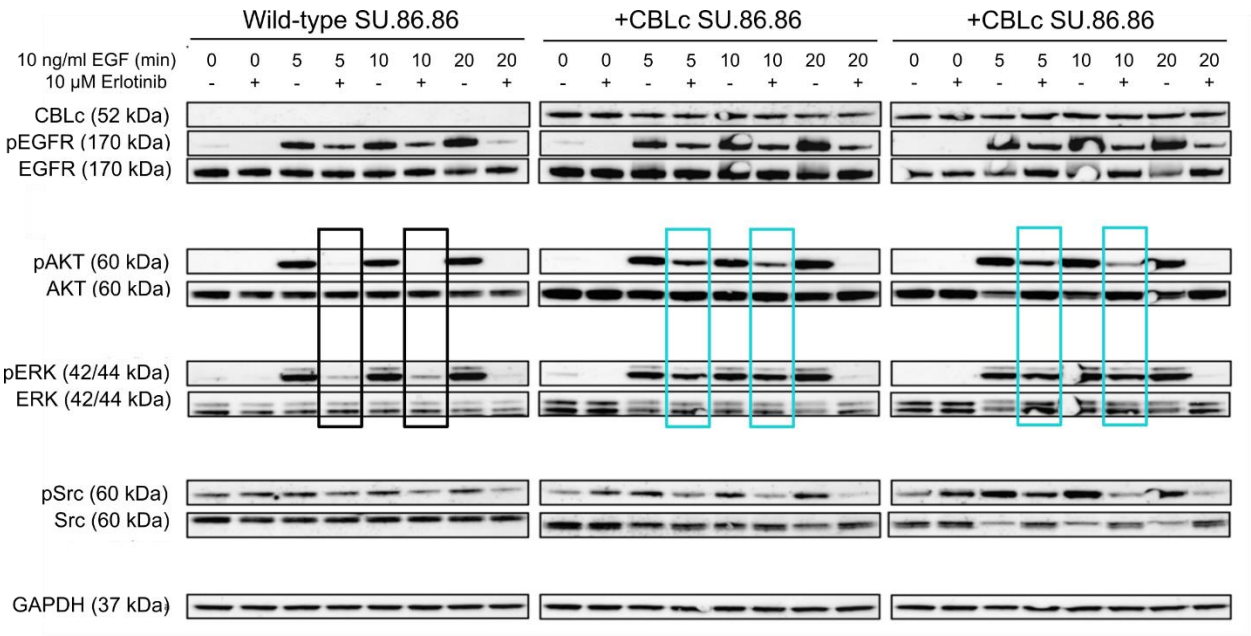


***Figure 7:*** *CBLc leads to drug resistance along the MAPK and PI3K/Akt pathway. SU.86.86 cells wt or stably transfected with CBLc were starved for 4 hours, treated with 10µM erlotinib (or drug-free medium) for 1 hour, then exposed to EGF (10 ng/ml) for up to 20 minutes. Several proteins along the pathways were investigated to observe the effect of CBLc on pathway activation. Erlotinib strongly affects the phosphorylated forms of Akt and Erk (black boxes) and minimizes the activation of the pathways in wt cells. By contrast, CBLc-expressing clones exhibit higher levels of pErk and pAkt in presence of chemotherapy 5 and 10 minutes after EGF exposure (turquoise boxes), suggesting a residual pathway activation. Data provided by Dr. K. Hu.*

### *2.3.3 PDAC and cervix cancer cells expressing CBLc are less sensitive to erlotinib*

The response of the MAPK and PI3K/Akt pathways was tested for different concentrations of erlotinib to investigate if CBLc is responsible for the residual activation of the cancer clones in presence of erlotinib and EGF treatment, as suggested by the experimental data presented in the previous section. Since CBLc is expressed in many epithelial tissues, it might potentially affect the activation dynamics not only in PDAC but rather be a pan-cancer mechanism of resistance. Therefore, an experimental setting was defined for two established cell lines deriving from cervical cancer (HeLa) and pancreatic cancer (SU.86.86) to characterise cancer-specific activation trajectories that can impact the dosing time and efficacy of erlotinib.

To test the response to chemotherapy, it is common practice to observe the toxicity of cells during drug treatment. However, from the experimental analysis presented so far, the role of CBLc in the activation of the MAPK and PI3K pathways seems prevalent on the short time scale of about 60 minutes where cells viability is not affected by chemotherapy, whereas the effect of the drug can modify intracellular mechanisms. Therefore, Erk and Akt phosphorylation were used as *de facto* measurements of the pathway activity in the two cell lines in a drug-response analysis.

To characterise the differences in cells expressing or not CBLc, exposure times related to the peak of activation of pErk and pAkt were selected to detect the maximal difference in the effect of erlotinib on the activation of the pathways. From preliminary tests, it could be observed that the

two cell lines present slightly different activation trajectories and peak times for Erk and Akt after drug exposure. Specifically, in HeLa cells, pAkt activity reaches a peak around 5 minutes after EGF exposure whereas pErk shows higher activity at 10 minutes EGF exposure. At the same time, SU.86.86 cells exposed to chemotherapy show peak activity for both Erk and Akt around 5 minutes after EGF treatment. These time points were therefore used in the analysis (**fig. 8** and **9**).

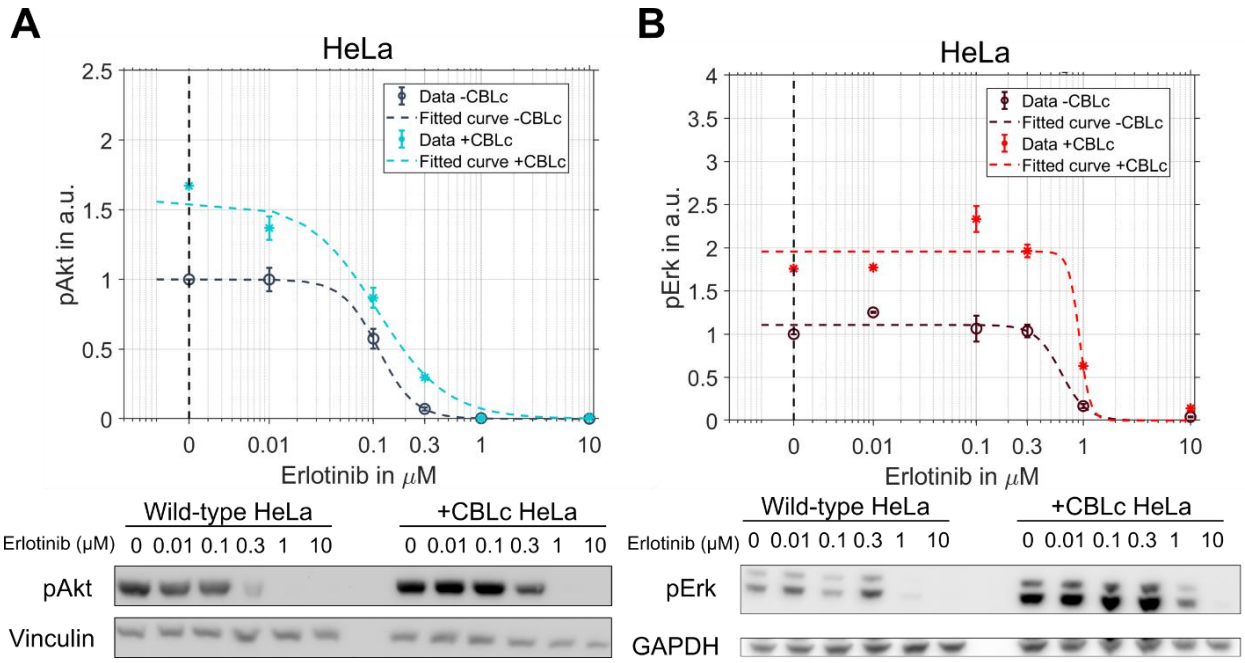


***Figure 8:*** *Dose-response curve of erlotinib-treated HeLa cells.* ***A.*** *(Top) Immunoblotting analysis of pAkt in HeLa cells starved overnight and treated with different concentrations of erlotinib, then exposed to EGF (10 ng/ml) for 5 minutes (means of n = 3 replicates; error bars, S.E.M; samples were normalized to untreated HeLa wt). Results show higher phosphorylation fraction of the PI3K downstream effector Akt in CBLc-expressing cells after 5 minutes EGF exposure. Estimated IC50 values for both cell lines: 0.11 μM for CBLc non-expressing cells, 0.12 μM for CBLc-expressing cells. (Bottom) Example of immunoblotting data collected for the dose-response analysis.* ***B.*** *(Top) Immunoblotting analysis of pErk in HeLa cells starved overnight and treated with different concentrations of erlotinib, then exposed to EGF (10 ng/ml) for 10 minutes (means of n = 3 replicates; error bars, S.E.M; samples were normalized to untreated HeLa wt). CBLc-expressing cells show higher phosphorylation fractions of the MAPK downstream effector Erk after 10 minutes EGF exposure. Estimated IC50 values: 0.9 μM for CBLc-expressing cells, 0.6 μM for CBLc non-expressing cells. (Bottom) Example of immunoblotting data collected for the dose-response analysis.*

The results showed two interesting effects that might potentially impact dosing strategies for cancer treatment of CBLc-expressing tissue.

On the one hand, CBLc overexpression caused a higher phosphorylated fraction of Erk and Akt, in both HeLa and SU.86.86 cells. Hence, although cells were under chemotherapy treatment, the ability to proliferate is potentially higher in clones with high CBLc expression.

In HeLa cells, the fraction of phosphorylation of Akt and Erk was higher in CBLc-expressing cells below the threshold of 1μM erlotinib, where this effect was almost independent of the chemotherapy drug concentration applied to the cells. Over this threshold, the effect of pathway

inactivation by erlotinib could not be compensated by the overexpression of CBLc, and no significant difference was visible. CBLc-expressing HeLa cells treated with less than 1μM erlotinib exhibited ~1.5 to 2-fold higher pAkt and pErk activation than wild-type cells (fig. 8).

Similarly, CBLc-positive SU.86.86 cells expressed pAkt and pErk at higher levels than CBLc-negative cells for every drug concentration used in the analysis. As in the data in fig. 7, SU.86.86 cells pathways were active even in presence of high drug concentration (10 μM), although the ratio between CBLc-expressing and non-expressing cells was lower in pAkt activation than pErk (fig. 9). Potentially this indicates that the MAPK pathway is less affected by erlotinib treatment than the PI3K/Akt one and combining erlotinib with an inhibitor of the MAPK pathway might be more relevant than targeting proteins in the other cascade.

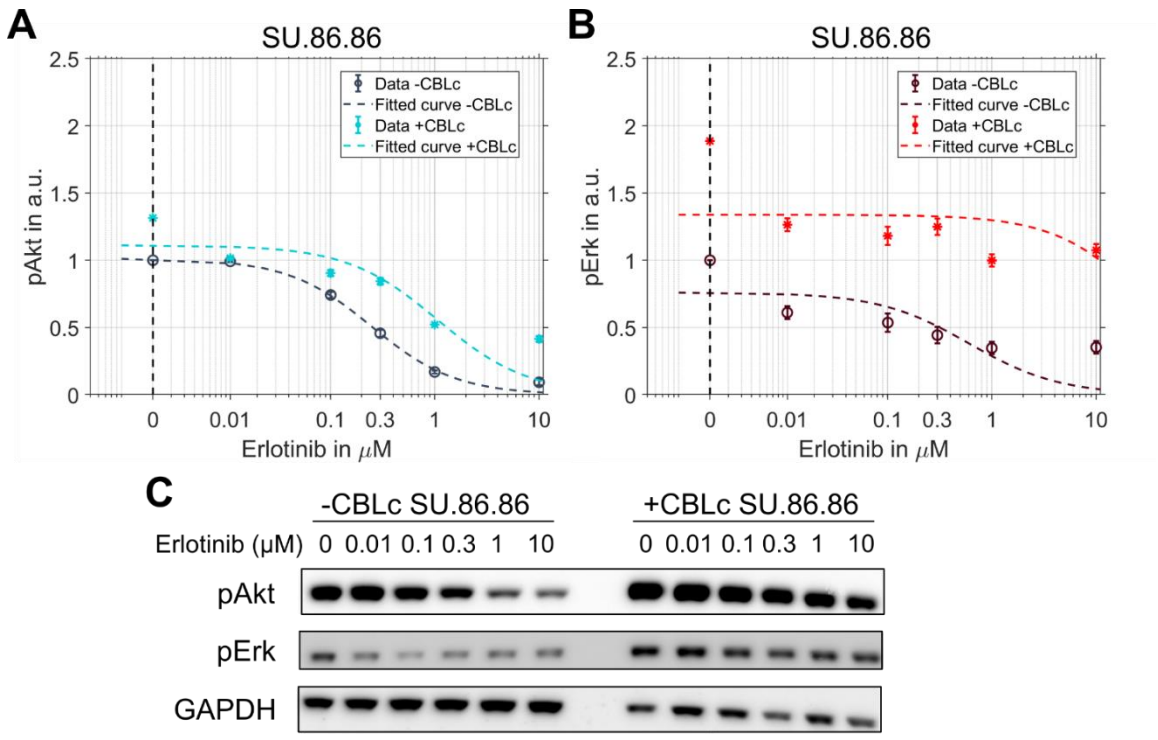


*Figure 9: Dose-response curve of erlotinib-treated SU.86.86 cells.* ***A.*** *Immunoblotting analysis of pAkt in transiently transfected SU.86.86 cells starved for 6 hours and treated with different concentrations of erlotinib, then exposed to EGF (10 ng/ml) for 5 minutes (means of n = 3 replicates; error bars, S.E.M; samples were normalized to untreated CBLc non-expressing SU.86.86). CBLc-expressing cells exhibit higher phosphorylation fractions of the PI3K downstream effector pAkt after 5 minutes EGF exposure. Estimated IC50 values: 0.25 μM for CBLc-expressing cells, 1 μM for CBLc non-expressing cells* ***B.*** *Immunoblotting analysis of pErk in transiently transfected SU.86.86 cells. Same experimental setting as per* ***A****. (means of n = 3 replicates; error bars, S.E.M; samples were normalized to untreated CBLc non-expressing SU.86.86). Results show that CBLc-expressing cells exhibit higher phosphorylation fractions of the MAPK downstream effector pErk after 5 minutes of EGF exposure. Estimated IC50 value: 0.6 μM for CBLc-expressing cells and 32 μM for CBLc non-expressing cells.* ***C.*** *Example of immunoblotting data collected for the dose-response analysis.*

On the other hand, CBLc causes a shift in IC50 values and, therefore, higher resistance to erlotinib. SU.86.86 cells overexpressing CBLc exhibit reduced sensitivity to the activity of the tyrosine kinases

inhibitor for high drug concentrations (10 μM) in comparison to wild-type SU.86.86 cells, in fact, the IC50 value for CBLc-positive cells is significantly increased for pAkt (from 0.25 μM to 1 μM) and more than 10-fold higher for pErk (from 0.6 μM to more than 10 μM). In HeLa cells pAkt is affected by similar drug concentration independent of CBLc (IC50 about 0.1 μM for both cell lines) whereas pErk shows an increase of IC50 values in CBLc-expressing cells (from 0.6 μM to 1 μM). Once again, in both cell lines, resistance to erlotinib seems more prominent in the MAPK than in the PI3K pathway, suggesting a more robust compensation of the network inhibition upstream of pErk than pAkt.

Interestingly, in HeLa cells, the effect of CBLc expression on the IC50 values was minor, whereas amplitudes were increased by 50% and 100% for pAkt and pErk, respectively. By contrast, In SU.86.86 cells the IC50 shift was considerable in both pathways, whereas the overexpression of CBLc caused a limited increase in the amplitude of pAkt and a 2-fold increase in the amplitude of pErk. The different response of the cell types investigated might be due to different abundance of adaptor proteins that modify the dynamics of activation of the pathways. The higher activity of the two downstream proteins might have implications on the transcription of early genes involved in cell fate regulation and cause the anomalous proliferation of cancer subtypes over-expressing CBLc. Thus, the effect of CBLc on proteins peak activity might compensate for the inhibition of EGFR erlotinib by enhancing the cell proliferation and, in turn, cell survival. At the same time, the reduced sensitivity of cells to erlotinib might translate into the necessity for higher doses of TKIs in the treatment of PDAC and cervical cancer subclones that express CBLc and supports the hypothesis that CBLc might be a marker for drug resistance.

### *2.3.4 CBLc amplifies the activation of signalling proteins in MAPK and PI3K/Akt pathways*

The results presented so far suggested an interesting effect of CBLc expression in PDAC drug resistance on the short time frame, in contrast with its established role.

As visible from the untreated samples in **fig. 8** and **9**, CBLc seems to affect the pathway dynamics also in absence of erlotinib. The higher peak of activation of pErk and pAkt in absence of erlotinib might be a potential mechanism of innate resistance and might indicate how cells behave before undergoing any drug-induced modification. Therefore, a time-course analysis was performed to observe the evolution of the MAPK and PI3K/Akt pathways in absence of chemotherapy in HeLa and SU.86.86 cells on four key proteins along the MAPK and PI3K pathways (EGFR, Src, Akt, Erk) in the timeframe of 20 minutes or 1 hour. Specifically, HeLa cells were tested for up to 20 minutes of EGF exposure (**fig. 10**) to compare the dynamics with results observed on PDAC cells, whereas the analysis on SU.86.86 was extended to a longer timescale of 60 minutes EGF treatment (**fig.11**). As

visible in **fig. 7**, in absence of drug treatment the proteins along the pathways were still highly active after 20 minutes EGF exposure.
The analysis showed that the dynamics of activation of the proteins in the pathways are quite different in HeLa and SU.86.86 cells due to cancer-specific regulation of the signalling pathways. On the one hand, Erk and Akt presented similar dynamics in HeLa cells and reached a peak about 5 minutes after EGF exposure, followed by a fast decay. On the other hand, Erk activity in PDAC cells did not decrease but rather increased after 20 minutes of EGF treatment similarly to EGFR, whereas pAkt reached a peak around 10 minutes after EGF treatment followed by a steady state of activation. Interestingly, the timing of activation of all the proteins was comparable between CBLc-expressing and non-expressing cells in both cell lines and was not influenced by the presence of CBLc.

Independent of cell-specific dynamics, the trajectories of activation of pErk and pAkt increase in presence of CBLc compared to the wild-type case both in HeLa and in SU.86.86 cells. The higher activation of downstream effectors of the MAPK and PI3K pathways might lead to changes in cell proliferation patterns and gene transcription influenced by Erk and Akt. It is known that Erk activation is generally pulsatile and heterogeneous, based on a series of fast and repeated peaks which influence the activity of different transcription factors [94], [95] and is often responsible for the tumorigenic behaviour of cells. On the one hand, spike dynamics of Erk with high peaks can lead to the accumulation of transcription factors with rapid degradation kinetics, such as c-Fos and Egr-1, which causes higher rates of early oncogenes transcription. On the other hand, the increased time integral of pErk and pAkt activation can cause the long-term accumulation of transcription factors with slow decay rates, such as Fra-1 (half-life longer than 5 hrs) [36] or FOXO even in presence of moderate pErk and pAkt levels. These mechanisms have relevance in the cell response to drugs since the anomalous transcription of oncogenes impairs the efficacy of chemotherapy and promotes cancer development.

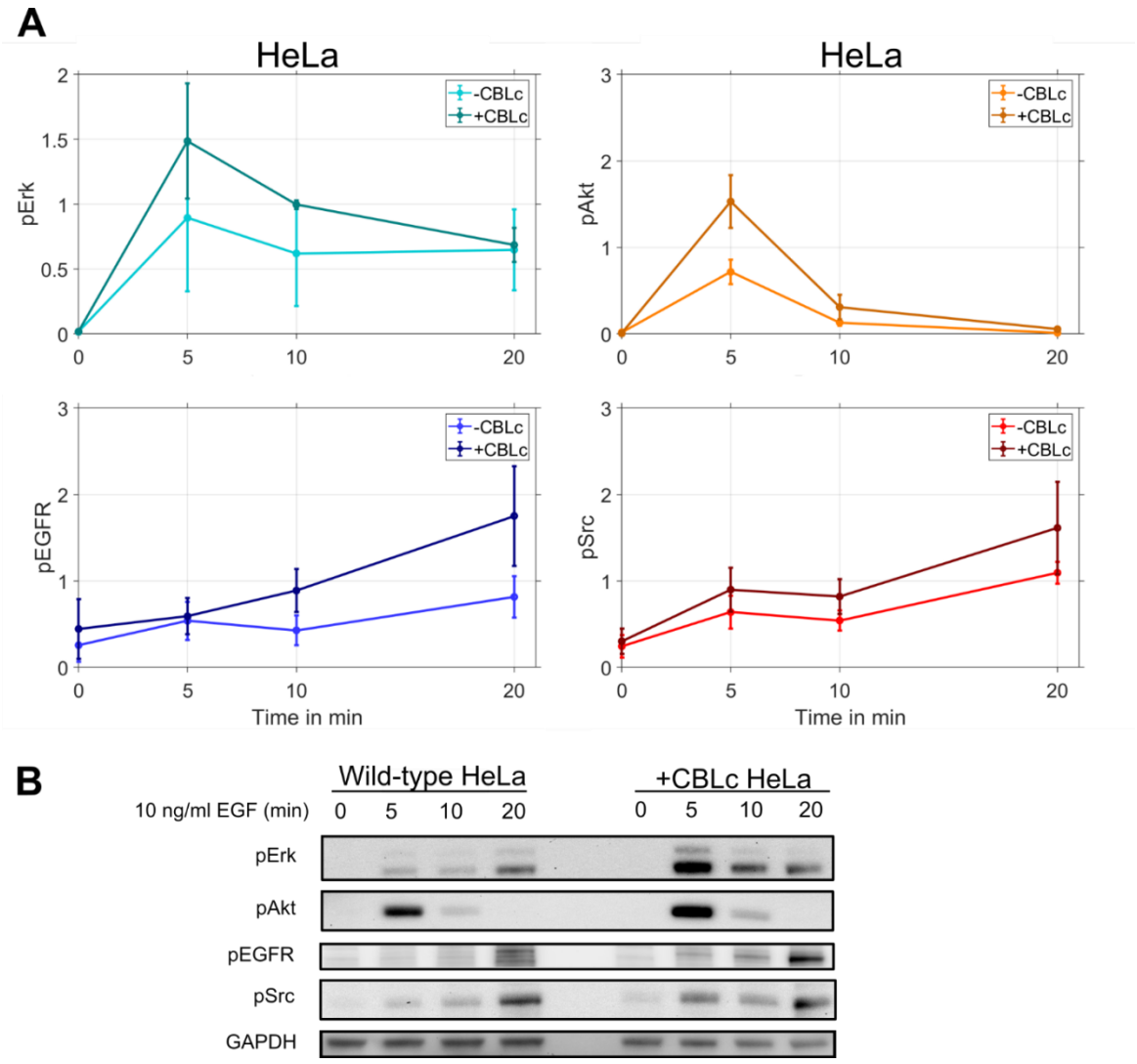


***Figure 10:*** *Time course analysis of MAPK and PI3K/Akt pathway activation in untreated HeLa cells. HeLa cells stably transfected with CBLc or wt were starved overnight, then exposed to EGF (10 ng/ml) for up to 20 minutes. Four proteins along the pathways were investigated to observe the effect of CBLc on pathway activation.* ***A.*** *Phosphorylated forms of Akt, Erk, EGFR and Src were quantified in CBLc-expressing and non-expressing HeLa cells (means of n = 3 replicates; error bars, S.E.; samples were normalized to loading control). The dynamics of all proteins exhibit higher phosphorylated fraction in CBLc-expressing cells, with sustained activation of pEGFR and pSrc 20 minutes after EGF exposure.* ***B.*** *Example of immunoblotting data collected for the time course analysis performed on HeLa cells.*

At the membrane level, the activity of pEGFR is quite different between PDAC and cervical cancer cells. HeLa cells (**fig. 10**) exhibited a marked difference in pEGFR activation around 20 minutes after EGF exposure in CBLc-expressing and non-expressing cells, which might be explained by the novel role proposed for CBLc by Hong et al. [36]. According to this recent publication, CBLc might stabilize active EGF receptors and prolong the half-life of EGFR in Hek293T cells transfected with CBLc by binding to active EGFR and competing with other CBL isoforms, such as c-CBL and CBLb. This way, CBLc would protect EGFR from CBL-controlled ubiquitination and degradation. This hypothesis was tested both via computational and experimental investigation and is further explained in the following paragraph.

In parallel, SU.86.86 cells (**fig. 11**) showed comparable expression of the active EGFR between CBLc-expressing and non-expressing SU.86.86 cells, similarly to the evidence collected in **fig.7**. CBLc did not affect the stability of EGFR and in turn the dynamics of EGFR degradation as a ubiquitin ligase, but instead exerted a function downstream of the membrane receptors short after EGF exposure as an activator of the pathways.

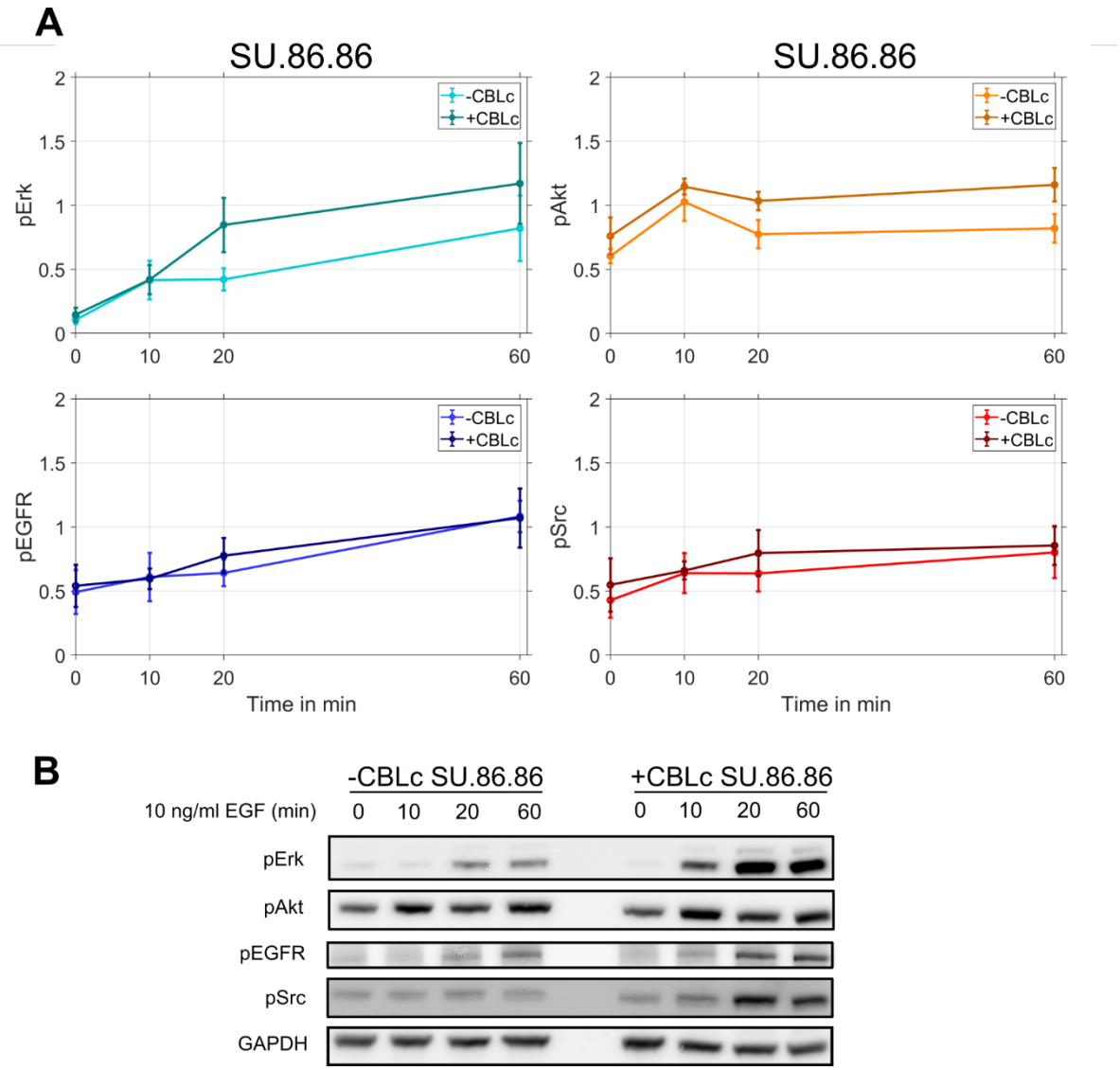


***Figure 11:*** *Time course analysis of MAPK and PI3K/Akt pathway activation in untreated SU.86.86 cells. SU.86.86 cells transiently transfected with CBL-c or empty vector were starved for 6 hours, then exposed to EGF (10 ng/ml) for up to 60 minutes. Four proteins were investigated to observe the effect of CBLc on pathway activation.* ***A.*** *Phosphorylated forms of Akt, Erk, EGFR and Src were quantified in CBLc-expressing and non-expressing SU.86.86 cells (means of n = 4 replicates; error bars, S.E.; samples were normalized to loading control). Although pEGFR is not significantly different at any time point between the two cell lines, downstream proteins show higher phosphorylated fraction in CBLc-expressing cells.* ***B.*** *Example of immunoblotting data collected for the time course analysis performed on SU.86.86 cells.*

### *2.3.5 Mechanistic model of pathways activation suggests a new role for CBLc*

As known for other CBL isoforms, the proline-rich region mediates the interactions of CBLc with a broad spectrum of SH3-containing proteins, such as GRB2, which act as adaptor proteins in EGFR signalosomes. Therefore, the observed activation of Akt and Erk might be explained by the role of CBLc as an adaptor protein on the time scale of one hour rather than its ubiquitin ligase function. To test this hypothesis, a novel ODE model was designed to describe EGFR complex formation with GAB1 (associated with GRB2) and CBLc, as well as protein interactions in the MAPK and PI3K/Akt pathways and their crosstalk.

Different versions of our mathematical framework were initially tested based on previously published models [68], [71], which included quite detailed descriptions of the signal transmission among proteins along the MAPK pathway. Fitting our data with these complex models returned poor goodness of fit, which was not sufficient to consider the model predictions accurate for our datasets. Therefore, the model was simplified, and the number of variables was reduced to essential proteins in EGFR complexes, i.e. EGFR, GAB1, CBLc, and in the MAPK and PI3K/Akt pathways (**fig. 5**). This simplified approach allowed more flexibility to the model, which could be then applied to evaluate some hypotheses on the activity of CBLc.

First, the influence of CBLc was tested on the activity of its main effectors along the pathways, Src, Ras and PI3K, by creating two nested models which differ only for the parameters that represent CBLc as an enhancer of the activity of the pathways. In one of the two versions (Version 2 and 3 in **fig. 12**), these parameters are fixed to 1 (see **table 7** in appendix), whereas in the other (Version 1 and 4 in **fig. 12**) they are estimated in the interval $[10^{-1},10^{2}]$. The estimated values of these parameters indicate whether CBLc serves as an activator of the pathways or if the presence of the enzyme does not modify the downstream dynamics. Second, the two model variants were extended to include reactions that describe the effect of CBLc on EGFR degradation and test the hypothesis by Hong et al. [36] that CBLc reduces the degradation of the receptors.

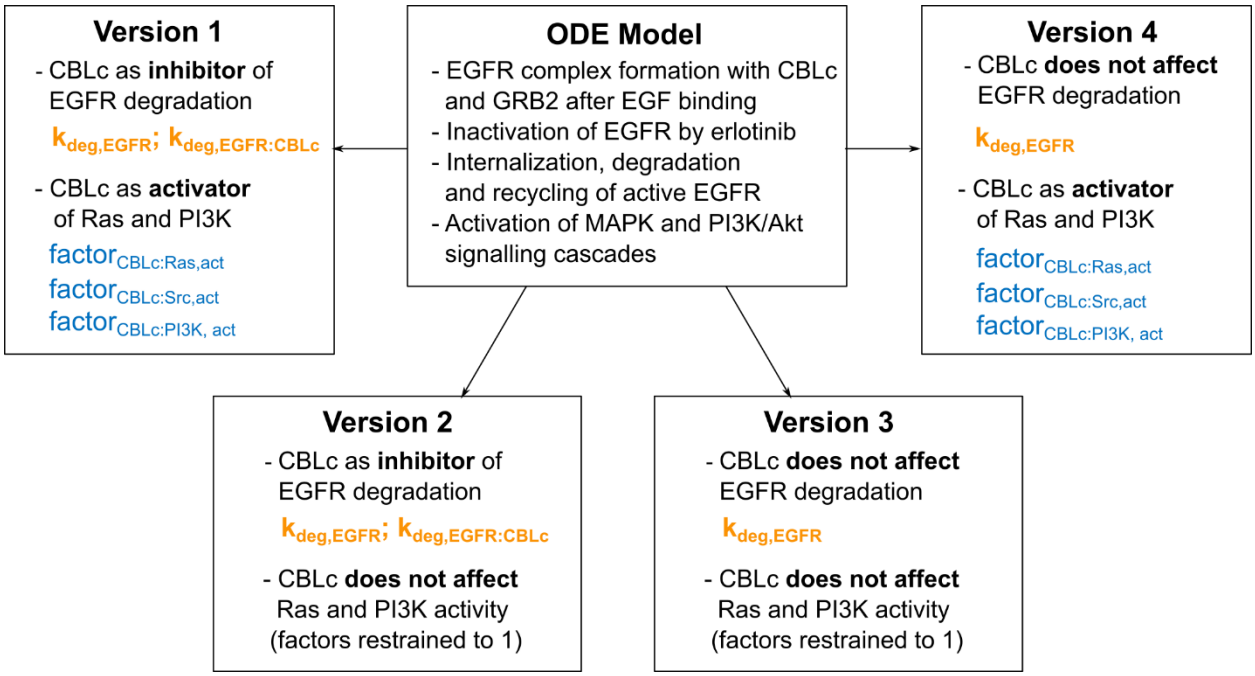


***Figure 12:*** *Versions of MAPK and PI3K/Akt ODE model tested on data collected from SU.86.86 and HeLa cells. Four versions of the main ODE model were defined including or not the assumption that* ***a.*** *CBLc acts as an inhibitor of EGFR degradation;* ***b.*** *CBLc increases the activity of the MAPK and PI3K pathways by enhancing the activity of active Src, active Ras and active PI3K, and in turn of downstream effectors.*

$\chi^2$ values were used to discriminate among the variants and compare the fitting results (**fig.13A**). The model describing CBLc as an activator of the pathways and an inhibitor of EGFR degradation (Version 1, in orange) presented the lowest values of $\chi^2$. According to this version, CBLc should impair the degradation of EGFR, which should translate into an increase in the total level of EGFR in CBLc-expressing cells. Therefore, this hypothesis was tested by investigating whether EGFR levels in HeLa cells are affected by the presence of CBLc on the time scale of 20 minutes of EGF treatment (**fig. 13C-D**) as in [36]. By immunoblotting EGFR, no significant difference was found in protein abundance in HeLa expressing and non-expressing CBLc (two-sample t-test scored a p-value > 0.05, corrected for multiple comparisons) both before and after EGF exposure, suggesting that CBLc does not act on EGFR degradation in this short timeframe. Therefore, the two model variants including the inhibition effect of CBLc on EGFR degradation were neglected.

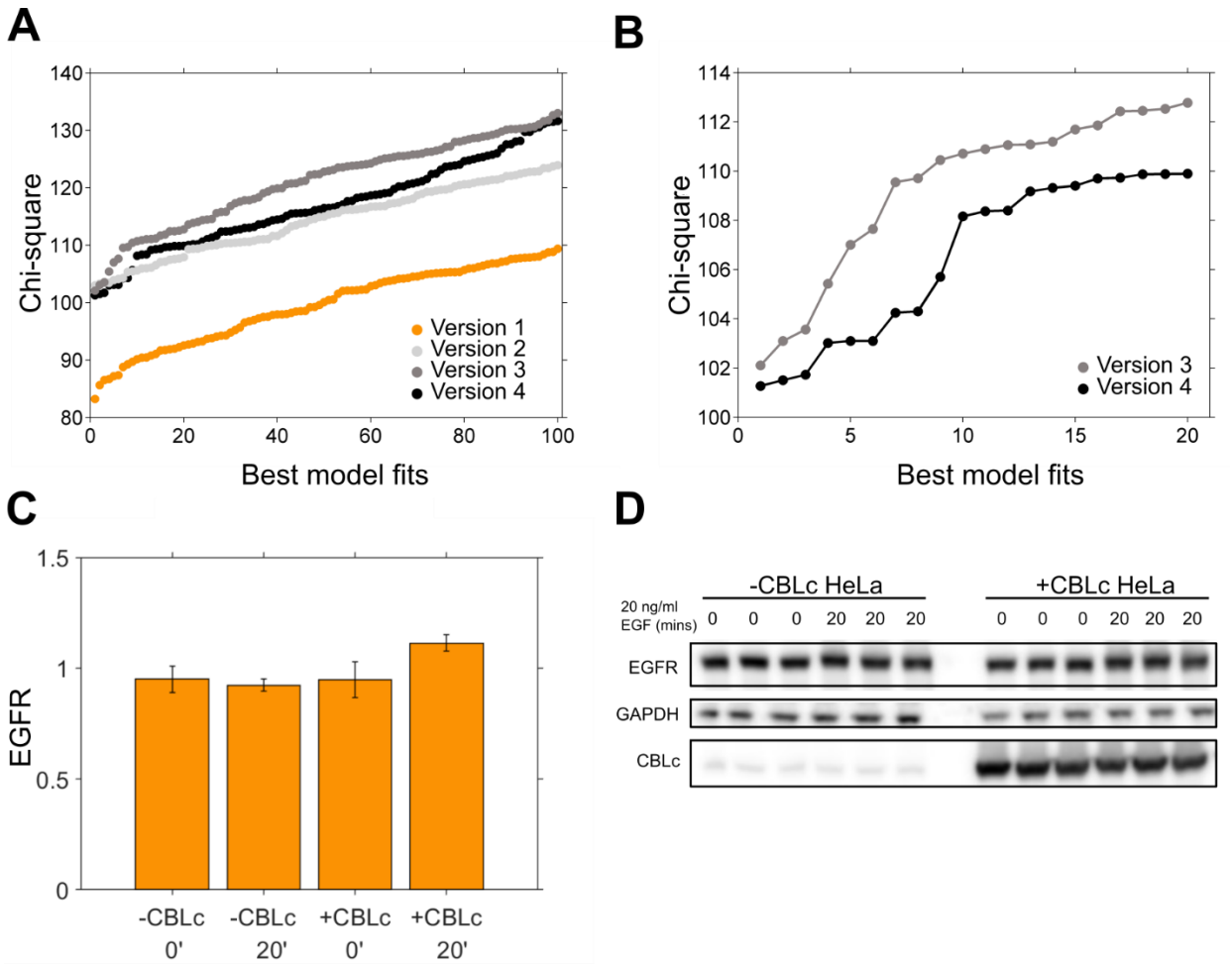


***Figure 13:*** *Optimization of mathematical model describing the role of CBLc in the activation of MAPK and PI3K/Akt pathways.* ***A.*** *Goodness of fit ($\chi^2$) of four model variants, tested on the time course data collected from HeLa and SU.86.86 cells. Best 100 fits out of 1500 are shown.* ***Version 1****, model including CBLc as an inhibitor of EGFR degradation and activator of downstream pathways;* ***Version 2****, model including CBLc as an inhibitor of EGFR degradation but not an activator of downstream pathways;* ***Version 3****, model neither including CBLc as an inhibitor of EGFR degradation nor as an activator of downstream pathways;* ***Version 4****, model not including CBLc as an inhibitor of EGFR degradation but only an activator of downstream pathways.* ***B.*** *Best fits of model variants not including CBLc as an inhibitor of EGFR degradation. Restricting parameters of the activity of CBLc as an enhancer of pathways activity (version 3) impairs model fitting* ***C.*** *Total EGFR expression recorded to test the hypothesis that CBLc inhibits EGFR degradation (means of n = 3 replicates; error bars, S.E.; samples were normalized to loading control). HeLa cells transiently transfected with CBLc or empty vector were starved overnight and exposed to EGF (20 ng/ml) for up to 20 minutes. No significant difference in EGFR levels was recorded between CBLc-expressing and non-expressing cells.* ***D.*** *Immunoblotting data of results presented in* ***C.***

The remaining model versions share most parameters but differ in the activity of CBLc on the activation of the MAPK and PI3K/Akt pathways. Restricting the activity of CBLc (Version 3, **fig. 13B**) impaired the data fitting and increased the $\chi^2$ value of the best fits. To further discriminate between the models, the trajectories estimated with the two variants were evaluated to verify if the activity of the proteins observed experimentally could be described. Although both models could reproduce the increased pathways' activation in presence of CBLc over-expression on the timescale of 60 minutes, the restricted model predicted a peak of activation of EGFR in absence of erlotinib in both cell lines within few minutes from EGF exposure, followed by a substantial decrease (data not

shown). As visible from the dataset of PDAC cells exposed to EGF for 20 minutes (**fig. 7**), in absence of erlotinib EGFR reaches a peak after around 5 minutes followed by a steady-state of activation retained over the timeframe of 20 minutes. Therefore, the model predictions are not realistic compared to the experimental evidence.

Taken together, the model including CBLc as an activator of the pathways (Version 4) proved to be the most accurate in reproducing our experimental data (**fig. 14**). This suggests that CBLc does not exert an activity as a ubiquitin ligase but instead acts as a scaffold in EGFR signalosomes on the timescale of one hour and amplifies signal transmission to downstream effectors.

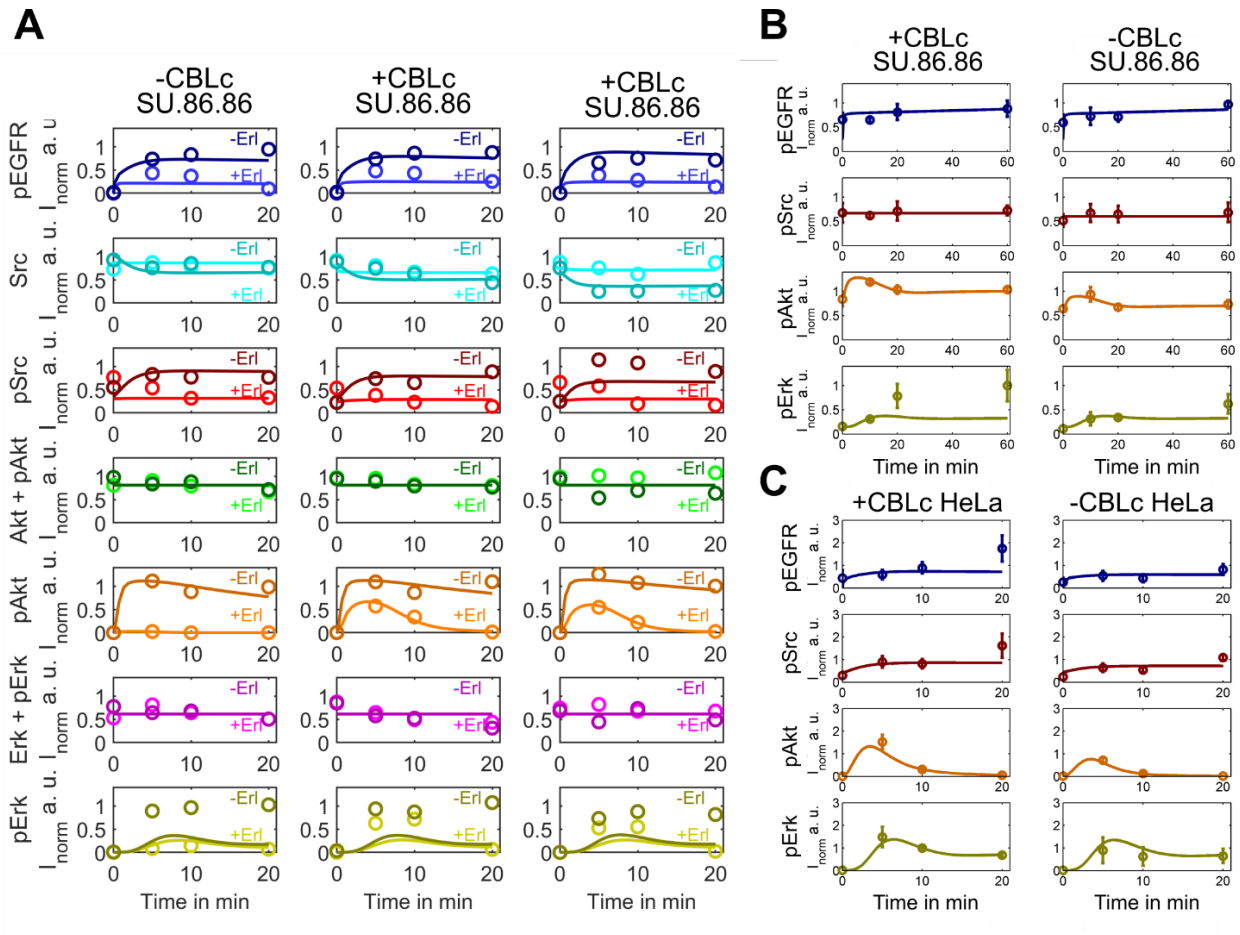


***Figure 14:*** *Time-resolved immunoblot data can be mechanistically explained by the mathematical model.* ***A.*** *Immunoblot data (circles) collected from SU.86.86 cells in presence and absence of erlotinib and model fits (lines) for pEGFR, unphosphorylated Src, pSrc, total Akt (Akt + pAkt), pAkt, total Erk (Erk + pErk) and pErk. (Erl, erlotinib; dark colors, -Erl; light colors +Erk).* ***B.*** *Immunoblot data (circles) collected from SU.86.86 cells in absence of erlotinib and model fits (lines) for pEGFR, pSrc, pAkt and pErk.* ***C.*** *Immunoblot data (circles) collected from HeLa cells in absence of erlotinib and model fits (lines) for pEGFR, pSrc, pAkt and pErk (means of n = 3 replicates; error bars, S.E.; samples are normalized to loading control)*

## *2.3.6 CBLc increases GRB2 recruitment to the membrane*

The experimental evidence collected in this project pointed towards a new and undescribed role for CBLc as an adaptor protein in EGFR complexes. The effect of CBLc in EGFR signalosomes on the

dynamics of signal propagation from the membrane to the nucleus along the MAPK and PI3K cascades was quantitatively described through the computational ODE model presented in the previous paragraph. To verify the hypothesis that CBLc acts as an adaptor for signalling proteins rather than an inhibitor of EGFR, some validation experiments were performed on the activity of CBLc in EGFR signalosomes. Specifically, the association of CBLc with EGFR, the association of CBLc with adaptor proteins in EGFR complexes, and the influence of CBLc on the kinetics of adaptor proteins recruited to the membrane were tested.
Many adaptor proteins contribute to the propagation of EGFR signalling and bind to the receptor in signalosomes, but proteins like CIN85 do not form complexes with CBLc due to its truncated motifs. Therefore, the adaptor protein GRB2 and its interactions with CBLc were investigated, crucial in the internalization of EGFR [34], [37], [66].

First, a microscopy analysis was performed on HeLa cells transiently transfected with GRB2-GFP (**fig. 15**) to observe the basal evolution of GRB2 recruitment. Cells were starved for 6 hours and exposed to fluorophore-complexed growth factor at high concentration to verify if GRB2 migrates from cytosol to membrane and co-localizes with the growth factor.
In the analysis, GRB2 was visible at the membrane level after 8 to 10 minutes of EGF exposure, and EGF and GRB2 co-occurred in vesicles where the fluorescence signals of the two channels overlapped. The concentration of GRB2 attracted to the membrane increased slightly around 12 minutes after adding EGF and reached a steady-state.

To validate the presence of CBLc in membrane signalosomes and the interaction with GRB2, an immunoprecipitation analysis of EGFR and GRB2 complexes was performed.
The formation of EGFR, GRB2 and CBLc complexes in SU.86.86 cells was investigated on the time scale of 10 minutes when, according to the microscopy analysis on HeLa cells, the recruitment of scaffold proteins is already significant. Through the immunoprecipitation of EGFR (**fig. 16A**) the interaction between EGFR and CBLc after starvation was verified. Interestingly, evidence shows the recruitment of CBLc already in absence of EGF, which steadily continues along the treatment with EGF. Next, the interaction between GRB2, EGFR and CBLc was confirmed both in the presence and absence of EGF by immunoprecipitating GRB2 after starvation, before and after EGF exposure. CBLc interacts with GRB2 after starvation, but the expression of CBLc in complex with GRB2 slightly increases when cells are exposed to the growth factors. Importantly, although erlotinib treatment reduces the interaction of GRB2 with EGFR in both wild-type and CBLc-expressing cells, likely due to a lower fraction of active receptors, it does not impair the recruitment of CBLc. This finding suggests that the interaction between GRB2 and CBLc is critical in the signalosomes but is not dependent on the EGFR level, confirming that the effect of CBLc exerts its activity as scaffold in the complex.

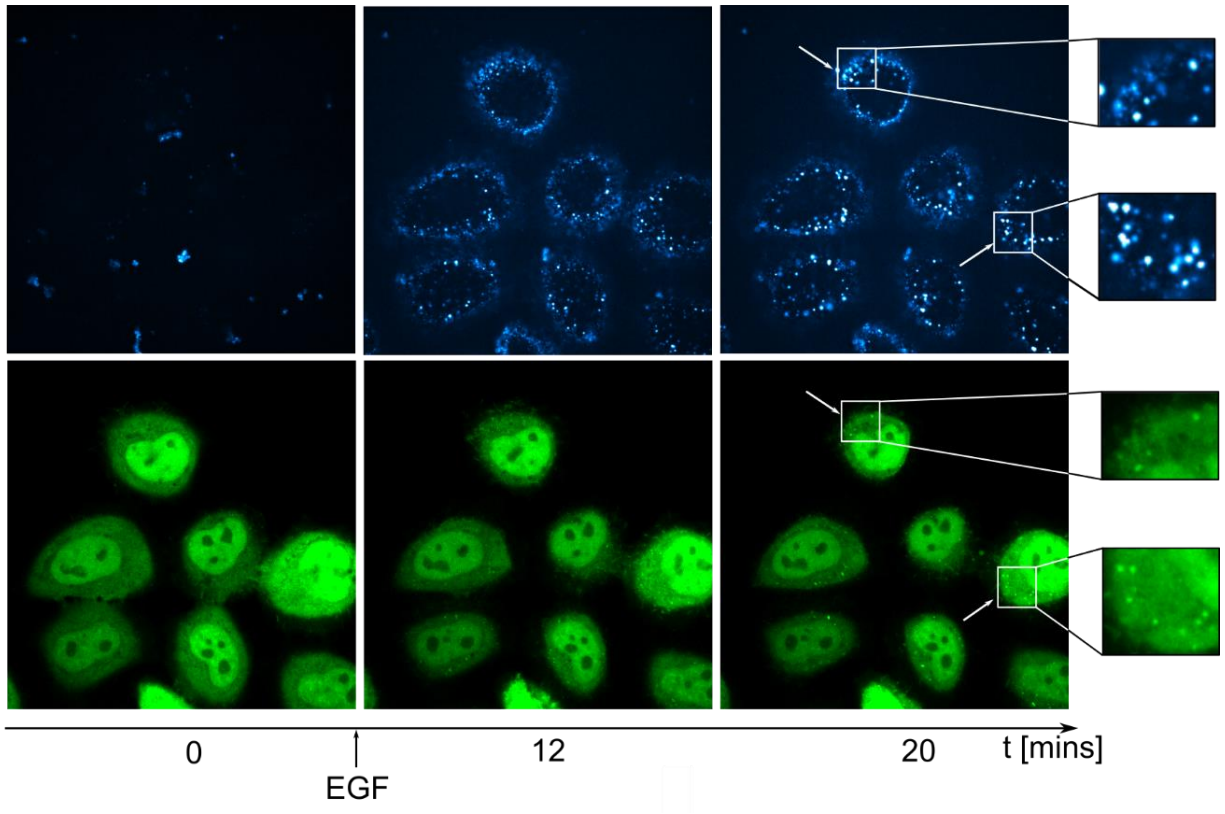


***Figure 15:*** *GRB2 is recruited to the membrane after EGF treatment. Microscopy analysis of GRB2 recruitment in HeLa cells transiently transfected with GRB2-GFP plasmid. After 4 hours of starvation, cells were exposed to EGF-AF647 (100 ng/ml) and analysed with confocal microscopy. GRB2 (in green) and EGF (in blue) channels were imaged before and after treatment with EGF. White arrows highlight the co-localization of GRB2 and EGF in vesicles (visible after 10 minutes of EGF treatment) during GRB2 recruitment to the membrane and EGF internalization.*

Next, the effect of CBLc expression on GRB2 recruitment to EGFR complexes was investigated. After co-transfecting with GRB2 and CBLc and starving HeLa cells, EGFR complexes were extracted before and after treating cells with EGF for 15 minutes (**fig. 16B**). The level of GRB2 in the complexes was quantified to compare differences between CBLc expressing and non-expressing cell lines, considering the untreated samples as the baseline for recruitment. GRB2 appeared in the complex after starvation and in absence of EGF stimuli. The observed recruitment in absence of an external source of growth factors could be due to auto-/paracrine stimulation. Nonetheless, the level of the adaptor protein was about 5-fold higher in CBLc-expressing cells than the cells lacking the enzyme both before and after treatment with EGF, which confirmed that the presence of CBLc influences the dynamics of GRB2 relocation.

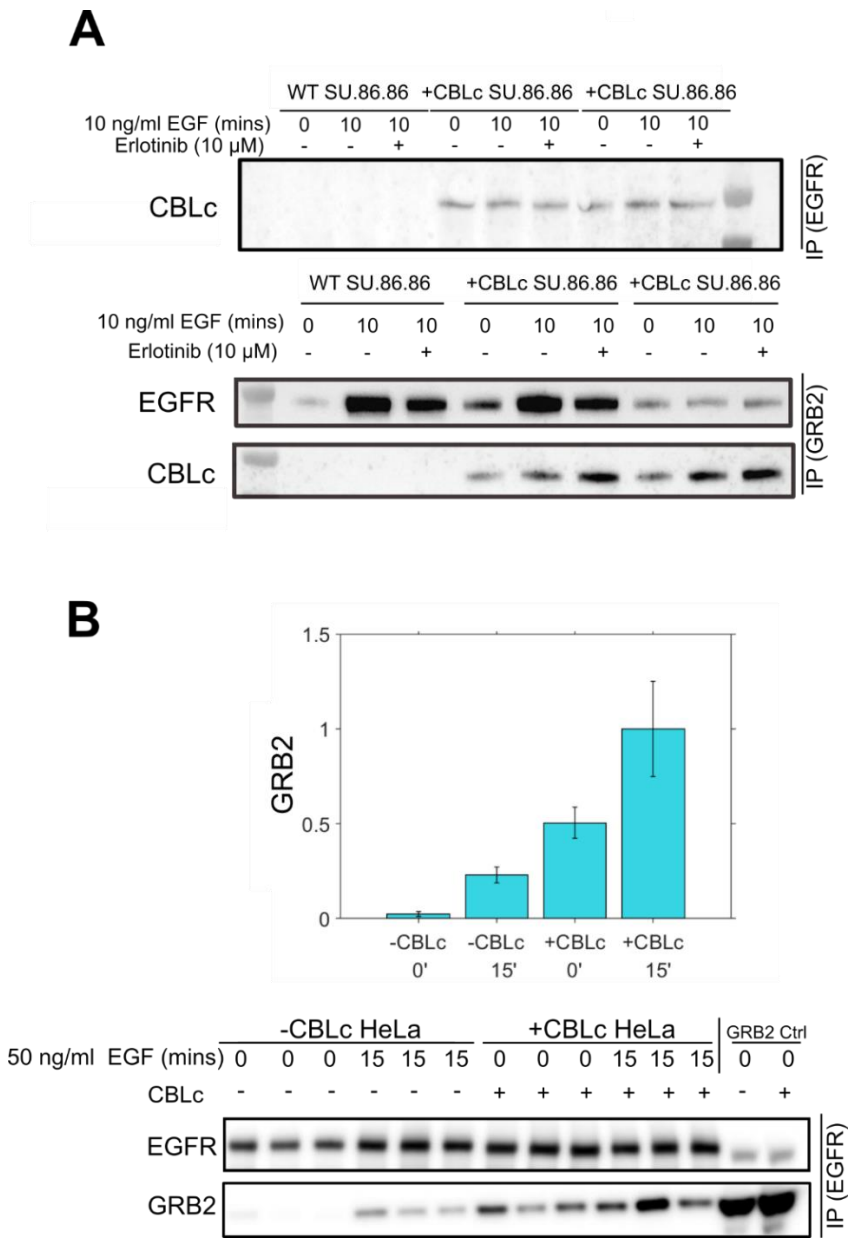


*Figure 16: CBLc interacts with EGFR and recruits higher levels of GRB2 to the membrane* ***A.*** *Cells were exposed to erlotinib or not treated for one hour, and then EGF treatment was performed for 10 minutes. (Top) Immunoprecipitation of EGFR complexes in SU.86.86 cells. Immunoblotting of CBLc confirms that EGFR interacts with CBLc in the presence and absence of erlotinib treatment. (Bottom) Immunoprecipitation of GRB2 complexes in SU.86.86 cells. The immunoblotting analysis confirms the interaction of GRB2 with EGFR and CBLc in the presence and absence of erlotinib.* ***B.*** *(Top) Immunoprecipitation of EGFR complexes in HeLa cells performed in absence of drug treatment before or 15 minutes after EGF treatment (50 ng/ml) (means of n = 3 replicates; error bars, SE; samples were normalized to EGFR). Results show that higher amount of GRB2 is recruited to EGFR complexes in CBLc-expressing cells in both time points. EGFR levels were used as loading control, and GRB2 levels of CBLc-expressing cells exposed to EGF for 15 minutes were used for normalization. (Bottom) Immunoblotting results of the immunoprecipitation analysis of EGFR complexes.*

Overall, these findings confirm that CBLc modifies the dynamics of membrane signalosomes by increasing the recruitment of GRB2 and changing the ratio of membrane receptor to adaptor protein. This way, the signalling potential of the receptor is amplified by the presence of more

adaptor molecules in the complex that transfer the signal of EGFR to downstream proteins and compensate for the activity of chemotherapeutic agents.

### *2.3.7 CBLc-expression is associated with a tendency towards lower paclitaxel sensitivity*

The activation of the MAPK and PI3K/Akt pathways shown in SU.86.86 and HeLa cells expressing CBLc suggests that CBLc might induce higher proliferative activity in the short timeframe of one hour. To prove if the enzyme also exerts a long-term effect on cells viability during drug treatment, a dose-response analysis was performed with paclitaxel, an established drug commonly used in clinical practice for pancreatic cancer patients. Paclitaxel was tested because the combination of paclitaxel and erlotinib is currently under investigation to improve the prognosis of patients with advanced pancreatic cancer [96], so understanding if CBLc interferes with the efficacy of either drug is fundamental.

Since paclitaxel blocks the cell cycle during mitosis, the experiment was performed on the timescale of the duplication rate of HeLa cells expressing or non-expressing CBLc, i.e. 24 hours. Cells were exposed to different concentrations of paclitaxel for up to 48 hours. The residual cell viability was quantified (**fig. 17**), and DMSO was used as control for each drug concentration to exclude the effect of DMSO toxicity. By fitting the data with a Hill function, IC50 values were estimated for the two cell lines, which resulted in a slightly higher value for HeLa cells expressing CBLc (0.01 μM for wild-type cells; 0.02 μM for CBLc-expressing cells). Also, a two-sample t-test confirmed a significant reduction ($p$-value $< 0.05$) in the residual viability of the cells lacking CBLc.

The analysis on HeLa and SU.86.86 cells suggested that CBLc increases cell proliferation by enhancing the activity of pErk and pAkt, and in turn of the transcription factors activated by the two kinases. Consistently, the higher residual viability of CBLc-expressing cells treated with paclitaxel might indicate that CBLc-overexpression confers a survival advantage on the time scale of two days. Although the difference in residual viability observed for almost all drug concentrations is statistically significant, the shift in IC50 value in CBLc-overexpressing HeLa cells is negligible. Therefore, the effect of paclitaxel on CBLc-expressing clones might be reduced due to increased proliferation, but further investigation will be necessary to better characterise the long-term effect of CBLc during chemotherapy treatment.

Taken together, the effect of CBLc on the short time frame of one hour at the molecular level and on the overall survival of HeLa cells in the timeframe of 48 hours suggests that CBLc is a modifier of both the transitory peak amplitude and the steady state behaviour of proteins involved in cell proliferation and drug response.

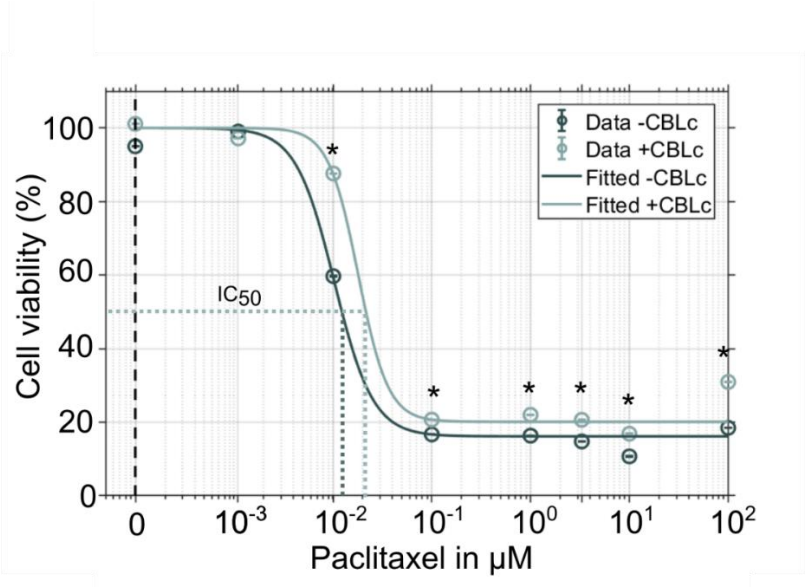


***Figure 17:*** *CBLc reduced the sensitivity to paclitaxel in HeLa cells. HeLa cells (wt and stably CBLc-transfected) were grown for 24 hours, then treated with serial dilutions of paclitaxel (means of n = 3 replicates; error bars, SE; samples were normalized to corresponding DMSO control). Viability was detected with CellTiter Glo3D assay after 48 hrs of drug exposure. CBLc-expressing HeLa cells show higher survival over the timeframe of 48 hours when exposed to the antimitotic drug. IC50 values were obtained by fitting the Hill equation to data (IC50: 0.01 µM for -CBLc HeLa, 0.02 µM for +CBLc HeLa). A two-sample t-test was applied to test mean deviations between the two cell lines (* indicates p-value<0.05).*

# 3. Modeling the protective effect of drug-metabolizing PDAC cells on surrounding cancer cells

## *Contributions*

In this project, I worked in collaboration with Dr. Manuel Reitberger (AG Sprick, DKFZ). Preliminary experimental evidence was collected by Dr. Reitberger. To improve the collection of data, I contributed to developing an automated live-cell imaging microscope [97] which was initially tested on 3D cell cultures grown in the context of this project.

## *3.1 Aim of the study*

The second sub-project of this dissertation focuses on a resistance mechanism related to the expression of drug-metabolizing enzymes in PDAC, which was investigated via computational and experimental analysis.

Recently, Noll et al. [23] described that patient-derived model cell lines of the exocrine-like PDAC subtype heterogeneously express CYP3A5, a member of the Cytochrome P450 (CYP) enzyme family which in physiologic circumstances is expressed in liver cells and is capable of metabolizing toxins and drugs. Post-treatment immunohistochemical stainings of the tumour cross-section indicated that cells strongly overexpressing CYP3A5 are heterogeneously distributed and interspersed with cells without detectable CYP3A5 expression, potentially creating a protective effect over PDAC tissue not expressing CYP3A5. Similarly, the heterogeneous expression of the drug-metabolizing enzyme in 3D cell cultures might result in localized tumour niches that resemble chemotherapy-resistant tumour subregions. To quantitatively study this resistance mechanism, a mathematical model was developed to describe drug response in cell populations and 3-dimensional spheroids heterogeneously expressing CYP3A5 or analogous drug-degrading enzymes. Different modelling strategies were established to characterize the spatio-temporal dynamics of drug resistance and the formation of tumour niches depending on the fraction of cells expressing drug-degrading enzymes. In the future, the developed models might help optimizing experimental strategies to test drug response in PDAC organoids characterised by subtype-specific mechanisms of resistance.

# *3.2 Materials and methods*

## *3.2.1 Experimental analysis*

### *3.2.1.1 Cell lines*

PDAC patient-derived cell lines (PACO) derived from different subtypes (exocrine, classical) were maintained in superior DMEM medium supplemented with a mix developed to avoid cell differentiation of cancer stem cells (recipe not disclosed for commercial reasons).

All cell lines were cultivated in 75cm$^2$ flasks (Corning Primaria) at 37 °C and 5% CO2 in a humidified tissue culture incubator and were passaged when reaching ~70-90% confluency. CO2-independent medium supplied with Glutamine (2mM) and lipid-rich bovine serum albumin (1%) was employed for passaging steps.

Several PACO cell lines were genetically manipulated via Crispr-Cas9 knock-out (see guide RNAs in **table 4**) or adenovirus-based knock-down of CYP3A5 to produce GFP-positive CYP3A5 non-expressing cells and mKate2-positive CYP3A5-overexpressing cells.

| Guide RNA construct name | Sequence |
|---|---|
| KO #1 | GATCACGTCGGGATCTGTGA PAM: TGG |
| KO #2 | CTTCACCAGCGGAAAACTCA PAM: AGG |

***Table 4:*** *Guide RNAs used for CYP3A5 knock-out. Sequences of guide RNAs used to perform two CRISPR-Cas9 based experiments of CYP3A5 knock-out. The guide RNAs were purchased from IDT.*

### *3.2.1.2 3D cell culture*

Different methods for 3D cell culturing were tested (Matrigel, Hydrogel, hanging drop plates), and ultimately ultra-low attachment (ULA) plates (Corning Costar) were selected. Cells were seeded in 96-well ultra-low attachment plates at a concentration of $10^4$ per well (200 µl medium). After seeding cells in ULA plates, PACO10 cells were briefly centrifuged (900 rpm for 3 minutes). PACO2 cells were grown for 24 hours in ULA-plates to form spheroids (round spheres appeared after one day), and the shape and aggregation rates were monitored by bright-field microscopy. PACO10 cells showed a slower aggregation rate and were therefore grown for two days after initial centrifugation. Growth time before treatment was limited to avoid the development of a necrotic core in the spheroids.

### *3.2.1.3 Immunoblotting analysis of CYP3A5 expression*

Several PACO cell lines from the classical and the exocrine-like subtype were tested for CYP3A5 expression levels, namely PACO2 wild-type (wt) and CYP3A5-overexpressing; PACO10 wt, CYP3A5 knock-down (2 clones) and transfected with empty-vector (termed shScrambled, encoding for

scrambled short hairpin (sh)RNAs); PACO3 wt and CYP3A5 knock-down; PACO14 CYP3A5 knock-down. For each line, cells were seeded in triplicates in 6-well plates (CytoOne) at a concentration of 0.1 x $10^5$ cells per well in cell growth medium. One day after seeding, cells were harvested with ice-cold lysis buffer [150 mM NaCl (58,44 g/mol), 10 mM Tris base (121.14 g/mol), 1 mM EDTA (292,24 g/mol), 0.5% NP-40, Protease inhibitor (cOmplete – Roche)], mixed with sample buffer (BioRad) and cooked at 95°C, followed by protein separation by SDS-PAGE. Proteins were then transferred onto a Polyvinylidenfluorid (PVDF) membrane [transfer buffer: 10% ethanol, 25mM Tris, 192 mM Glycine, 2lt, 1x), and the membrane was blocked using 2% BSA (brand) in PBS-T. Primary antibody (CYP3A5 - ab108624 (abcam); GAPDH – ab9484 (abcam)] was diluted in 2% BSA in PBS-T (1:2000) and applied for one hour, followed by incubation with secondary anti-mouse IgG for one hour. Chemiluminescence was detected using the SuperSignal West Pico Chemiluminescent Substrate (Thermo Scientific) and a ChemoCam Imager (Intas).

### *3.2.1.4 Drug treatment of PACO cells*

Drug treatment was performed on PACO10 cells both in 2D and 3D cell culture.

1. PACO10 cells were seeded in 2D in 96-well plates coated for primary cells (Corning Primaria) at a density of $10^4$ cells per well. After 24 hours, cells were treated with paclitaxel (Selleckchem) and erlotinib (LC laboratories) for up to 72 hours. Paclitaxel (10 mM) and erlotinib (10mM) stocks were diluted in medium to double the concentration to test, then further diluted 1:2 by substituting 100 µl of medium from each well with drug-containing medium (final drug concentrations: $10^{-3}$ to 33 µM). Staurosporine (1 µM) was used as positive control, while untreated and DMSO-treated cells were used as negative control. All results were recorded in triplicates.

2. 3-dimensional spheroids grown from PACO10 cells in 96-well ULA plates were treated with paclitaxel (Selleckchem) and erlotinib (LC laboratories) after 2 days of growth. Paclitaxel (10 mM) and erlotinib (10mM) stocks were diluted in medium to double the concentration to test, half medium volume was removed from each well, taking care of not perturbing the spheroids, and exchanged with drug-containing medium (final concentrations: $10^{-3}$ to 33 µM). Staurosporine (1 µM) was used as positive control, while untreated and DMSO-treated cells were used as negative control. All results were recorded in triplicates.

### *3.2.1.5 Cell viability assay*

To test drug sensitivity, CellTiter Glo3D (Promega) was used according to the manufacturer's guidelines after 72 hours of drug treatment on cells grown in 2D and on spheroids. Luminescence was recorded with an Infinite 200 plate reader with 500 ms exposure, and data were analysed with

custom codes in Matlab to perform background removal, data normalization to DMSO control and data averaging.

#### *3.2.1.6 Microscopy analysis*

To reproduce tumour heterogeneity, CYP3A5-positive and -negative PACO10 cells were co-cultured at different ratios (0, 50 or 100% CYP3A5-expressing cells). Spheroid growth and drug response were monitored before and after drug treatment by microscopy imaging using the Nikon Ti-TuCam technology equipped with Nikon S Plan Fluor ELWD 20x NA 0.45 (working distance 8.2 - 6.9mm). Bright-field channel was used to retrieve and focus on the middle section of the spheroid. Z-stacks of 10x10µm images were recorded for GFP, mKate2 and bright-field channels (30% laser power) every 24 hours for up to 144 hours.

### *3.2.2 Computational analysis*

#### *3.2.2.1 Computational workflow for microscopy image analysis*

A Matlab custom workflow was developed to analyse Z-stacks of 10x10µm images recorded in PACO10 spheroids. Images were recorded every 24 or 48 hours for up to 144 hours, before and during drug treatment.

The bioformat function *bfopen* was used to extract images obtained with Nikon Ti-Tucam microscope and available in the nd2 file format . The maximum intensity projection of spheroid voxels along the Z-axis was extracted to preserve the visualization of 3D spheroids from data attenuation and was used for the rest of the analysis.

To observe changes in the number of cells the radius of the spheroid was used as a reference due to the limited resolution of the Ti-Tucam microscope that does not allow the detection of single cells within the spheroid. By knowing the initial number of cells seeded and the diameter of a single cell (~10 µm), any change in the number of cells in the spheroid can be estimated for each time point. By a similar principle, the overall fluorescence level in the GFP and mKate2 channels was recorded to monitor changes in fractions of cells expressing or not expressing CYP3A5 (CYP3A5-positive PACO10 cells express mKate2, while CYP3A5 knock-down cells express GFP).

Due to the irregular shape of PACO10 spheroids, automated detection of the radius could not be performed, and a semi-automated method was established. More specifically a GUI was used to manually detect reference points of the spheroid, namely the centre, the top, bottom, left and right apices of the spheroid. This way, distances of the apices from the centre of the spheroid were computed and the average distance was used as the effective radius of the spheroid.

To extract the total GFP or RFP fluorescence, the area of the circles developing around the central point was computed, and the total fluorescence level in the circle area was extracted. Although

irregular, spheroids show a somewhat spherical section, and a sphere was therefore used as an approximation of their structure.
Finally, total fluorescence data were normalized by the minimum fluorescence level recorded each day. Although microscopy settings were not modified, data recorded on different days can show relative changes in position along the z-axis, which can affect the detected fluorescence and the comparability of the images. Therefore, to display the changes over time, the extracted values for the radius were normalized by the values of untreated spheroids (recorded before treating spheroids with chemotherapy drugs).

### *3.2.2.2 Mathematical modelling of PACO2 populations heterogeneously expressing CYP3A5*

In this thesis, a mathematical framework was developed to investigate the behaviour of cell populations heterogeneously expressing drug-degrading enzymes. As part of the modelling strategy, a computational model was developed describing drug-induced enzyme induction, cell growth inhibition and drug degradation. Model equations are available in **table 5**.
The model was fitted to published data, available in Noll et al. [23], i.e. PACO2 cell viability data obtained from cells exposed to paclitaxel. In the model simulations, the initial number was set to 8000 cells according to the performed experiments; cells were grown for 24 hours and treated for 48 hours.
PACO2 data fitting was performed with four variants of the model including or not enzyme induction for wt cells, to test whether basal CYP3A5 expression influences the dynamics of enzyme induction and drug-dependent growth inhibition and cell death. More details on the development of the models can be found in the results section. Drug concentrations corresponding to half-maximal enzyme induction ($K_E$), cell growth inhibition ($K_I$), and cell death ($K_D$) were defined based on the assumption that sub-lethal drug concentrations lead to enzyme induction and cell growth inhibition, whereas higher drug concentrations cause apoptosis. Therefore, the Hill parameters for cell growth inhibition and death were defined as:

$$K_I = K_E + dK_I$$
$$K_D = K_E + dK_I + dK_D$$

The four variants were fitted to PACO2 data with Matlab custom scripts using the *multistart* strategy, which allows the estimation of multiple local minima in parallel. The estimation problem was solved with the non-linear least square curve fitting method based on the trust-region-reflective algorithm. The optimization was performed by minimizing the distance between the simulated number of cells after 48 hours of drug treatment normalized to the number of cells in untreated cell population and the viability data from PACO2 cells.
Parameter values and intervals of estimation are available in **table 9** in the appendix.

| Equation | Description |
|---|---|
| $\frac{dC}{dt} = \left[ k_g \frac{1}{1+\left(\frac{D}{K_I}\right)^h}\left(1-\frac{C}{K_c}\right) - k_d \frac{\frac{1}{\alpha}+\left(\frac{D}{K_D}\right)^j}{1+\left(\frac{D}{K_D}\right)^j} \right] C$ | Cell number (C) variation dependent on the rate of growth in absence of drug treatment, on drug-induced growth inhibition and cell death. |
| $\frac{dE}{dt} = k_{syn} \frac{\frac{1}{\beta}+\left(\frac{D}{K_E}\right)^l}{1+\left(\frac{D}{K_E}\right)^l} - k_{deg} E$ | Enzyme turnover and induction in presence of drug treatment (D) |
| $\frac{dD}{dt} = -k_r ECD = -\tilde{k}_r \frac{EC}{E_0 C_{max}} D$ | Drug degradation dependent on the expression of the enzyme (E) |

***Table 5:*** *ODE model equations of drug-induced cell growth inhibition, enzyme induction and cell apoptosis. In the model, cell growth inhibition, cell death and enzyme induction are described as sigmoidal curves, respectively characterised by the Hill coefficients $K_I$, $K_D$ and $K_E$. Chemotherapy is degraded at a rate $k_r$ due to the expression of the drug-metabolizing enzyme.*

## *3.3 Results and discussion*

### *3.3.1 Testing patient-derived PDAC cells in 3D cell culture*

CYP3A5 is ectopically expressed in patient-derived PDAC cell lines (PACO) and causes the survival of cancer tissue in mice by degrading established chemotherapeutic drugs [23]. The protective effect of CYP3A5-expressing cells on the surrounding environment in 3D cell culture was investigated to verify if cells surviving drug exposure form resistant tumour niches.

The following criteria were established to select an optimal cell line and the best experimental setting to observe how heterogeneous CYP3A5 expression affects the dynamics of drug response at the tissue level:

1. Cells must be able to grow into 3D structures and the cell culture method must be suitable to monitor cell death and drug diffusion in single spheroids.
2. PDAC cells used in the mixture must show a strong difference in CYP3A5 levels to resemble the heterogeneous environment of PDAC tissues.
3. CYP3A5-expressing and non-expressing cells must express different fluorescent proteins to monitor the evolution of different subtypes separately.

Different systems to grow 3D cell culture were tested on several PDAC cell lines (PACO) previously used in Noll et al.[23]. As in organs, cells can be grown on gels that resemble the extra-cellular matrix (ECM), such as hydrogel and Matrigel. Cells dispersed in the ECM formed small colonies of 3-dimensional spheres stochastically aggregating from CYP3A5-expressing and non-expressing cells. In our setting, the initial cell composition of each spheroid is crucial to track how the drug response changes based on the fraction of CYP3A5-expressing cells. Therefore, this method was discarded in favour of ultra-low attachment microplates, 96-well round-bottomed plates coated with covalently bonded hydrogel that minimizes cell attachment. In ULA plates, cells are kept in a suspended state and forced to aggregate to keep cell-to-cell contact, so they create one single spheroid on the bottom of each well, without any external matrix to support the 3D structure.

Nonetheless, it must be noted that not all cell lines are suitable for this method due to the suspension in which they are forced to aggregate. Several PACO cell lines (PACO2, PACO3, PACO10, PACO14, PACO17, PACO18, PACO43) were tested but only one of them, the classical subtype PACO2, showed significant aggregation into spheres within 24 hours. Most exocrine-like cells did not form spheroids but rather irregular 3D structures and underwent necrosis in the core within few hours from the aggregation of cells. The only exception among the exocrine-like cell lines is the PACO10 line which showed a somewhat intermediate behaviour. These cells did not aggregate into regular spheroids, but when facilitating the aggregation by centrifugation, spheroids formed in 24 to 36 hours and showed almost no necrotic cells in the core within few days.

## 3.3 Results and discussion

Co-culturing of cell lines that exhibit strongly different levels of CYP3A5 was essential to monitor whether CYP3A5 influences drug response in 3D. Therefore, the CYP3A5 expression of several PACO cell lines was tested, including PACO2 and PACO10 cells, provided by our collaborators (**fig. 18A**). Based on Noll et al. [23], exocrine-like cells should express CYP3A5 at the highest level in the wild-type state, whereas the classical subtype should have almost no CYP3A5 enzyme at the basal level. Unfortunately, a residual enzyme expression was visible in several CYP3A5 knock-down lines, which were therefore neglected. Consistent with previous data, CYP3A5 expression was significant in PACO10 cells in the unmodified (wild-type, wt) and the empty-transfection (shScrambled) case. PACO2 wt cells on the other hand presented a higher expression of CYP3A5 than expected. Nonetheless, PACO2 and PACO10 cells were selected due to their capability to form spheroids in ULA plates.

First, the knock-down of CYP3A5 cells was performed in PACO10 with a plasmid containing and shRNA for the enzyme conjugated with GFP expression. In parallel, PACO10 wt cells were transfected with an empty plasmid containing the fluorescent protein mKate2 (**fig. 18B**). This way, two different fluorescent proteins were induced to monitor the evolution of the two clones during chemotherapy treatment. Similarly, the knock-out of CYP3A5 in PACO2 wt cells was performed via CRISPR-Cas9 (**fig. 18C**), followed by the over-expression of CYP3A5.

Once genetically optimized, PACO2 and PACO10 cells were treated with established chemotherapy agents to test their drug response, as described in the following paragraph.

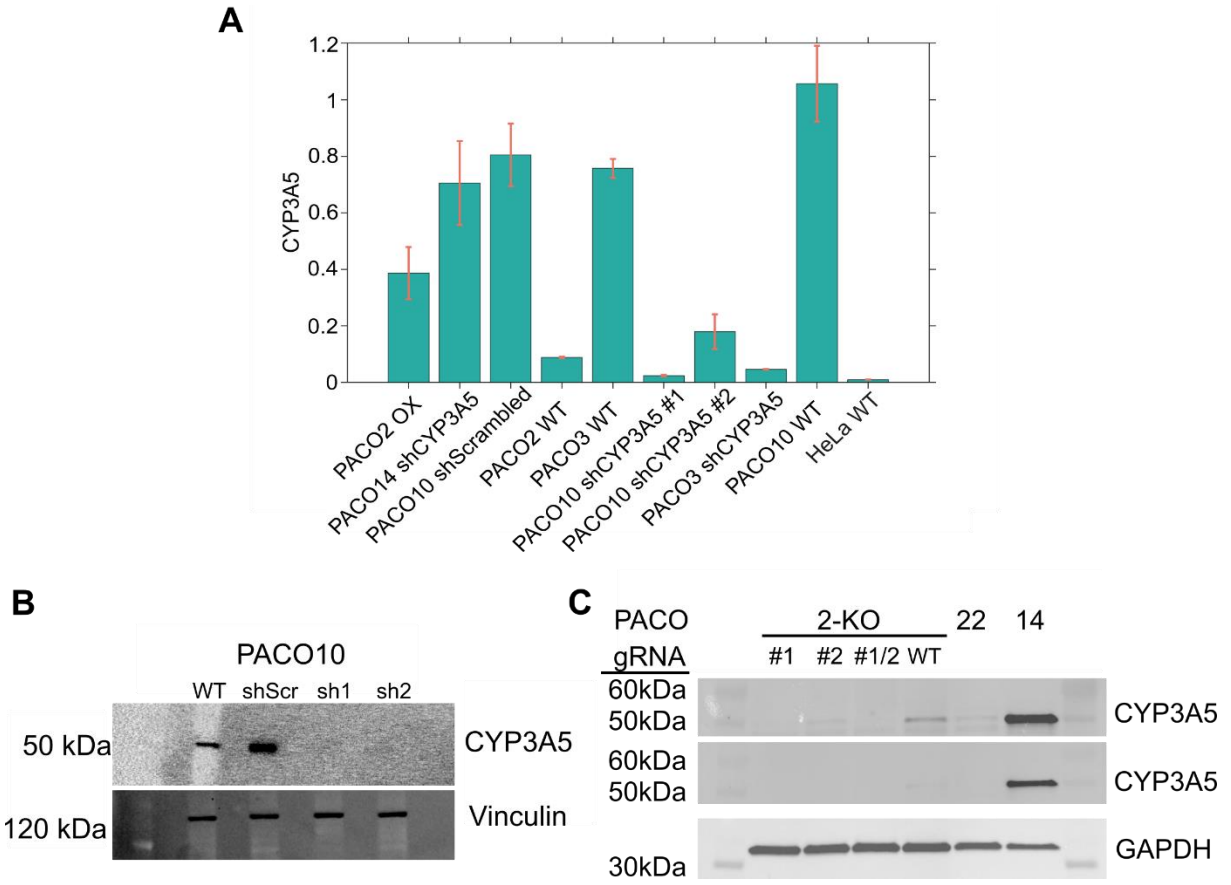


***Figure 18:*** *CYP3A5 expression in different subtypes of patient-derived PDAC cells (PACO).* ***A.*** *CYP3A5 levels were determined in genetically modified PACO2 (classical subtype), PACO3 (exocrine-like subtype), PACO10 (exocrine-like subtype) and PACO14 (exocrine-like subtype) cells from for Noll et al.* [23] *HeLa wt cells were used as a reference. (bars represent means of n=3 replicates; error bars, SE; samples were normalized to loading controls). OX, CYP3A5 overexpressing; shCYP3A5, vector encoding for CYP3A5 short hairpin (sh)RNA; WT, unmodified patient-derived cell line; shScrambled, empty vector encoding for scrambled shRNA.* ***B.*** *CYP3A5 expression of genetically modified PACO10 cells. Two plasmids were tested for CYP3A5 knock-down (sh1 and sh2). Vinculin was used as a loading control. Data provided by Dr. M. Reitberger (WT, unmodified patient-derived cell line; shScr, empty vector encoding for scrambled short hairpin (sh)RNA).* ***C.*** *CYP3A5 expression of genetically modified PACO2 and wt PACO22 and PACO14. Two guide RNAs (#1 and #2) and the combination of the two (#1/2) were used for the knock-out of CYP3A5 with Crispr-Cas9 in PACO2. GAPDH was used as loading control. Data provided by Dr. M. Reitberger.*

## *3.3.2 PACO cells do not benefit from CYP3A5 expression during drug treatment*

To verify the hypothesis that CYP3A5-expressing tumour niches survive drug treatment in 3D cell cultures, a fundamental step was to reproduce the finding that CYP3A5 confers higher drug resistance to cells in 2D.

Therefore, a viability assay was performed on PACO10 cells expressing or non-expressing CYP3A5 separately grown in 2D for 24 hours and exposed to paclitaxel for 72 hours (**fig. 19A**). The time frame was selected based on the observation that PACO10 cells duplicate every 48-72 hours and cytostatic drugs, such as paclitaxel, exert a visible effect on the timescale of the duplication rate. Viability was quantified by using a luminescence-based cell viability assay. In parallel, our

collaborators performed a similar experiment on PACO2 cells (**fig. 19B**). Specifically, four genetically modified PACO2 cell lines – namely CYP3A5-overexpressing (OX), two CYP3A5-knock out (#1 and #2 KO) lines and unmodified wt PACO2 cells – were grown in two-dimensional plates and exposed to paclitaxel for 48 hours. In this case, viability was recorded through a fluorescence-based cell viability assay (CellTiter Blue).

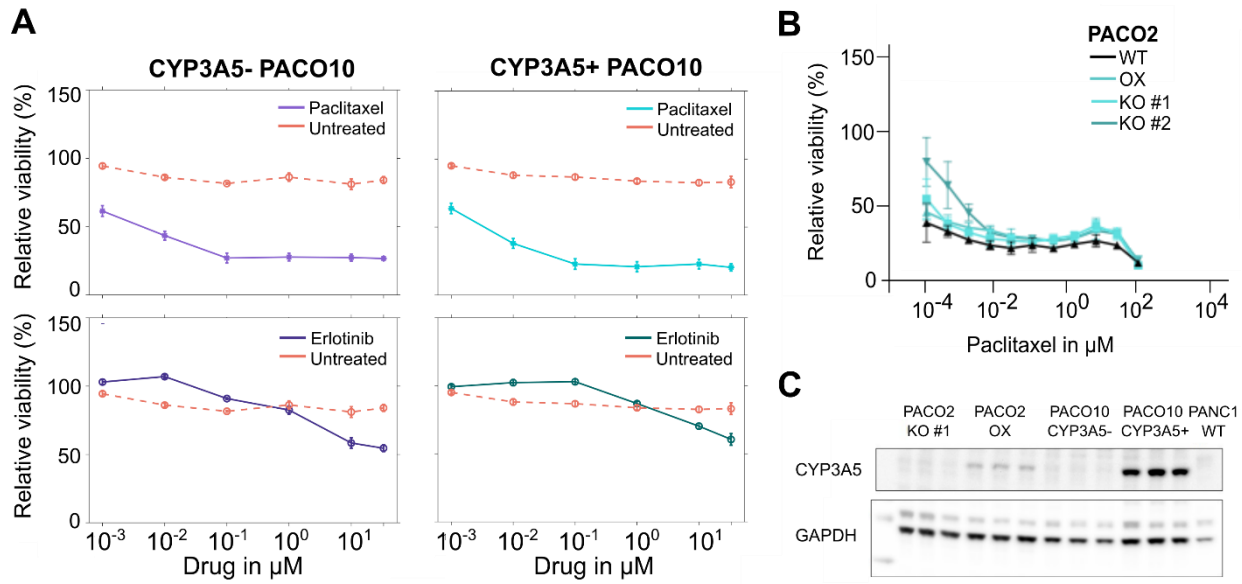


***Figure 19:*** *Drug response of genetically modified PACO cells grown in 2D.* ***A.*** *PACO10 cells non-expressing (left column) or expressing CYP3A5 (right column) were exposed to paclitaxel (top row) or erlotinib (bottom row) for 72 hours (means of n = 3 replicates; error bars, S.E.; samples are normalized DMSO control). Red data points represent untreated cell viability normalized to relative DMSO control. PACO10 cells are highly affected by paclitaxel treatment at low concentrations - independent of CYP3A5 expression - while erlotinib exhibits a weak effect on cell viability.* ***B.*** *PACO2 cells (WT, unmodified cells; OX, CYP3A5 overexpressing; KO, CRISPR-Cas9 knock-outs presented in fig. 18C as #1 and #2) were treated for 48 hours with several concentrations of paclitaxel. No significant difference was detected in cell response to paclitaxel, independent of the expression of CYP3A5. Data provided by Dr. M. Reitberger.* ***C.*** *Immunoblotting analysis of CYP3A5 expression in genetically modified PACO2 and PACO10 cells; PANC1 cells were used as negative control. GAPDH was used as loading control. (KO, Crispr-Cas9 based CYP3A5 knock-out; OX, CYP3A5 overexpression; CYP3A5-, adenovirus-based CYP3A5 knock-down; CYP3A5+, cells transfected with an empty vector).*

While trying to reproduce experiments published in Noll et al. [23], we found deviating results while being in discussion with the group. In contrast with what reported, we could not observe a resistant behaviour in PACO cells expressing CYP3A5 when treated with established chemotherapeutic agents.

The analyses on PACO10 and PACO2 cells share some common evidence in the response to paclitaxel. Independent of the subtype difference, a strong effect of paclitaxel was visible for quite low concentrations ($10^{-3}$ µM) on both CYP3A5-expressing and non-expressing cell lines. Based on what was previously shown, one would have expected a substantial reduction in the viability of

CYP3A5 non-expressing cells compared to the CYP3A5-expressing ones, especially in the case of PACO10 cells that exhibit markedly different expression of CYP3A5 (**fig. 19C**).
The overexpressing PACO2 line presents CYP3A5 at a lower level than PACO10. In this case, the comparable response between enzyme-expressing and non-expressing PACO2 cells could be explained by an insufficient expression of CYP3A5 in the over-expressing line, which cannot contrast the effect of paclitaxel especially for high drug concentrations.
In both cases, the unexpected sensitivity to paclitaxel could be justified by a batch effect of the drug used in our protocol. Further analyses showed that the batch of paclitaxel used for the rounds of testing presented in this thesis affected cells significantly more than in previous results. Also, due to the long storage of the cells in liquid nitrogen, epigenetic or genetic modifications might have occurred when thawing the PACO2 and PACO10 cancer stem cells. Recent studies have suggested that the freezing/thawing cycles of stem cells may affect some cellular processes, such as protein expression and DNA integrity, or their epigenetic profile. This would also explain the unpredicted expression of CYP3A5 in PACO cells which were genetically modified for the publication of Noll et al. [23].

Erlotinib, on the other hand, exerted no effect on PACO10 cells even for high drug concentrations, both in presence and absence of CYP3A5 (**fig. 19A**). As for paclitaxel, one would have expected strong sensitivity to erlotinib only in the PACO cells not expressing CYP3A5, but the drug response was comparable in the two conditions.
It remains unclear why PACO10 cells do not respond to erlotinib since the drug concentrations applied ranged from relatively small to high values compared to realistic chemotherapeutic strategy - the therapeutic range of erlotinib in patients is typically around 1 µg/ml (~2µM) [98]. One hypothesis is that mutations in the MAPK and PI3K pathways might be present in PACO10 cells, as often shown in PDAC tissue. The compensatory effect of mutated proteins acting along the signalling cascades, as activating mutations of Ras and RAF in PDAC, might overcome the inactivation of EGF receptors and minimize the efficacy of chemotherapy. However, this hypothesis is purely speculative and was not of major interest for the success of this project, therefore it was not further investigated.

Overall, the datasets here presented were not sufficient to explain discrepancies between the data collected in this project and previous evidence provided on PACO cells, although the experimental setting was replicated according to the published protocol. Nonetheless, further investigation is ongoing to confirm that other CYP3A5-expression confers chemotherapy resistance to PDAC cell lines.

### *3.3.3 PDAC spheroids are highly sensitive to chemotherapy treatment in the presence and absence of CYP3A5*

To further assess the behaviour of PACO cells, a new round of testing was performed on PACO10 spheroids grown in ULA plates. Based on previous literature [50], [51], [99], one would expect that the response of cells grown in 3D is different than in 2D. Specifically, it was proved that 3D cancer structures are more resistant to drug exposure due to different diffusion dynamics and metabolic response compared to 2D cell culture. To test any possible differences between the two cell culture methods, the protocol used in 2D was applied to spheroids treated with paclitaxel and erlotinib and viability was monitored with an assay optimized for 3D cell cultures.

Once again, no substantial difference was visible between spheroids grown from cells expressing and non-expressing CYP3A5 (**fig. 20**). As in the 2D experiment, paclitaxel exerted a strong effect on the cell lines for drug concentrations in the sub-lethal range, whereas erlotinib affected the cells only for high drug concentrations independent of the CYP3A5 expression level.

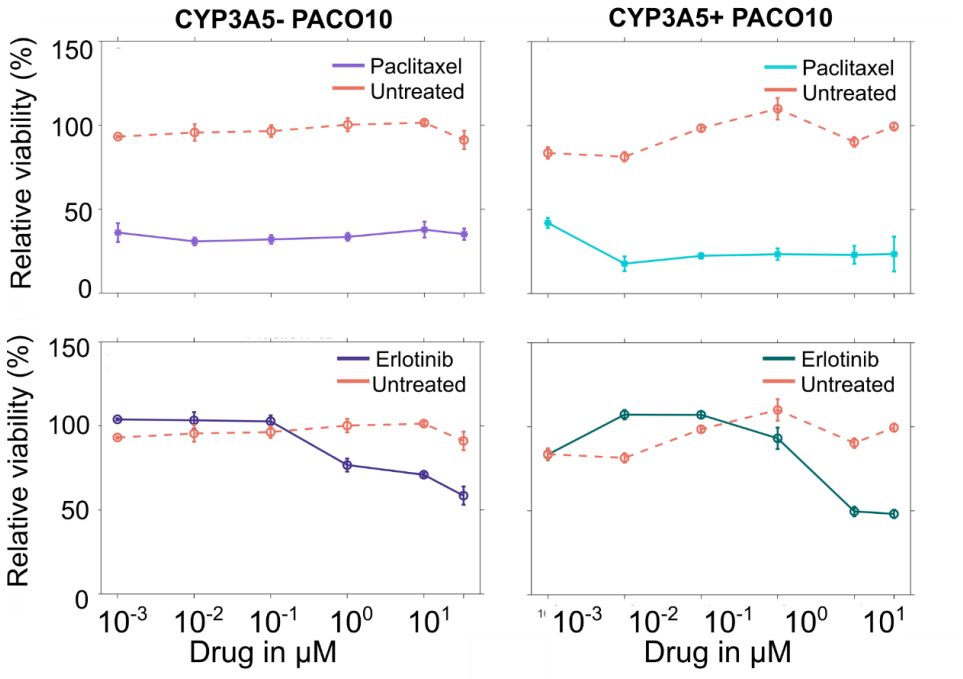


***Figure 20:*** *Drug response of genetically modified PACO10 cells grown in 3D. PACO10 cells non-expressing (left column) or expressing CYP3A5 (right column) were grown in 3D cell culture (ultra-low attachment plate) for 24 hours, then exposed to paclitaxel (top row) or erlotinib (bottom row) for 72 hours. Residual viability was recorded with CellTiter Glo3D assay (means of n = 3 replicates; error bars, S.E.; samples are normalized DMSO control). Red data points represent untreated cell viability normalized to relative DMSO control to monitor DMSO toxicity. PACO10 cells are highly affected by paclitaxel treatment at low concentrations – independent of CYP3A5 expression levels - while erlotinib does not exert a significant effect on cell viability.*

Although viability and toxicity assays are widely established to test drug efficacy, they rely on the metabolism effects of cells and can sometimes fall short when working with cells with slow metabolic and replication rate. Therefore, to rule out that the results deviate from previous evidence

for experimental reasons, a microscopy analysis of PACO10 spheroids was performed before and after drug treatment. In detail, PACO10 spheroids grown in ultra-low attachment plates were treated with paclitaxel and erlotinib for up to 144 hours. To observe co-cultures that resemble the heterogeneity of PDAC tissues during drug exposure, three mixtures of CYP3A5 expressing and non-expressing cells were tested, namely 0%, 50% and 100% of CYP3A5-expressing PACO10 cells. Z-stacks of spheroids were recorded after aggregation and during drug exposure and the radius of the spheroids was used to estimate the change in the number of cells in the structure. The results showed that spheroids treated with relatively low concentrations of paclitaxel (0.1 and 1 μM) were strongly affected by chemotherapy exposure, i.e. the radius of these spheroids was strongly reduced compared to the untreated control (**fig. 21A**). Interestingly, paclitaxel caused a reduction of the spheroid radius of about 50% after one day independent of CYP3A5 expression. Moreover, a high number of detached cells accumulated around the spheroid was visible in wells treated with paclitaxel, whereas the amount of apoptotic cells was negligible in erlotinib treated spheroids. In fact, erlotinib did not significantly affect the spheroids at both concentrations and growth was comparable to the untreated spheroids (**fig. 21B**).

From the collected evidence, CYP3A5 does not play a relevant role in this experimental setting in drug response to paclitaxel and erlotinib. Nonetheless, the observations here presented are supported by consistent results obtained with both viability assays and microscopy imaging. Quick and easy-to-handle methods such as viability assays are a valuable option to test several experimental conditions in parallel when working with organoids as an alternative to microscopy analyses that are time-consuming and often expensive. In this perspective, the use of automated live-cell microscopy [97] could potentially bridge the gap between the two methods. Automated imaging could reduce the effort an costs of imaging spheroids on a daily basis and minimize perturbations during the experiments, while still providing more insight on the evolution of organoids than final-point toxicity assays. In future, more investigations on drug-degrading enzymes will be performed using this method to test the response of PDAC to single or combinations of established drugs.

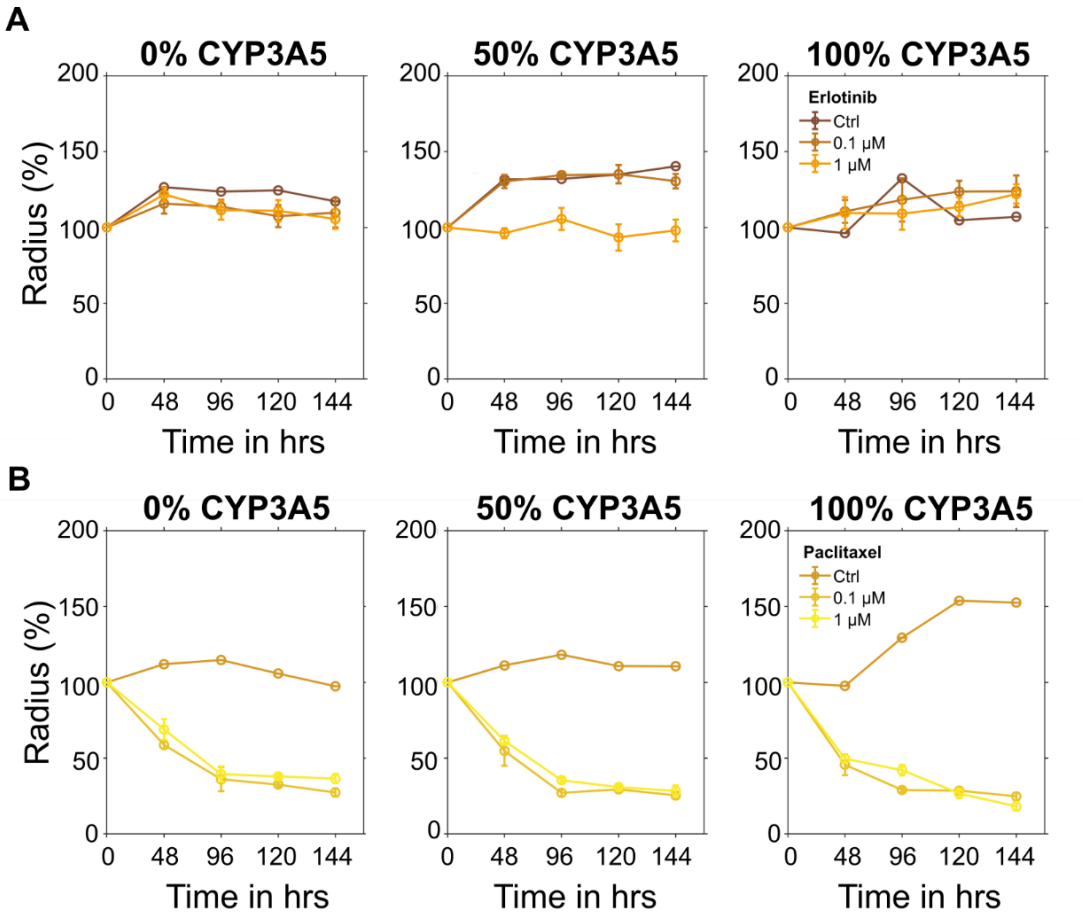


***Figure 21:*** *Real-time microscopy analysis of PACO10 spheroids treated with paclitaxel and erlotinib. Spheroids were grown in ultra-low attachment plates from different fractions of CYP3A5-expressing PACO10 cells, then treated with erlotinib (**A**) or paclitaxel (**B**) at 0.1 μM or 1 μM (in triplicates) or not treated (Ctrl, one replicate) 24 hours after seeding, for up to 144 hours. Z-stacks were recorded every 24 o 48 hours, and spheroids radius was extracted with custom Matlab code from bright-field images (for treated spheroids data represents means of n = 3 replicates; error bars, S.E.; samples were normalized to the initial time point). Analysis shows no significant difference in cell response to drug exposure.*

### *3.3.4 Mathematical model of cell populations expressing drug-degrading enzymes*

As explained in the previous paragraphs, the experimental analysis performed on PACO cells could not fully mirror the findings published by our collaborators. Nonetheless, the relevance of proteins in the cytochrome P450 family and other drug-degrading proteins in cancer resistance is established and represents a limitation in chemotherapy treatment.

Therefore, a modelling strategy was created by combining mechanistic models of cell populations characterised by drug-degrading enzymes in 2D and 3D to predict drug response in heterogeneous cancer populations. The method is based on two modelling approaches – presented in the following sections - to shed light on intra-cellular and systemic dynamics of PDAC during drug exposure and make use of experimental data from different sources.

*3.3.4.1 Cell population ODE model of cell growth inhibition, cell death and enzyme induction*

PDAC cells may express cytochrome enzymes that degrade chemotherapeutic drugs [48]. It is well known that cytochrome P450 enzymes are induced, dependent on the activity of xenobiotic sensors as PXR and CAR [100]. Therefore, a mathematical model (**fig. 22**) was created to study the role of enzyme induction, drug degradation and consequences for growth inhibition or cell death induction by chemotherapeutic drugs.

The model was developed under the following assumptions (**fig. 22A**): the number of cells $C$ of a cell population depends on cell growth and proliferation inhibition and cell death induction dependent on the concentration of a drug $D$. Degradation of the drug added to the cells depends on the number of cells $C$ and the average cellular enzyme concentration $E$.

Inhibition of proliferation, cell death, and enzyme induction dependent on drug exposition (**fig. 22B**) are processes linked to transcriptional regulation. In the case of proliferation inhibition or stimulation of cell death, chemotherapeutic drugs might affect DNA stability or, more specifically, inhibit pathways involved in growth or survival. In the case of cytochrome P450 enzymes, enzyme induction depends on the action of xenobiotic sensors that are activated by multiple drugs. The described effects of drug exposition can be assumed to be absent at extremely low drug concentrations and saturated at high drug concentrations. Due to the involvement of responses at the transcriptional level and dependency on drug concentration ranges, drug actions were described as transcriptional activators or repressors. The equation describing cell growth is:

$$\frac{dC}{dt} = \left[ k_g \frac{1}{1+\left(\frac{D}{K_I}\right)^h}\left(1-\frac{C}{K_c}\right) - k_d \frac{\frac{1}{\alpha}+\left(\frac{D}{K_D}\right)^j}{1+\left(\frac{D}{K_D}\right)^j} \right] C \qquad (1)$$

where the first part that depends on the parameters $k_g$, $K_I$, h and $K_C$ describes cell growth and growth inhibition by the drug with concentration $D$. The parameter $k_g$ describes the speed of cell growth in the absence of the drug. Growth inhibition is modelled as a sigmoidal function with a Hill coefficient $h$ with half-maximal inhibition when $D$ equals $K_I$. Cell growth is assumed to be limited by the carrying capacity $K_C$[23]. The second part of Eq. 1 describes cell death dependent on the parameters $k_d$, $K_D$, $\alpha$ and $j$. In absence of the drug, cells are removed by a basal cell death rate $k_d/\alpha$. To account for the concentration range between a sublethal drug concentration and a drug concentration resulting in a maximal death rate, cell death was simulated by a sigmoidal function with Hill coefficient $j$. The model works under the assumption that $K_D > K_I$ equivalent to the hypothesis that drugs inhibit proliferation at lower concentrations and stimulate cell death at higher concentrations. In absence of the drug, the maximal number of cells equals:

$$C_{max} = K_C \left(1 - \frac{k_d}{\alpha k_g}\right) \quad (2)$$

Turnover of the enzyme depends on the parameter $k_{syn}$ for synthesis and $k_{deg}$ for degradation. Its average cellular concentration is described by

$$\frac{dE}{dt} = k_{syn} \frac{\frac{1}{\beta} + \left(\frac{D}{K_E}\right)^l}{1 + \left(\frac{D}{K_E}\right)^l} - k_{deg} E \quad (3)$$

Enzyme induction was described by a sigmoidal function with Hill coefficient $l$. In absence of the drug, the enzyme is synthesized at a basal rate $k_{syn}/\beta$. If $D$ equals $K_E$, the synthesis rate is half-maximal. In absence of the drug, the enzyme is expressed at a basal level $E_0 = \frac{k_{syn}}{\beta k_{deg}}$.

After adding the drug to the cells, its removal depends on the parameter $k_r$ and, besides the drug concentration $D$, on the average cellular enzyme concentration $E$ as well as the number of cells $C$.

$$\frac{dD}{dt} = -k_r ECD = -\tilde{k}_r \frac{EC}{E_0 C_{max}} D \quad (4)$$

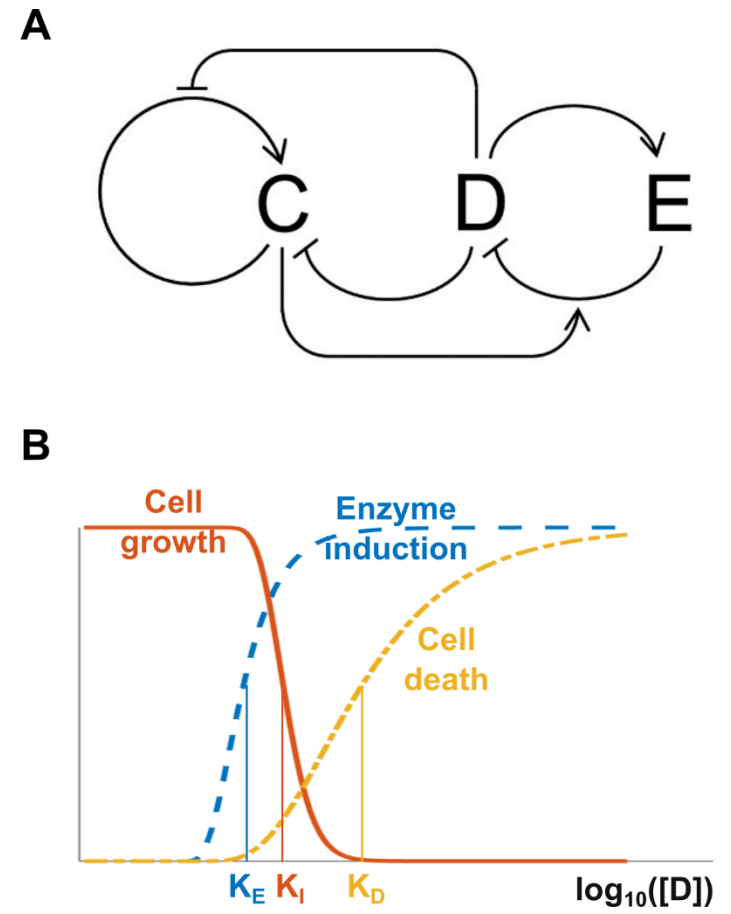


*Figure 22: Drug-dependent proliferation inhibition, cell death and enzyme induction.* ***A.*** *ODE model describes the proliferation of cells (C) inhibited by a drug (D). Drug exposure induces cell death and increases the expression of drug-degrading enzymes (E). In turn, drug degradation depends on the concentration of the enzyme and the number of cells.* ***B.*** *Drug concentration influences the cell population response: for low drug concentrations, drug-degrading enzymes are induced as a reaction to cytotoxicity; for increasing concentrations, chemotherapy first causes the inhibition of cell growth, then apoptosis of cells exposed to lethal amounts of the drug.*

Simulations of the cell population ODE model are available in fig. 23. The timeframe of the simulations was defined according to the experimental protocol tested on PACO cells. More specifically, to investigate cell response to chemotherapy, cells in the simulation were grown for 24 hours and treated with chemotherapy for up to 72 hours.

PACO cells tend to duplicate every 48 to 72 hours, and apoptosis appears after 24 to 48 hours from drug treatment; therefore, growth and death rate were set respectively to log(2)/72 and log(2)/24 according to exponential population dynamics. Enzyme production rate and growth inhibition rate were defined assuming that for low drug concentrations transcriptional modifications cause increased enzyme expression and growth arrest, whereas for higher drug concentrations cells cannot minimize drug toxicity by expressing the enzyme and undergo apoptosis. The half-maximal

drug-induced death rate was set at 1 µM since the evidence collected from PACO10 cells in 2D and 3D suggests that CYP3A5-expressing spheroids are affected by erlotinib around this drug concentration – which also represents the range of the average plasma concentration of erlotinib in patients after 24 hours treatment [98]. $K_E$ and $K_I$ values were selected consequently.

The maximal carrying capacity $K_C$ was set to $5x10^4$, the average number of cells at maximum confluency in 96-well plates used in most cell viability assays.

All the other parameter values are available in **table 8** in the appendix, and drug concentrations were equally distributed between 0 and 100 µM as used in some of the dose-response analyses presented in this dissertation.

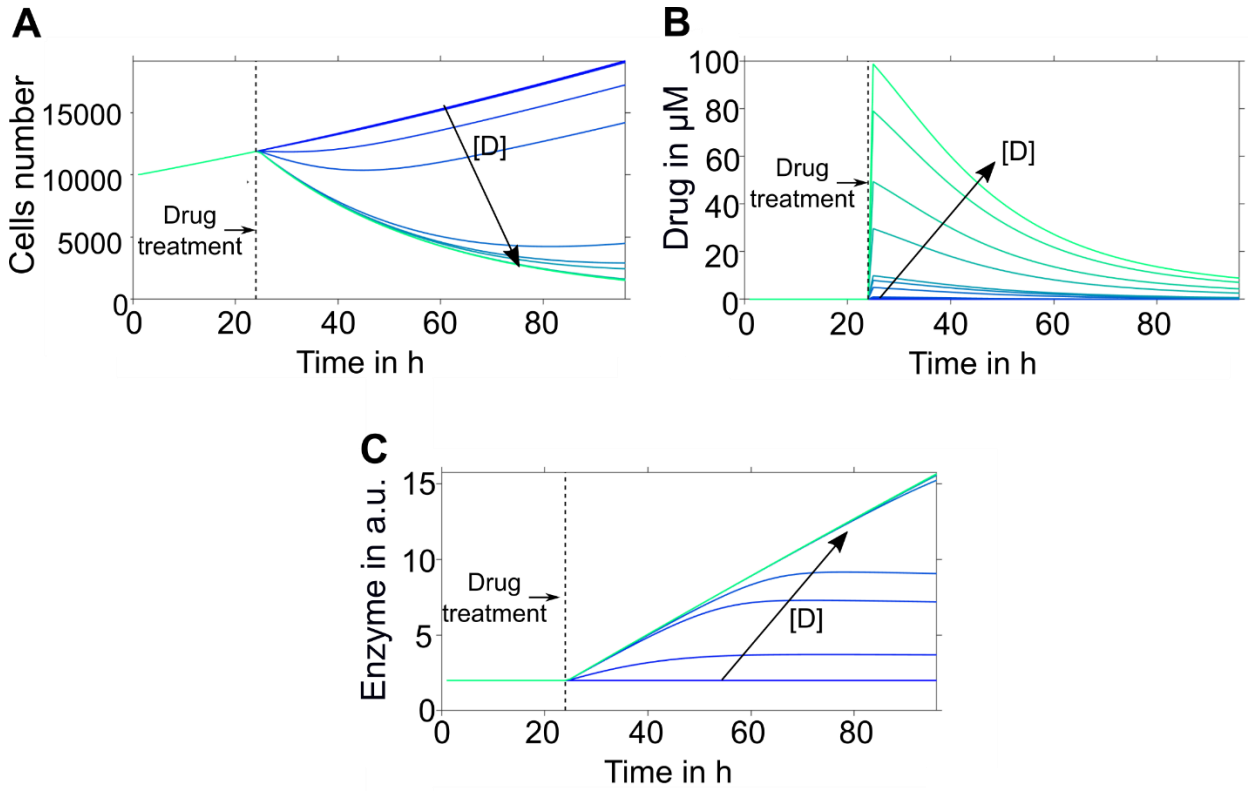


***Figure 23:*** *Simulations of ODE model of cell growth, drug-induced apoptosis, drug-induced enzyme expression and drug degradation by enzymes like CYP3A5.* ***A.*** *Variation of the number of cells depending on drug concentration [D] applied to the cell population.* ***B.*** *Drug concentration changes due to drug-degrading enzyme expressed in the simulated cell population.* ***C.*** *Dynamics of enzyme induction depending on the drug concentration [D] applied to the cell population. Drug concentration was varied between 0 and 100 µM.*

The model simulations represent the evolution of cell populations under the effect of chemotherapy in presence of enzymes, like CYP3A5. The simulated number of cells in the treated population decreases dramatically for the higher drug concentrations but does not reach zero thanks to drug-degrading enzymes that are strongly induced in presence of chemotherapy (**fig. 23C**) and cause a drop in drug concentration (**fig. 23B**). The simulations indicate that treating the tumour with constant drug exposure for up to 4 days might not kill a population of about 10000 cells and might allow the tissue to recover.

Similar considerations might be tested experimentally on cells to optimize the treatment of tumours characterised by drug-degrading enzymes and have a better understanding of subtype- or cancer-specific dynamics.

### *3.3.4.2 Cell growth, cell death and enzyme induction ODE model describes viability data of PACO2 cells*

To validate that the trajectories predicted by the model realistically represent the evolution of cells treated with chemotherapy in presence or absence of CYP3A5, the ODE model of cell growth, cell death and enzyme induction was fitted to dose-response data published in Noll et al. [23] The dataset represents residual cell viability of CYP3A5-expressing and non-expressing PACO2 cells exposed to paclitaxel for 48 hours.

Since the cell lines were derived from the same original tissue, one can assume that the rates of cells turnover, drug removal, enzyme synthesis and degradation are comparable. Nonetheless, due to the differential expression of CYP3A5, the cell population's response might differ in drug sensitivity and enzyme induction dynamics. Consequently, four variants of the model were tested to gain insight into the behaviour of PACO2 cell lines (**fig.24**).

PACO2 cells are classified as classical subtype and, according to previous evidence, they should not express CYP3A5 in the wild-type form. Therefore, the first version of the model assumes that enzyme induction only occurs in the genetically modified cells, i.e. CYP3A5-overexpressing PACO2. More specifically, this variant of the model includes that paclitaxel treatment in wt PACO2 does not lead to enzyme induction but causes growth inhibition for lower drug concentrations and cell apoptosis for higher ones.

Three other variants of the model were implemented to investigate drug response dynamics assuming that enzyme induction occurs in both cell lines. The model was developed under the assumption that sub-lethal drug concentrations lead to enzyme induction and cell growth inhibition, whereas higher concentrations cause cell apoptosis.

In each model, growth inhibition, enzyme induction and cell death were modelled as sigmoidal curve and Hill constants (respectively $K_I$, $K_E$ and $K_D$) were defined in different ways to discriminate how the basal and the acquired expression of CYP3A5 affect drug response (**fig.24**). Specifically, the second model variant includes the same $K_E$ and $K_I$ for both cell lines, but separate $K_D$. The third variant considers different enzyme induction rates, $K_E$, that translate into different inhibition and death rates, although the increments $dK_I$ and $dK_D$ are shared between the cell lines. Finally, the last variant includes separate values for both the enzyme induction and the cell death parameters.

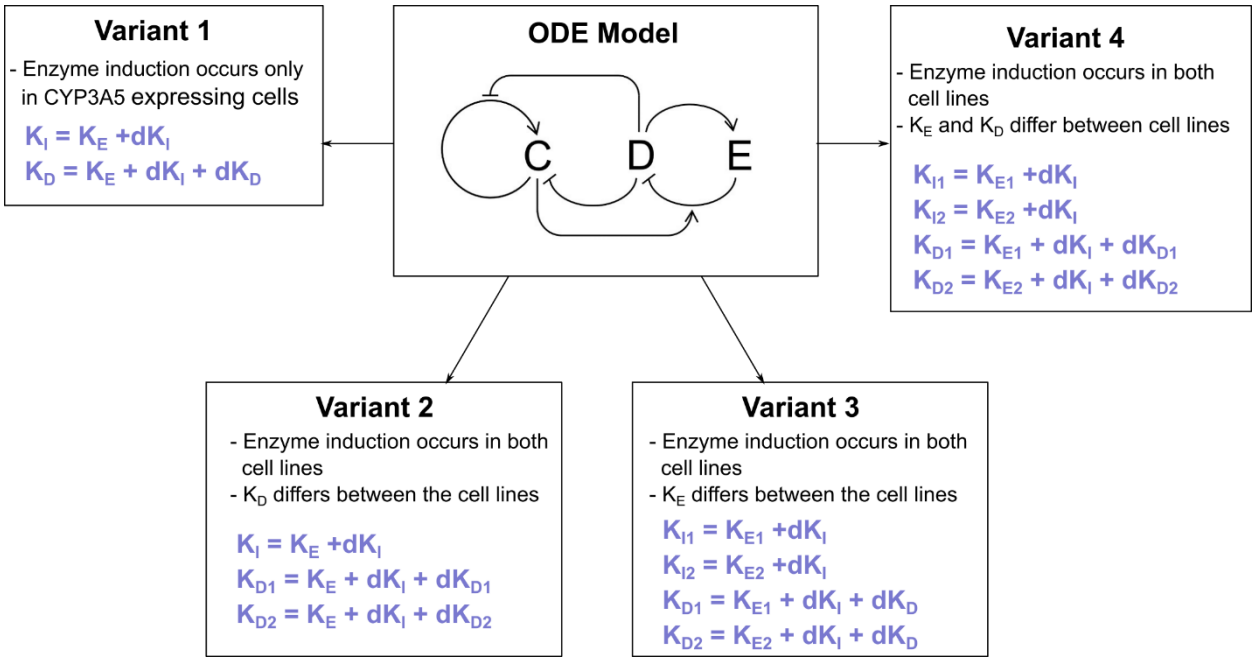


***Figure 24:*** *Variants of the ODE model of cell growth, cell death, enzyme induction and drug degradation tested on PACO2 cell viability data from Noll et al.* [23]. *The model assumes that $K_D > K_I > K_E$, estimated differently in each model variant (definition of the parameters in violet). In the parameters, the subscript 1 refers to wt PACO2 cells and the subscript 2 refers to CYP3A5-expressing cells.*

The goodness of fit for each model, i.e. the squared norm of the residuals, is presented in **fig.25A**. The best results were obtained by fitting the most flexible version of the model, including different enzyme induction and cell death half-maximal rates, i.e. variant 4 (**fig. 25B**). As visible from the estimated trajectories, the model can accurately reproduce the response of both cell lines to increasing concentrations of paclitaxel. Estimated parameters are available in **table 9** in the appendix.

The $K_D$ of the two cell lines, i.e. the IC50 value, is a quantitative indication of the sensitivity of cells to chemotherapy. The model predicts that paclitaxel inhibits PACO2 cells expressing CYP3A5 at a 50% rate at a concentration of about 95 µM and CYP3A5-negative cells in the range of 1.5 µM. The significant difference in drug sensitivity might translate into quite a diverse drug response in mixtures of cells grown from over-expressing and non-expressing PACO2 cells. Experimentally these values might be relevant to test whether cell lines deriving from the same PDAC subtype exposed to paclitaxel exhibit a similar behaviour.

Furthermore, the model fitting indicates that wild-type cells will undergo enzyme induction in the range of $5x10^{-4}$ µM and CYP3A5-expressing cells in the range of 0.1 µM.

The observation that wild-type cells react to drug exposure by expressing the drug metabolizer even at low drug concentrations highlights that induced resistance could occur in the classical subtype for minimal drug dosage. Therefore, PDAC cells that initially do not express the enzyme might react

to low dug concentrations by expressing drug-metabolizer hence surviving drug treatment in the long term.

These results indicate that the plasticity of PDAC cells leads to quite diverse resistance mechanisms over the drug range used in the experimental analysis. On the one hand, the efficacy of commonly used drugs might be strongly impaired in PDAC subtypes characterised by basal expression of CYP3A5. Consequently, significant drug dosage might be necessary to treat PDAC tissue with high enzyme expression, thus causing severe side effects in clinical practice. On the other hand, the genomic instability of PDAC cells for low dosage of chemotherapy causes the expression of CYP3A5 to contrast drug toxicity. Therefore, in the future, the combination of paclitaxel with CYP3A5 inhibitors might be crucial to render cells more sensitive to chemotherapy and decrease the effect of enzyme induction, hence drug resistance.

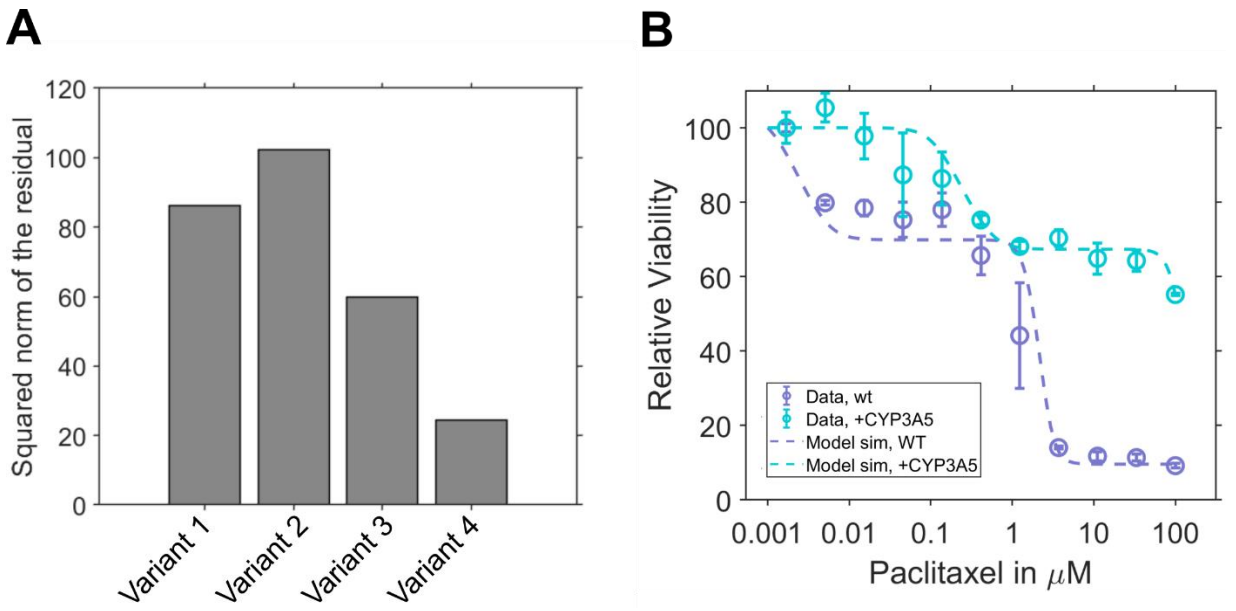


***Figure 25:*** *Mathematical model of drug degradation, cell growth and cell death describes PACO2 viability data (Noll et al.* [23]*). PACO2 data were fitted in Matlab with the ODE model in fig. 22 to extract relevant information on the population behaviour.* ***A.*** *Goodness of fit of model variants tested on PACO2 viability data. Variants are described in fig. 24. Bars represent the squared norm of the residual of the best fit of each model variant out of up to 100 iterations.* ***B.*** *Fitting of PACO2 viability data with the model variant 4. Data (circles) represents means of n = 4 replicates; error bars, S.E.; samples were normalized to DMSO. Trajectories estimated by the model (dashed line) can accurately reproduce the dose-response dataset.*

The model gave insight on the dynamics of PACO2 cells by estimating relevant parameters from published data. This approach could be tested on other publicly available datasets to investigate the dynamics of drug resistance in other cancer tissues expressing drug-metabolizing enzymes. Due to the extensive qualitative data available in many publications, the model could be applied to predict optimal drug concentrations for different cellular contexts and optimise further experimental analyses inexpensively.

In the context of this project, cell death rates estimated from PACO2 cells expressing or not CYP3A5 were implemented in an agent-based model to predict the dynamics of drug-diffusion and drug degradation in 3D cell cultures exposed to chemotherapy, described in the following section.

### *3.3.4.3 3D model of drug diffusion, drug degradation and cell apoptosis*

Drug molecules dispersed in a homogeneous cell medium passively diffuse from areas with higher to areas with lower concentration, creating diffusion gradients. Due to the role of CYP3A5 in drug degradation [23], one can assume that the heterogeneous expression of CYP3A5 in cancer tissues will influence the profiles of drug concentration during drug exposure. Therefore, an agent-based model of drug diffusion in 3D cell cultures was defined to resemble cancer tissue dynamics.

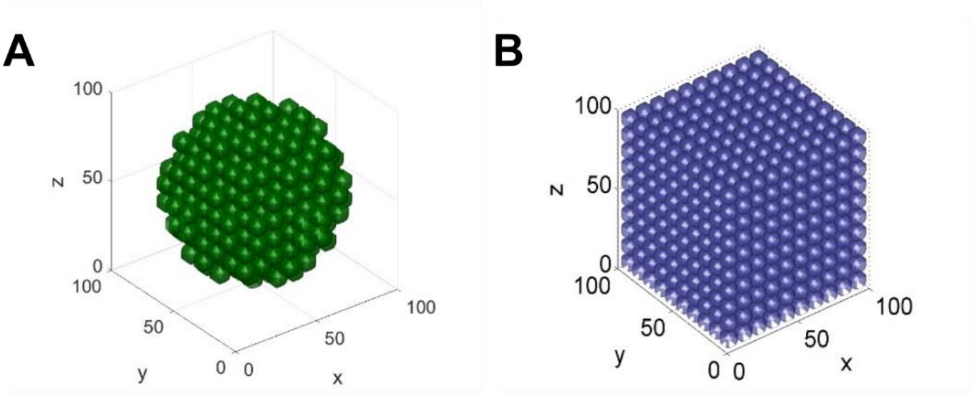


***Figure 26:*** *Geometry of 3D cell cultures simulated in reaction-diffusion model describing drug degradation and drug diffusion. To simulate realistic cell culture, a spherical (A) and a cubic geometry (B) were defined, containing respectively ~500 and 1000 spheres. Each sphere represents a cell as an agent capable (or not) to degrade drugs.*

Drug gradients form due to drug diffusion and degradation, which can be modelled according to Fick's second law (a) for symmetric diffusion,

$$\partial_t C = D\nabla^2 C - k_{deg} C \qquad \text{(a)}$$

Where C represents the drug concentration, D is the drug diffusion coefficient and $k_{deg}$ represents that drug degradation coefficient.

Cells in the 3D cell culture were represented as spheres characterised either by the presence or total absence of CYP3A5 expression, i.e. cells are single agents capable (or not) to degrade the diffusing drug with a rate of degradation $k_{deg}$.

To represent a 3-dimensional cell culture, Fick's second law was solved with the finite difference method in a custom Matlab code, simulated over a cube or a sphere in the range of 0.1 mm of side

or diameter (fig. 26). The choice of including two cell culture shapes derived from the most established techniques developed in the last decade and used to test 3D cell structures [99], [101], [102]. Cells can be grown in a solid gel that imitates the extracellular matrix and forced into different shapes or in a suspended state where the shape of the 3D structure depends on the capability of the cell line to aggregate. In the former case, cells can be forced into a more cubic environment, while in the latter, the shape of the organoid depends on the cell lines and acquires a more spherical appearance in the early stages of aggregation. In the model, 3D structures are made of cells along a regular lattice to minimize the simulation time. This approach allows quick testing of several cellular contexts in short time.

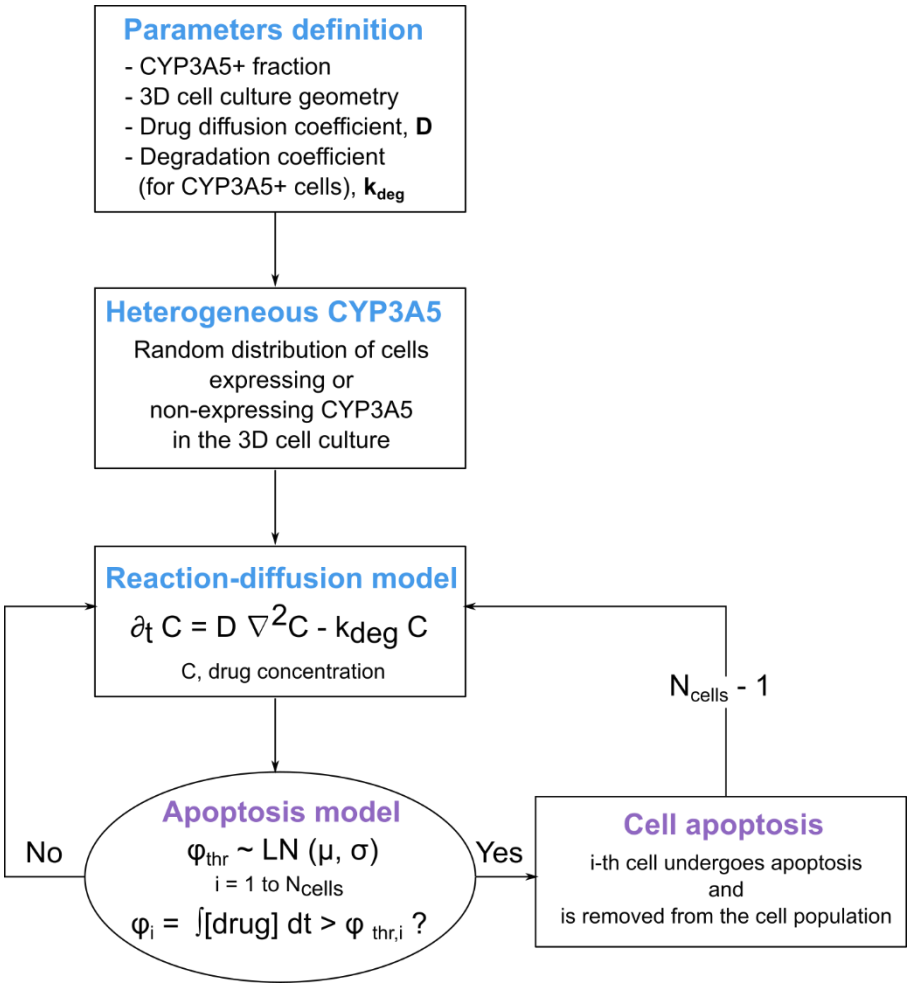


***Figure 27:*** *Workflow of agent-based model of drug diffusion, degradation, and cell apoptosis in 3D cell culture. First, model parameters, such as the fraction of CYP3A5-expressing cells, diffusion coefficient and degradation coefficient of CYP3A5-expressing cells, are defined. Then, random labels are assigned to cells in the 3D population and Fick's law of diffusion is simulated assuming that CYP3A5-expressing cells can degrade drugs with a rate $k_{deg}$. When the time integral of drug concentration within the volume of a single cell exceeds a pre-defined threshold (based on a log-normal function with mean μ and standard deviation σ), the cell undergoes apoptosis and is removed from the 3D population.*

An auxiliary model was developed to include the effect of drug-induced cell apoptosis (**fig. 27**), based on the assumption that cells undergo apoptosis – and therefore detach and disappear from the 3D cell culture – when a certain concentration of drug accumulates in the cell, i.e. the time integral of drug concentration within the cell volume reaches a certain threshold, according to the following:

$$\varphi = \int_0^{t_{apt}} [drug]dt \geq \varphi_{thr} \qquad \text{(b)}$$

where φ represents the time integral of the drug concentration, while $\varphi_{thr}$ indicates a log-normal threshold function:

$$\varphi_{thr} \sim \mathcal{L}\mathrm{N}(\mu, \sigma) \qquad \text{(c)}$$

*3.3.4.4 3D model of drug diffusion, drug degradation and cell apoptosis predicts the formation of tumour resistant niches*

The basic version of the 3D model does not include cell apoptosis and can be used to estimate the diffusion rate of small molecules in 3D cell cultures that are degraded by cells, as in the case of xenobiotics. For instance, simulations of drug diffusion and degradation were performed in a cubic 3D cell culture to test if the model can reasonably describe the distribution of chemotherapy in dense mixtures of cells (**fig. 28**) on a short timeframe in which the cells do not undergo apoptosis, but drugs can diffuse in the system. Due to a lack of evidence on PDAC cells about drug diffusion and degradation coefficients, arbitrary parameter values were based on previous literature [101], [103]. Most chemotherapeutic strategies are cyclic: patients undergo drug treatment followed by a drug-free period to recover, during which the cancer tissue often detoxifies or develops resistance.

On the scale of a 3D cell culture, this can be translated into exposing cells to a constant concentration of chemotherapy diluted in growth medium (colour coded in red in the **fig. 28A**) and then including a wash-out phase where the drug is removed from the medium (colour coded in blue in the **fig. 28A**).

Interestingly, the model simulations suggest that the fraction of drug-degrading cells influences the depth of drug penetration in the cell population during the drug exposure phase: the higher the fraction of CYP3A5-expressing cells, the least drugs can penetrate in the 3D structure. One can observe that drug diffusion, hence drug efficacy, will be limited to a particular volume of the cell culture, i.e. limited to a certain border over which cells are protected from the drug. Consequently, the volume of the protected niche (**fig. 28B**) depends on the fraction of drug-degrading cells and the diffusion rate of the drug, mostly related to the dimension of the diffusing molecule.

At the same time, the simulations suggest another interesting effect: the fraction of cells capable of degradation controls not only the depth of penetration but also the retention of the drug within the 3D structure. This suggests that although outer layers are not constantly exposed to the drug, the drug retains its effect during the wash-out phase, mostly in spheroids with low percentages of drug-degrading cells.

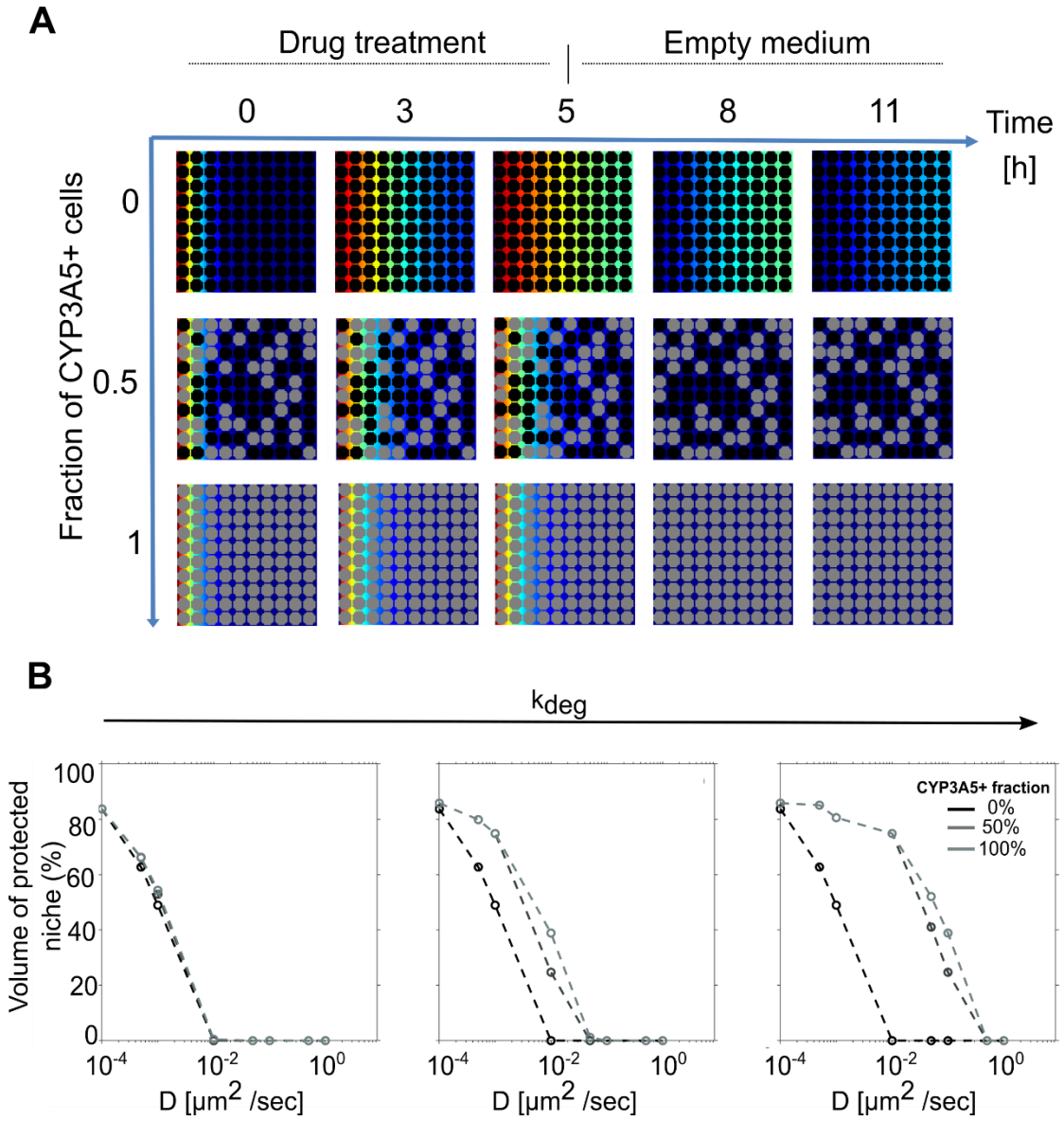


***Figure 28:*** *Simulation of drug diffusion and degradation in 3D cubic cell culture (0.1 mm per side) for different CYP3A5-expressing cell fractions.* ***A.*** *Cells positioned on a regular cubic lattice were randomly labelled as CYP3A5-expressing or non-expressing, to simulate heterogeneous populations of cells. CYP3A5-expressing cells were assigned a degradation rate of 0.001/sec and a drug diffusion rate of 0.05 µm²/sec was simulated. Drug treatment of 1 µM was simulated over a period of ~5 h, followed by an equal period with empty medium (absence of drug treatment).* ***B.*** *Volume of niches protected from drug effect due to CYP3A5 degradation. Simulations were performed over the timeframe used in* ***A.*** *assuming first drug exposure and then a wash-off period in spherical 3D cell culture in absence of drug apoptosis for different degradation coefficients (left to right: $10^4$, $10^3$, $10^2$ [1/sec]).*

## 3.3 Results and discussion

As previously mentioned, this model can be extended to include the effect of drug-induced apoptosis on the overall behaviour of the 3D cell culture and predict drug response and cell survival in conditions that match real cell culture experiments. Interestingly, PACO cells from the classical subtype tend to aggregate in a sphere-like geometry; therefore, drug treatment was simulated on spherical 3D cell cultures to predict the behaviour of PACO2 spheroids exposed to substrates of CYP3A5.

In the model, drug-induced apoptosis occurs if the concentration of drug within the cell over the time of treatment exceeds a certain threshold and the cell cannot neutralize the cytotoxic effect.

Simulations were performed for three percentages of CYP3A5-expressing cells, namely 0%, 50% and 100%, over a timeframe of 48 hours treatment with 1 μM drug, based on established protocols for drug toxicity assays. Parameters for drug diffusion and degradation were based on [101], [104]. IC50 values for CYP3A5-expressing and non-expressing cell lines estimated by fitting dose-response data collected from PACO2 cells and used as mean values for the threshold log-normal function in the apoptosis model.

The results of the simulation of drug diffusion, drug degradation and cell apoptosis (**fig. 29**) suggest that on the timeframe of 48 hours, residual tumour niches survive after drug exposure, but the number of dead cells, hence the dimension of the niches, depends on the percentage of CYP3A5 expressing cells. Consequently, if cells from PDAC subtypes are randomly dispersed in spheroids, drug-degrading cells will shield CYP3A5 non-expressing ones in the inner layers of the sphere from the effect of chemotherapy.

Interestingly, according to the model if the drug molecule diffuses with high rate, i.e. if the diffusion coefficient is in the range of 1 $\mu m^2$/min, the simulated drug degradation will not be sufficient to protect cancer cells from apoptosis on the timeframe of 48 hours of treatment. This range of diffusivity is typical of monoclonal antibodies in tumour spheroids of melanoma and colon adenocarcinoma spheroids [105], whereas more recent literature on the diffusion of small molecule drugs, generally smaller than monoclonal antibodies, in hepatocyte spheroids [106] - simulated as the diffusion of drug molecules in an aqueous environment - identifies the diffusion coefficient of these chemotherapy agents in the range of $10^2$-$10^3$ $\mu m^2$/min. Testing PDAC spheroids treated with both categories of drugs could be supported by the agent-based model to estimate degradation rates of CYP3A5 substrates and predict the sysemic spheroid response to treatment.

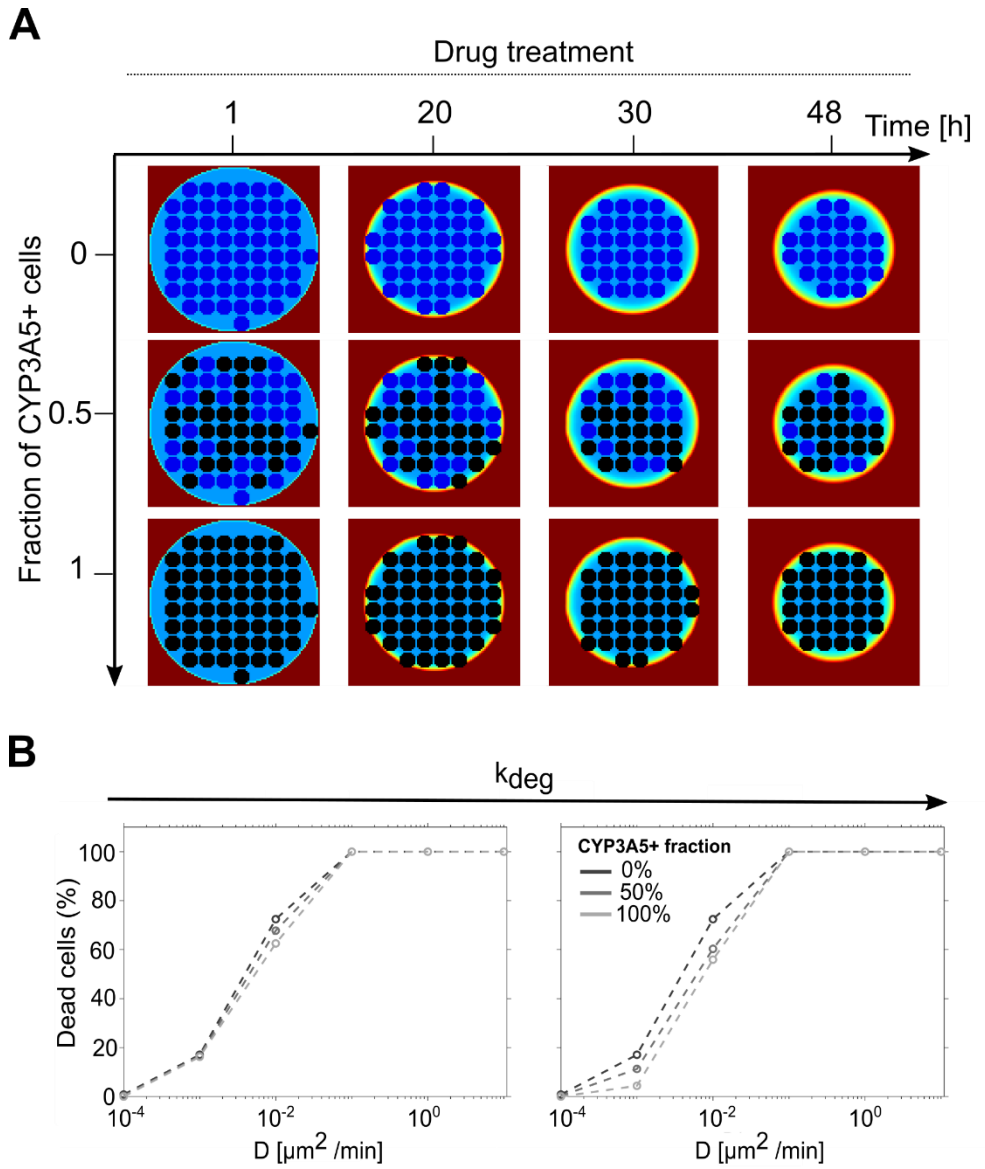


***Figure 29:*** *Simulation of drug diffusion, drug degradation and cell death in 3D spherical cell culture with a diameter of 0.1 mm for different CYP3A5-expressing cells fractions* ***A.*** *Spheroids exposed to drug treatment (1 µM) for 48 hours. Degradation rate of 0.001/min and a drug diffusion rate of 0.01 µm²/min were simulated in mixtures of cells with 0%, 50% and 100% CYP3A5-expressing cells. IC50 values for PACO2 cells (1.5 µM for wt, 95 µM for CYP3A5+ cells) were used to define a log-normal threshold for apoptosis.* ***B.*** *Simulations of drug diffusion, degradation, and cell death over a period of 48 hours for different values of diffusion rates and degradation coefficients (left to right: $10^{-3}$, $10^{-2}$ [1/min]). Data represent the percentage of dead cells at the end of the simulation in the cell culture.*

The added value of this model is the resemblance between real and computational spheroids. Therefore, this mathematical framework could support pre-clinical research on the efficacy of novel chemotherapeutic molecules in 3D cell culture. On a systemic level, the diffusion rate depends on the size and solubility of the chemotherapy agent. Based on the model predictions (**fig. 29B**), developing highly soluble or small chemotherapy molecules might be beneficial to contrast the degradation effect of drug-metabolizers as CYP3A5.

## 3.3 Results and discussion

Thanks to the limited number of parameters required in the model to describe the behaviour of 3D cell culture, drug diffusion could be simulated in a wide range of experimental conditions. Similar to what was proposed in this dissertation, previous studies might be used as a reference for pharmacokinetic parameters of drug diffusion and turnover. Moreover, results from drug toxicity or cell viability assays could be directly compared with the simulations to validate pharmacokinetics studies on the distribution of chemotherapy in 3D cancer tissue. Such experimental methods are inexpensive and quick to apply, and this approach will, in the future, further reduce the experimental costs and time necessary to test drug treatments *in vitro*.

# 4. Conclusions

## *4.1 Summary of achievements of this project*

In this study, the role of two proteins, CBLc and CYP3A5, responsible for different mechanisms of drug resistance was investigated in pancreatic ductal adenocarcinoma (PDAC). Such mechanisms have been discussed extensively in different cancer contexts, but little is still known about their effect in PDAC.

In this perspective, the systems biology approach used in this dissertation represents a platform to predict drug response in PDAC due to the occurrence of pre- and post-treatment expression of proteins involved in cell proliferation and drug degradation. By combining *in silico* modelling and experimental data, the first sub-project elucidated the impact of CBLc on PDAC and cervical cancer cells not as a ubiquitin ligase, its established protein activity, but as an activator of signalling pathways, so far investigated for other CBL isoforms [107]. At the same time, a novel quantitative description of the dynamics of innate and acquired drug resistance in 2D and 3D PDAC cell cultures characterised by the expression of drug-metabolizing enzymes was proposed. Overall, these studies provide a reliable mathematical framework to support further experimental investigation on the drug response of cell populations expressing enzymes involved in signalling and metabolic pathways.

## *4.2 CBLc is an activator of the MAPK and PI3K/Akt pathways in PDAC and cervix cancer*

Proteins of the CBL ubiquitin family are mainly characterised as inhibitors of the signalling activity of the MAPK and PI3K/Akt pathways due to the negative effect they exert on active membrane receptors. CBL proteins localize in membrane complexes, called signalosomes, where they can act as a scaffold to allow the binding of ubiquitin molecules to receptors or adaptor proteins involved in pathway activation.

Our collaborators observed that overexpression of CBLc results in an increased activation of the MAPK and PI3K/Akt pathways in presence of drug treatment with erlotinib, an established drug that acts on EGF receptors to inhibit signal transduction and arrest cell proliferation. The observed resistance effect opened new hypotheses on the role of CBLc as an enhancer of intracellular signal transmission, which was tested in PDAC and cervix cancer cells via a combination of mathematical modelling and experiments.

First, the analysis highlighted that, in both kinds of cancers, peak amplitude and IC50 values of the activation of the main effectors of the MAPK and PI3K pathways, pErk and pAkt, during erlotinib treatment were increased in cells expressing CBLc compared to CBLc-negative ones. Specifically,

HeLa cells exhibited a significant increase in the amplitude of both proteins, while the effect on drug sensitivity was negligible. On the other hand, the sensitivity to erlotinib of the proteins in SU.86.86 cells was significantly reduced, with an IC50 value more than 10-fold higher for pErk and 4-fold higher for pAkt in CBLc-expressing cells.

Furthermore, time-course analyses of the main proteins along the pathways, namely pAkt, pErk, pSrc and pEGFR, in absence of drug treatment, showed that the over-activation of the pathways is independent of drug treatment and happens mainly downstream of EGFR. This resistance mechanism might be a feature of tumour cells before drug exposure and over-activation of signalling pathways due to CBLc might represent an evolutionary advantage for cancer cells over normal tissue.

It was recently shown [108] that in breast cancer cells, the isoform CBL is often highly expressed and increases the tumorigenic activity of cells rather than suppressing cancer development. Similarly, CBLc might have an oncogenic role in PDAC and cervix cancer by enhancing the activity of Erk and Akt and dysregulating essential transcription factors, such as Fra-1, c-Fos and Egr-1, NF-kB, connected to oncogenesis and influenced by both the peak level and time integral of pErk and pAkt activity [94], [95], [109].

To validate the hypothesis that CBLc has a role as an activator of the pathways, a comprehensive ODE model describing EGFR internalization, degradation, and complex formation with CBLc and adaptor protein GAB1, as well as the activation of downstream MAPK and PI3K/Akt pathways was developed. This model is, to our knowledge, the most comprehensive mechanistic model describing the influence of CBLc on the intricate network of signalling proteins and represents a platform to investigate the activity of adaptor proteins in cells treated with targeted inhibitors.

The model could elucidate that CBLc acts as an activator on a short time scale by increasing the activity of proteins along the MAPK and PI3K pathways, i.e. Ras, PI3K and Src, in both PDAC and cervical cancer cells.

Consequently, further experiments were conducted to validate that the activity of CBLc is mainly downstream of the receptor. Immunoprecipitating EGFR complexes confirmed that CBLc leads to higher recruitment of the adaptor protein GRB2 and does not influence the dynamics of EGFR at the membrane level, but rather mediates the interaction between receptors and other proteins in signalosomes and amplifies signal transmission to downstream effectors. Also, the treatment of HeLa cells with paclitaxel highlighted a slightly reduced effect of chemotherapy on CBLc-expressing cells in the timeframe of 48 hours. Although further analysis will be necessary to assess the role of CBLc on the long term, the higher viability showed by CBLc-expressing cells is consistent with the hypothesis that the enzyme overexpression might give cells a survival advantage during drug treatment.

Overall, this study highlights the importance of CBLc as a modulator of the MAPK and PI3K pathways, responsible for increased activity of downstream enzymes. CBLc acts as scaffold for signalling proteins in the pathways and modifies the peak and steady state activity of enzymes that translate external information into transcriptional patterns and regulate the proliferation of cancer cells. The observed effect visible in two cancer cell lines suggests that this role of CBLc is not limited to pancreatic cancer and should be further investigated in pan-cancer studies. Inhibiting CBLc might be a new and improved approach to regulate the proliferation of PDAC and cervical cancer cells in combination with compounds targeting membrane receptors to reduce the chances of cancer survival.

## *4.3 Mathematical model predicts the formation of drug-resistant PDAC niches in 3D cell populations*

CYP3A5, a protein from the cytochrome P450 family usually expressed in the liver, is known to de-activate xenobiotics, such as chemotherapeutics drugs. Our collaborators from DKFZ recently showed that CYP3A5 is ectopically expressed in some subtypes of pancreatic ductal adenocarcinoma before drug exposure and is further induced under treatment. The extensive analysis presented in their publication on CYP3A5 in PDAC cancer stem cells (PACO) [23] showed a strong effect of resistance to established drug treatments in CYP3A5-expressing subtypes. Nonetheless, experiments that were part of this thesis showed no significant difference in drug responses based on the expression of CYP3A5 in PACO cells derived from the classical (PACO2) and exocrine-like (PACO10) subtypes in 2D and 3D cell culture. On the one hand, low concentrations of paclitaxel strongly affected PACO2 and PACO10 cells in 2D cell culture independent of the expression of CYP3A5; on the other hand, erlotinib was inefficient on PACO10 cells, which also survived for high drug concentrations. Moreover, evidence collected via toxicity assay and fluorescence microscopy on PACO10 spheroids confirmed the results of the 2D analysis and was consistent between the two methods.

To further characterise the role of drug-degrading enzymes in chemotherapy resistance, a reaction-diffusion model of cellular agents was developed to simulate the behaviour of heterogeneous cell cultures under drug treatment. Though it is known that cells capable of drug degradation play a major role in patients relapse in cancer, to our knowledge, no model has so far described the effect of drug degrading enzymes, such as CYP3A5, in the three-dimensional environment.

Our modelling strategy based on two mathematical approaches gives a comprehensive overview of the evolution of cell populations heterogeneously expressing enzymes such as CYP3A5, which impair the efficacy of established drug treatments.

The cell population ODE model describes cell growth, cell death, drug degradation and enzyme induction with a limited number of equations. Therefore, it can be used to simulate a wide range of drug concentrations or parameter sets on tumours expressing drug-degrading enzymes [110].
In this dissertation, the cell population model was applied to published data by Noll et al. [23] to estimate drug-induced death rates of PACO2 cells with different levels of CYP3A5, treated with paclitaxel. This way, the model provided more insight into the cell death and enzyme induction dynamics of PACO2 cells during chemotherapy without further experiments. In future, this approach might be used to estimate optimal conditions for drug treatment of a wide range of solid tumours from publicly available datasets.

The death rate parameters extracted from PACO2 viability data were used to simulate the evolution of 3D cell cultures with an agent-based model of drug diffusion, drug degradation and cell apoptosis in different biochemical contexts, e.g. different drug diffusion rates related to the drug molecule size. Our simulations predict the formation of tumour niches protected from drug-induced apoptosis in heterogeneous 3D cell culture expressing drug-degrading enzymes. The dimension of these niches depends on the diffusion and degradation rate of the drug molecules and, most importantly, on the percentage of cells that express the drug-degrading enzyme. This prediction is a reasonable representation of what might happen in patients' tissue based on the abundance of subtypes capable of degrading drugs, as the exocrine-like subtype in PDAC. Similar to the model simulations, it is reasonable to believe that patients' tissues that do not express drug-degrading enzymes would retain the drug molecules in the tissue for a longer time.
Predicting how cells respond to drugs in 3D might be crucial to optimize the *in vitro* treatment conditions used for established and novel compounds that are substrates of enzymes such as CYP3A5 and CYP3A4. The result of our 3D model could be directly matched with datasets of viability assays or microscopy analyses performed on organoids to estimate parameters like drug degradation and diffusion rates straightforwardly.
Overall, although further experiments will be necessary to validate the model predictions of cells survival in PDAC, our models could be crucial to predict the evolution of different subtypes in solid tumours characterised by drug-degrading enzymes.

## *4.4 Future perspectives and outlook*

The plasticity of cancer cells affects drug discovery due to the unpredictable long-term response to chemotherapy of cells that adapt both in the intracellular environment and at the systemic level to survive drug toxicity. In this perspective, systems biology can support the investigation of cell dynamics on different scales and partially compensate for the lack of experimental data available for pancreatic ductal adenocarcinoma.

## 4.4 Future perspectives and outlook

As shown in this thesis, combining computational modelling and experimental analysis can elucidate the dynamics of cancer response to drugs in quantitative terms from few datasets and highlight critical points in the evolution of drug resistance based on subtype-specific features. Also, mathematical modelling can be used to create a comprehensive description of distinct resistance mechanisms that might co-exist in cancer cells.

A new frontier of modelling is the multi-scale approach, which favours integrating multiple scales of resolution in cancer, from the molecular to the system level. This dissertation is the initial step for the development of a comprehensive method to integrate different layers of complexity in PDAC. For instance, our models might be a valuable support to predict the response of heterogeneous tumours to chemotherapy targeting signalling proteins. The expression of CYP3A5 in PDAC cells affects the concentration of drugs, such as erlotinib, which target proliferation pathways and are substrates for the enzyme. A decrease of the drug concentration due to CYP3A5 impairs the inhibiting effect of erlotinib on the activation of the signalling pathways. Therefore, the ODE model describing the MAPK and PI3K pathways could be used to characterise the intracellular response in single cells in the agent-based model of 3D cell culture to account for the different concentrations of erlotinib modulated by CYP3A5-expressing cells. This way, different proliferation activity in single agents could be specified to predict the systemic response of organoids. Finally, CYP3A5 induction due to drug exposure could be further simulated in the model to predict how the fluctuations of the enzyme affect the concentration of drug in the cells and, in turn, the inhibition of the signalling pathways.

Thanks to the flexibility of our computational models, hypotheses on the cancer response to erlotinib and other compounds could be tested in many biological conditions to optimize further experimental analyses. Our comprehensive modelling strategy can be applied to several mechanisms of drug resistance in multiple contexts to gain a systemic view of the cancer environment which will in the future support precision medicine.

# Appendix

**Table 6:** Ordinary differential equations of the model describing MAPK and PI3K/Akt pathways activation. Model versions do or not include:

1. **CBLc as an activator of MAPK and PI3K/Akt pathways.** Parameters in blue are restricted to 1 in the model neglecting the role of CBLc as an enhancer of pathways activation.
2. **CBLc as an inhibitor of EGFR degradation.** Parameters in red are included only in the version describing CBLc as an inhibitor of EGFR degradation.

In the model equations, the subscript *m* denotes the membrane compartment, and *c* indicates the cytosolic compartment.

| Model equations | Description |
|---|---|
| $\frac{d[EGFR_m]}{dt} = -(k_{EGFR,act} * [EGFR_m] * [EGF] - k_{EGFR,inact} * [EGFR_{m,act}]) - (k_{EGFR,inh,on} * [EGFR_m] * Erlotinib - k_{EGFR,inh,off_{inh}} * [EGFR_{m,Erlo}]) - (k_{EGFR,in} * [EGFR_m] - k_{EGFR,ex} * [EGFR_c]) + (k_{EGFR,inact} * [EGFR_{C,m,act}]) + (k_{EGFR,inact} * [EGFR_{G,m,act}]) + (k_{EGFR,inact} * [EGFR_{C,G,m,act}]) + (k_{EGFR,rec} * [EGFR_{RE}])$ | Total EGFR at the plasma membrane |
| $\frac{d[EGFR_{m,Erlo}]}{dt} = (k_{EGFR,inh,on} * [EGFR_m] * Erlotinib - k_{EGFR,inh,off} * [EGFR_{m,Erlo}]) - (k_{EGFR,in} * [EGFR_{m,Erlo}] - k_{EGFR,ex} * [EGFR_{c,Erlo}])$ | Total EGFR at the plasma membrane bound to Erlotinib |
| $\frac{d[EGFR_{c,Erlo}]}{dt} = k_{EGFR,in} * [EGFR_{m,Erlo}] - k_{EGFR,ex} * [EGFR_{c,Erlo}]$ | Total EGFR in cytosolic compartment bound to Erlotinib |
| $\frac{d[EGFR_{m,act}]}{dt} = (k_{EGFR,act} * [EGFR_m] * EGF - k_{EGFR,inact} * [EGFR_{m,act}]) - (k_{CBLc,act,on} * CBLc_{act} * [EGFR_{m,act}] - k_{CBLc,act,off} * [EGFR: CBLc_{m,act}]) - (k_{GAB1,on} * [GAB1] * [EGFR_{m,act}] - k_{GAB1,off} * [EGFR: GAB1_{m,act}]) - (k_{EGFR,act,in} * [EGFR_{m,act}])$ | Active EGFR at membrane level |
| $\frac{d[EGFR_c]}{dt} = k_{EGFR,in} * [EGFR_m] - k_{EGFR,ex} * [EGFR_c]$ | Total EGFR in cytosolic compartment |

| | |
|---|---|
| $\frac{d[EGFR_{c,act}]}{dt} = (k_{syn,EGFR} - k_{deg,EGFR} * [EGFR_{c,act}]) - (k_{CBLc,act,on} * [CBLc_{act}] * [EGFR_{c,act}] - k_{CBLc,act,off} * [EGFR: CBLc_{c,act}]) - (k_{GAB1,on} * [GAB1] * [EGFR_{c,act}] - k_{GAB1,off} * [EGFR: GAB1_{c,act}]) + (k_{EGFR,act,in} * [EGFR_{m,act}]) - (k_{EGFR,c,inact} * [EGFR_{c,act}])$ | Active EGFR in cytosolic compartment |
| $\frac{d[EGFR: GAB1_{m,act}]}{dt} = -(k_{CBLc,act,on} * [CBLc_{act}] * [EGFR: GAB1_{m,act}] - k_{CBLc,act,off} * [EGFR: GAB1: CBLc_{m,act}]) + (k_{GAB1,on} * [GAB1] * [EGFR_{m,act}] - k_{GAB1,off} * [EGFR: GAB1_{m,act}]) - (k_{EGFR,inact} * [EGFR: GAB1_{m,act}]) - (k_{EGFR,act,in} * [EGFR: GAB1_{m,act}]) - ((k_{deg,EGFR} + k_{deg,EGFR:CBLc}) * [EGFR: GAB1_{m,act}])$ | Active EGFR:GAB1 complex at membrane level |
| $\frac{d[EGFR: GAB1_{c,act}]}{dt} = -(k_{CBLc,act,on} * [CBLc_{act}] * [EGFR: GAB1_{c,act}] - k_{CBLc,act,off} * [EGFR: GAB1: CBLc_{c,act}]) + (k_{GAB1,on} * [GAB1] * [EGFR_{c,act}] - k_{GAB1,off} * [EGFR: GAB1_{c,act}]) + (k_{EGFR,act,in} * [EGFR: GAB1_{m,act}]) - (k_{EGFR,c,inact} * [EGFR: GAB1_{c,act}]) - ((k_{deg,EGFR} + k_{deg,EGFR:CBLc}) * [EGFR: GAB1_{c,act}])$ | Active EGFR:GAB1 complex in cytosolic compartment |
| $\frac{d[EGFR: CBLc_{m,act}]}{dt} = (k_{CBLc,act,on} * [CBLc_{act}] * [EGFR_{m,act}] - k_{CBLc,act,off} * [EGFR: CBLc_{m,act}]) - (k_{GAB1,on} * [GAB1] * [EGFR: CBLc_{m,act}] - k_{GAB1,off} * [EGFR: GAB1: CBLc_{m,act}]) - (k_{EGFR,inact} * [EGFR: CBLc_{m,act}]) - (k_{EGFR,act,in} * factor_{EGFR,int,Cbl} * [EGFR: CBLc_{m,act}]) - (k_{deg,EGFR:CBLc} * [EGFR: CBLc_{m,act}])$ | Active EGFR:CBLc complex at membrane level |
| $\frac{d[EGFR_{C,c,act}]}{dt} = (k_{CBLc,act,on} * [CBLc_{act}] * [EGFR_{c,act}] - k_{CBLc,act,off} * [EGFR: CBLc_{c,act}]) - (k_{GAB1,on} * [GAB1] * [EGFR: CBLc_{c,act}] - k_{GAB1,off} * [EGFR: GAB1: CBLc_{c,act}]) + (k_{EGFR,act,in} * factor_{EGFR,int,Cbl} * [EGFR: CBLc_{m,act}]) - (k_{EGFR,c,inact} * [EGFR: CBLc_{c,act}]) - (k_{deg,EGFR:CBLc} * [EGFR: CBLc_{c,act}])$ | Active EGFR:CBLc complex in cytosolic compartment |

| | |
|---|---|
| $\frac{d[EGFR_{C,G,m,act}]}{dt} = (k_{CBLc,act,on} * [CBLc_{act}] * [EGFR: GAB1_{m_{act}}] - k_{CBLc,act,off} * [EGFR: GAB1: CBLc_{m,act}]) + (k_{GAB1,on} * [GAB1] * [EGFR: CBLc_{m,act}] - k_{GAB1,off} * [EGFR: GAB1: CBLc_{m,act}]) - (k_{EGFR,inact} * [EGFR: GAB1: CBLc_{m,act}]) - (k_{EGFR,act,in} * factor_{EGFR,int,Cbl} * [EGFR: GAB1: CBLc_{m,act}]) - (k_{deg,EGFR:CBLc} * [EGFR: GAB1: CBLc_{m,act}])$ | Active EGFR:GAB1:CBLc complex at membrane level |
| $\frac{d[EGFR: GAB1: CBLc_{c,act}]}{dt} = (k_{CBLc,act,on} * [CBLc_{act}] * [EGFR: GAB1_{c,act}] - k_{CBLc,act,off} * [EGFR: GAB1: CBLc_{c,act}]) + (k_{GAB1,on} * [GAB1] * [EGFR: CBLc_{c,act}] - k_{GAB1,off} * [EGFR: GAB1: CBLc_{c,act}]) + (k_{EGFR,act,in} * factor_{EGFR,int,Cbl} * [EGFR: GAB1: CBLc_{m,act}]) - (k_{EGFR,inact} * [EGFR: GAB1: CBLc_{c,act}]) - (k_{deg,EGFR:CBLc} * [EGFR: GAB1: CBLc_{c,act}])$ | Active EGFR:GAB1:CBLc complex in cytosolic compartment |
| $\frac{d[EGFR_{RE}]}{dt} = (k_{EGFR,c,inact} * [EGFR_{c,act}]) + (k_{EGFR,c,inact} * [EGFR: GAB1_{c,act}) + (k_{EGFR,c,inact} * [EGFR: CBLc_{c,act}]) + (k_{EGFR,c,inact} * [EGFR: GAB1: CBLc_{c,act}]) - (k_{EGFR,rec} * [EGFR_{RE}])$ | Recycled EGFR |
| $\frac{d[GAB1]}{dt} = -(k_{GAB1,on} * [GAB1] * [EGFR_{m,act}] - k_{GAB1,off} * [EGFR: GAB1_{m,act}]) - (k_{GAB1,on} * [GAB1] * [EGFR_{c,act}] - k_{GAB1,off} * [EGFR: GAB1_{c,act}]) - (k * [GAB1] * [EGFR: CBLc_{m,act}] - k_{GAB1,off} * [EGFR: GAB1: CBLc_{m,act}]) - (k_{GAB1,on} * [GAB1] * [EGFR: CBLc_{c,act}] - k_{GAB1,off} * [EGFR: GAB1: CBLc_{c,act}]) + (k_{EGFR,inact} * [EGFR: GAB1_{m,act}]) + k_{EGFR,inact} * [EGFR: GAB1: CBLc_{m,act}] + k_{EGFR,c,inact} * [EGFR: GAB1_{c,act}] + k_{EGFR,c,inact} * [EGFR: GAB1: CBLc_{c,act}] + (k_{deg,EGFR} + k_{deg,EGFR:CBLc}) * [EGFR: GAB1_{m,act}] + (k_{deg,EGFR} + k_{deg,EGFR:CBLc}) * [EGFR: GAB1_{c,act}] + k_{deg,EGFR:CBLc} * [EGFR: GAB1: CBLc_{m,act}] + k_{deg,EGFR:CBLc} * [EGFR: GAB1: CBLc_{c,act}] - (k_{GAB1,ph} * [GAB1] * [Erk_{act}] - k_{GAB1,deph} * [GAB1_i])$ | Complex formation, complex activation and inactivation, phosphorylation and dephosphorylation of GAB1 |
| $\frac{d[GAB1_i]}{dt} = k_{GAB1,ph} * [GAB1] * [Erk_{act}] - k_{GAB1,deph} * [GAB1_i]$ | Inactivation of GAB1 |

| | |
|---|---|
| $\frac{d[Src]}{dt} = -(k_{Src,act,basal} * [Src]) - (k_{Src,act,EGFR} * [Src] * ([EGFR_{m,act}] + [EGFR_{c,act}] + [EGFR{:}\ GAB1_{m,act}] + [EGFR{:}\ GAB1_{c,act}])) - (k_{Src,act,EGFR} * factor_{CBLc:Src,act} * [Src] * ([EGFR{:}\ CBLc_{m,act}] + [EGFR{:}\ CBLc_{c,act}] + [EGFR{:}\ GAB1{:}\ CBLc_{m,act}] + [EGFR{:}\ GAB1{:}\ CBLc_{c,act}])) + (k_{Src,inact} * [Src_{act}])$ | Synthesis and complex formation of total Src |
| $\frac{d[Src_{act}]}{dt} = (k_{Src,act,basal} * [Src]) + (k_{Src,act,EGFR} * [Src] * ([EGFR_{m,act}] + [EGFR_{c,act}] + [EGFR{:}\ GAB1_{m,act}] + [EGFR{:}\ GAB1_{c,act}])) + (k_{Src,act,EGFR} * factor_{CBLc:Src,act} * [Src] * ([EGFR{:}\ CBLc_{m,act}] + [EGFR{:}\ CBLc_{c,act}] + [EGFR{:}\ GAB1{:}\ CBLc_{m,act}] + [EGFR{:}\ GAB1{:}\ CBLc_{c,act}])) - (k_{Src,inact} * [Src_{act}])$ | Activation, complex formation and inactivation of active Src, i.e. phosphorylation of Src |
| $\frac{d[CBLc]}{dt} = -(k_{CBLc,act} * [CBLc] * [Src_{act}]) + (k_{CBLc,inact} * [CBLc_{act}])$ | Activation and inactivation of CBLc through Src |
| $\frac{d[CBLc_{act}]}{dt} = -(k_{CBLc,act,on} * [CBLc_{act}] * [EGFR_{m,act}] - k_{CBLc,act,off} * [EGFR{:}\ CBLc_{m,act}]) - (k_{CBLc,act,on} * [CBLc_{act}] * [EGFR_{c,act}] - k_{CBLc,act,off} * [EGFR{:}\ CBLc_{c,act}]) - (k_{CBLc,act,on} * [CBLc_{act}] * [EGFR{:}\ GAB1_{m,act}] - k_{CBLc,act,off} * [EGFR{:}\ GAB1{:}\ CBLc_{m,act}]) - (k_{CBLc,act,on} * [CBLc_{act}] * [EGFR{:}\ GAB1_{c,act}] - k_{CBLc,act,off} * [EGFR{:}\ GAB1_{c,act}]) + (k_{EGFR,inact} * [EGFR{:}\ CBLc_{m,act}]) + (k_{EGFR,inact} * [EGFR{:}\ GAB1{:}\ CBLc_{m,act}]) + (k_{EGFR,c,inact} * [EGFR{:}\ CBLc_{c,act}]) + (k_{EGFR,c,inact} * [EGFR{:}\ GAB1{:}\ CBLc_{c,act}]) + (k_{deg,EGFR:CBLc} * [EGFR{:}\ CBLc_{m,act}]) + (k_{deg,EGFR:CBLc} * [EGFR{:}\ CBLc_{c,act}]) + (k_{deg,EGFR:CBLc} * [EGFR{:}\ GAB1_{m,act}]) + (k_{deg,EGFR:CBLc} * [EGFR{:}\ GAB1{:}\ CBLc_{c,act}]) + (k_{CBLc_{act}} * [CBLc] * [Src_{act}]) - k_{CBLc,inact} * [CBLc_{act}]$ | Complex formation, scaffold activity and inactivation of active CBLc |
| $\frac{d[PI3K]}{dt} = -(k_{PI3K,act} * [PI3K] * ([EGFR{:}\ GAB1_{m,act}] + [EGFR{:}\ GAB1_{c,act}]) - k_{PI3K,inact} * [PI3K_{act}]) - (k_{PI3K,act} * factor_{CBLc:PI3K,act} * [PI3K] * ([EGFR{:}\ GAB1{:}\ CBLc_{m,act}] + [EGFR{:}\ GAB1{:}\ CBLc_{c,act}]) - k_{PI3K,inact} * [PI3K_{act}])$ | Synthesis, complex formation, and turnover of PI3K |

| | |
|---|---|
| $\frac{d[PI3K_{act}]}{dt} = (k_{PI3K,act} * [PI3K] * ([EGFR:GAB1_{m,act}] + [EGFR:GAB1_{c,act}]) - k_{PI3K,inact} * [PI3K_{act}]) + (k_{PI3K,act} * factor_{CBLc:PI3K,act} * [PI3K] * ([EGFR:GAB1:CBLc_{m,act}] + EGFR:GAB1:CBLc_{c,act}]) - k_{PI3K,inact} * [PI3K_{act}])$ | Complex formation, activation, and inactivation of PI3K |
| $\frac{d[Akt]}{dt} = -(k_{Akt,act} * [Akt] * [PI3K_{act}] - k_{Akt,inact} * [Akt_{act}])$ | Activation and inactivation of total Akt |
| $\frac{d[Akt_{act}]}{dt} = k_{Akt,act} * [Akt] * [PI3K_{act}] - k_{Akt,inact} * [Akt_{act}]$ | Activation and inactivation of active Akt, i.e. phosphorylated Akt |
| $\frac{d[Ras]}{dt} = -(k_{Ras,act} * [Ras] * ([EGFR_{m,act}] + [EGFR_{c,act}] + [EGFR:GAB1_{m,act}] + [EGFR:GAB1_{c,act}]) - k_{Ras,inact} * [Ras_{act}]) - (k_{Ras,act} * factor_{CBLc:Ras,act} * [Ras] * ([EGFR:CBLc_{m,act}] + [EGFR:CBLc_{c,act}] + [EGFR:GAB1:CBLc_{m,act}] + [EGFR:GAB1:CBLc_{c,act}]) - k_{Ras,inact} * [Ras_{act}])$ | Activation, complex formation, inactivation of total Ras |
| $\frac{d[Ras_{act}]}{dt} = (k_{Ras,act} * [Ras] * ([EGFR_{m,act}] + [EGFR_{c,act}] + [EGFR:GAB1_{m,act}] + [EGFR:GAB1_{c,act}]) - k_{Ras,inact} * [Ras_{act}]) + (k_{Ras,act} * factor_{CBLc:Ras,act} * [Ras] * ([EGFR:CBLc_{m,act}] + [EGFR:CBLc_{c,act}] + [EGFR:GAB1:CBLc_{m,act}] + [EGFR:GAB1:CBLc_{c,act}]) - k_{Ras,inact} * [Ras_{act}])$ | Activation, complex formation, inactivation of active Ras, i.e. phosphorylated |
| $\frac{d[Raf]}{dt} = -(k_{Raf,act} * [Raf] * [Ras_{act}] - k_{Raf,inact} * [Raf_{act}]) - (k_{Erk,inh} * [Raf] * [Erk_{act}] - k_{Raf,deph} * [Raf_i])$ | Activation, inactivation of total Raf and interaction with Ras |
| $\frac{d[Raf_{act}]}{dt} = (k_{Raf,act} * [Raf] * [Ras_{act}] - k_{Raf,inact} * [Raf_{act}]) - (k_{Erk,inh} * [Raf_{act}] * [Erk_{act}] - k_{Raf,deph} * [Raf_{act,i}])$ | Activation, inactivation of phosphorylated Raf and interaction with Ras, feedback from active Erk to Raf |
| $\frac{d[Raf_{act,i}]}{dt} = (k_{Erk,inh} * [Raf_{act}] * [Erk_{act}] - k_{Raf,deph} * [Raf_{act,i}]) + (k_{Raf,act} * [Raf_i] * [Ras_{act}] - k_{Raf,inact} * [Raf_{act,i}])$ | Activation, inactivation of phosphorylated Raf and interaction with Ras, feedback from active Erk to Raf |

| | |
|---|---|
| $\frac{d[Raf_i]}{dt} = (k_{Erk,inh} * [Raf] * [Erk_{act}] - k_{Raf,deph} * [Raf_i]) - (k_{Raf,act} * [Raf_i] * [Ras_{act}] - k_{Raf,inact} * Raf_{act,i}])$ | Inactivation and inhibition of Raf through feedback from Erk |
| $\frac{d[Mek]}{dt} = -(k_{Mek,act} * [Mek] * [Raf_{act}] - k_{Mek,inact} * [Mek_{act}])$ | Activation and inactivation of total Mek |
| $\frac{d[Mek_{act}]}{dt} = k_{Mek,act} * [Mek] * [Raf_{act}] - k_{Mek,inact} * [Mek_{act}]$ | Activation and inactivation of active Mek (phosphorylated) |
| $\frac{d[Erk]}{dt} = -(k_{Erk,act} * [Erk] * [Mek_{act}] - k_{Erk,inact} * [Erk_{act}])$ | Activation and inactivation of total Erk |
| $\frac{d[Erk_{act}]}{dt} = k_{Erk,act} * [Erk] * [Mek_{act}] - k_{Erk,inact} * [Erk_{act}]$ | Activation and inactivation of active Erk (phosphorylated) |

**Table 7** Parameters estimated by fitting the ODE model of MAPK and PI3K/Akt pathways activations to SU.86.86 cells in presence or absence of erlotinib treatment (EGF treatment of up to 20 and up to 60 minutes) and HeLa cells in absence of chemotherapy (EGF treatment of up to 20 minutes). Model versions do or do not include:

1. **CBLc as an activator of MAPK and PI3K/Akt pathways.** Parameters in blue are fixed to 1 in the model neglecting the role of CBLc as an enhancer of pathways activation.
2. **CBLc as an inhibitor of EGFR degradation.** Parameters in red are included only in the variant describing CBLc as an inhibitor of EGFR degradation.

Estimated parameter values in the table were obtained by fitting the model variant including CBLc as an activator and not an inhibitor of EGFR degradation (Version 4). Values of the parameters in red are related to the model version accounting also for the reduced EGFR degradation due to CBLc (Version 1).

| **Scaling factors** | **Estimated value** | **Values range [min,max]** | **Unit** |
|---|---|---|---|
| **SU.86.86 [0-20 minutes], +/- Erlotinib** | | | |
| $scale_{pEGFR}$ | 0.18 | $[10^{-4},10^{4}]$ | $nM^{-1}$ |
| $scale_{Src}$ | 0.04 | $[10^{-4},10^{4}]$ | $nM^{-1}$ |
| $scale_{pSrc}$ | 0.06 | $[10^{-4},10^{4}]$ | $nM^{-1}$ |
| $scale_{Akt}$ | 0.29 | $[10^{-4},10^{4}]$ | $nM^{-1}$ |
| $scale_{pAkt}$ | 563.04 | $[10^{-4},10^{4}]$ | $nM^{-1}$ |
| $scale_{Erk}$ | 0.02 | $[10^{-4},10^{4}]$ | $nM^{-1}$ |
| $scale_{pErk}$ | 0.04 | $[10^{-4},10^{4}]$ | $nM^{-1}$ |
| | | | |
| **SU.86.86 [0-60 minutes], - Erlotinib** | | | |
| $scale_{pEGFR,SU8686}$ | 195.44 | $[10^{-4},10^{4}]$ | $nM^{-1}$ |
| $scale_{pSrc,SU8686}$ | 0.67 | $[10^{-4},10^{4}]$ | $nM^{-1}$ |
| $scale_{pAkt,SU8686}$ | 181.55 | $[10^{-4},10^{4}]$ | $nM^{-1}$ |
| $scale_{pErk,SU8686}$ | 0.41 | $[10^{-4},10^{4}]$ | $nM^{-1}$ |
| | | | |
| **HeLa [0-20 minutes], - Erlotinib** | | | |
| $scale_{pEGFR,HeLa}$ | 0.25 | $[10^{-4},10^{4}]$ | $nM^{-1}$ |
| $scale_{pSrc,HeLa}$ | 0.07 | $[10^{-4},10^{4}]$ | $nM^{-1}$ |
| $scale_{pAkt,HeLa}$ | 70.92 | $[10^{-4},10^{4}]$ | $nM^{-1}$ |
| $scale_{pErk,HeLa}$ | 0.08 | $[10^{-4},10^{4}]$ | $nM^{-1}$ |

| Kinetic parameters | Estimated value | Values range [min,max] | Unit |
|---|---|---|---|
| $k_{EGFR,act}$ | 1.8 | [$10^{-4}$,10] | $nM^{-1}min^{-1}$ |
| $k_{EGFR,inact}$ | 9.17 | [$10^{-4}$,10] | $min^{-1}$ |
| $k_{EGFR,inh,on}$ | 0.10 | [$10^{-2}$,10] | $nM^{-1}min^{-1}$ |
| $k_{EGFR,inh,off}$ | 0.01 | [$10^{-2}$,10] | $min^{-1}$ |
| $k_{EGFR,in}$ | 5.32 | [$10^{-4}$,10] | $min^{-1}$ |
| $k_{EGFR,c,inact}$ | 0.60 | [$10^{-4}$,10] | $min^{-1}$ |
| $k_{EGFR,act,in}$ | 0.01 | [$10^{-4}$,10] | $min^{-1}$ |
| $factor_{EGFR,int,Cbl}$ | 96.11 | [1,$10^{2}$] | dimensionless |
| $k_{EGFR,ex}$ | 0.28 | [$10^{-4}$,10] | $min^{-1}$ |
| $k_{EGFR,rec}$ | 0.05 | [$10^{-4}$,10] | $min^{-1}$ |
| $k_{GAB1,on}$ | 1.82 | [$10^{-4}$,10] | $nM^{-1}min^{-1}$ |
| $k_{GAB1,off}$ | 0.01 | [$10^{-4}$,10] | $min^{-1}$ |
| $k_{GAB1,ph}$ | 0.18 | [$10^{-4}$,10] | $nM^{-1}min^{-1}$ |
| $k_{GAB1,deph}$ | 0.001 | [$10^{-4}$,10] | $min^{-1}$ |
| $k_{CBLc,act}$ | 0.002 | [$10^{-4}$,10] | $nM^{-1}min^{-1}$ |
| $k_{CBLc,inact}$ | 5.49 | [$10^{-4}$,10] | $min^{-1}$ |
| $k_{CBLc,act,on}$ | 1.28 | [$10^{-4}$,10] | $nM^{-1}min^{-1}$ |
| $k_{CBLc,act,off}$ | 1.86 | [$10^{-4}$,10] | [$min^{-1}$ |
| $k_{Src,act,EGFR}$ | 0.006 | [$10^{-4}$,10] | $nM^{-1}min^{-1}$ |
| $k_{Src,act,basal}$ | 0.20 | [$10^{-4}$,10] | $min^{-1}$ |
| $k_{Src,inact}$ | 0.84 | [$10^{-4}$,10] | $min^{-1}$ |
| $k_{PI3K,act}$ | 0.51 | [$10^{-4}$,10] | $nM^{-1}min^{-1}$ |
| $k_{PI3K,inact}$ | 1.73 | [$10^{-4}$,10] | $min^{-1}$ |
| $k_{Akt,act}$ | 0.02 | [$10^{-4}$,10] | $nM^{-1}min^{-1}$ |
| $k_{Akt,inact}$ | 3.04 | [$10^{-4}$,10] | $min^{-1}$ |
| $k_{Ras,act}$ | 0.02 | [$10^{-4}$,10] | $nM^{-1}min^{-1}$ |
| $factor_{CBLc,Src,act}$ | 31.14 | [$10^{-1}$,$10^{2}$] | dimensionless |
| $factor_{CBLc,Ras,act}$ | 0.59 | [$10^{-1}$,$10^{2}$] | dimensionless |
| $factor_{CBLc,PI3K,act}$ | 98.56 | [$10^{-1}$,$10^{2}$] | dimensionless |

| | | | |
|---|---|---|---|
| $k_{Ras,inact}$ | 0.32 | $[10^{-4},10]$ | $min^{-1}$ |
| $k_{Raf,act}$ | 0.012 | $[10^{-4},10]$ | $nM^{-1}min^{-1}$ |
| $k_{Raf,inact}$ | 0.43 | $[10^{-4},10]$ | $min^{-1}$ |
| $k_{Mek,act}$ | 4.76 | $[10^{-4},10]$ | $nM^{-1}min^{-1}$ |
| $k_{Mek,inact}$ | 0.54 | $[10^{-4},10]$ | $min^{-1}$ |
| $k_{Erk,act}$ | 1.15 | $[10^{-4},10]$ | $nM^{-1}min^{-1}$ |
| $k_{Erk,inact}$ | 0.27 | $[10^{-4},10]$ | $[min^{-1}]$ |
| $k_{Erk,inh}$ | 0.08 | $[10^{-4},10]$ | $nM^{-1}min^{-1}$ |
| $k_{Raf,deph}$ | 0.03 | $[10^{-4},10]$ | $min^{-1}$ |
| $k_{syn,EGFR}$ | 0.001 | $[10^{-4},10]$ | $min^{-1}$ |
| $k_{deg,EGFR}$ | 0.0002 | $[10^{-4},10]$ | $min^{-1}$ |
| $k_{deg,EGFR:CBLc}$ | 0.0003 | $[10^{-4},10]$ | $min^{-1}$ |
| | | | |
| | | | |
| **Initial concentrations** | **Estimated value** | **Values range [min,max]** | **Unit** |
| **SU.86.86 [0-20 minutes], +/- Erlotinib** | | | |
| $EGFR_m$ | 99.03 | $[10^{-1},10^{2}]$ | nM |
| $EGFR_c$ | 99.93 | $[10^{-1},10^{2}]$ | nM |
| GAB1 | 1.48 | $[10^{-1},10^{2}]$ | nM |
| Src | 17.32 | $[10^{-1},10^{2}]$ | nM |
| $Src_{act}$ | 2.595 | $[10^{-4},10^{2}]$ | nM |
| CBLc | 542.43 | $[10^{-1},10^{4}]$ | nM |
| $CBLc_{act}$ | 10.68 | $[10^{-1},10^{4}]$ | nM |
| PI3K | 0.13 | $[10^{-1},10^{2}]$ | nM |
| Akt | 2.71 | $[10^{-1},10^{2}]$ | nM |
| Ras | 0.139 | $[10^{-1},10^{2}]$ | nM |
| Raf | 9.48 | $[10^{-1},10^{3}]$ | nM |
| Mek | 14.02 | $[10, 10^{4}]$ | nM |
| Erk | 36.08 | $[10, 10^{4}]$ | nM |
| | | | |

| **SU.86.86 [0-60 minutes], - Erlotinib** | | | |
|---|---|---|---|
| $EGFR_{m,SU.86.86}$ | 0.11 | $[10^{-1},10^{2}]$ | nM |
| $EGFR_{c,SU.86.86}$ | 0.10 | $[10^{-1},10^{2}]$ | nM |
| $GAB1_{SU.86.86}$ | 99.96 | $[10^{-1},10^{2}]$ | nM |
| $Src_{SU.86.86}$ | 1.61 | $[10^{-1},10^{2}]$ | nM |
| $Src_{act,SU.86.86}$ | 3.51 | $[10^{-4},10^{2}]$ | nM |
| $CBLc_{SU.86.86}$ | 717.39 | $[10^{-1}, 10^{4}]$ | nM |
| $CBLc_{act,SU.86.86}$ | 29.54 | $[10^{-1}, 10^{4}]$ | nM |
| $PI3K_{SU.86.86}$ | 11.09 | $[10^{-1},10^{2}]$ | nM |
| $Akt_{SU.86.86}$ | 30.82 | $[10^{-1},10^{2}]$ | nM |
| $Ras_{SU.86.86}$ | 0.186 | $[10^{-1},10^{2}]$ | nM |
| $Raf_{SU.86.86}$ | 0.49 | $[10^{-1},10^{3}]$ | nM |
| $Mek_{SU.86.86}$ | 1190.23 | $[10, 10^{4}]$ | nM |
| $Erk_{SU.86.86}$ | 141.01 | $[10, 10^{4}]$ | nM |
| | | | |
| **HeLa [0-20 minutes] , - Erlotinib** | | | |
| $EGFR_{m,HeLa}$ | 95.29 | $[10^{-1},10^{2}]$ | nM |
| $EGFR_{c,HeLa}$ | 79.63 | $[10^{-1},10^{2}]$ | nM |
| $GAB1_{HeLa}$ | 0.10 | $[10^{-1},10^{2}]$ | nM |
| $Src_{HeLa}$ | 29.18 | $[10^{-1},10^{2}]$ | nM |
| $Src_{act,HeLa}$ | 0.36 | $[10^{-4},10^{2}]$ | nM |
| $CBLc_{HeLa}$ | 1421.07 | $[10^{-1},10^{4}]$ | nM |
| $CBLc_{act,HeLa}$ | 0.43 | $[10^{-1},10^{4}]$ | nM |
| $PI3K_{HeLa}$ | 9.22 | $[10^{-1},10^{2}]$ | nM |
| $Akt_{HeLa}$ | 2.10 | $[10^{-1},10^{2}]$ | nM |
| $Ras_{HeLa}$ | 0.52 | $[10^{-1},10^{2}]$ | nM |
| $Raf_{HeLa}$ | 0.89 | $[10^{-1},10^{3}]$ | nM |
| $Mek_{HeLa}$ | 53.56 | $[10, 10^{4}]$ | nM |
| $Erk_{HeLa}$ | 117.84 | $[10, 10^{4}]$ | nM |

**Table 8:** Parameter values used to simulate drug-induced cell growth inhibition, cell apoptosis and enzyme induction in cancer cell population expressing drug-degrading enzymes and treated with chemotherapy.

| Parameter | Value | Unit |
|---|---|---|
| Time before treatment | 24 | h |
| Time of treatment | 72 | h |
| $k_g$ | log (2)/72 | 1/h |
| $K_I$ | 0.5 | μM |
| h | 2 | dimensionless |
| $K_c$ | 50000 | dimensionless |
| $k_d$ | log (2)/24 | 1/h |
| alpha | 1000 | dimensionless |
| $K_D$ | 1 | μM |
| J | 2 | dimensionless |
| $k_{syn}$ | 0.2 | 1/h |
| beta | 100 | dimensionless |
| $K_E$ | 0.1 | μM |
| l | 2 | dimensionless |
| $k_{deg}$ | 0.001 | 1/h |
| $k_r$ | 0.000001 | 1/h |

**Table 9:** Parameter values estimated by fitting drug-induced cell growth inhibition, cell apoptosis and enzyme induction model to PACO2 viability data by Noll et al[23].

| Parameter | Value | Values range [min,max] | Unit |
|---|---|---|---|
| Time before treatment | 24 | - | h |
| Time of treatment | 72 | - | h |
| $k_g$ | 0.01 | [log(2)/96, log(2)/12] | 1/h |
| $dK_I$ | $5.7x10^{-4}$ | $[10^{-4},10^{2}]$ | µM |
| h | 3.24 | [2,10] | dimensionless |
| $K_c$ | $5.5x10^{4}$ | $[10^{3},10^{6}]$ | dimensionless |
| $k_d$ | 0.04 | [log(2)/96, log(2)/12] | 1/h |
| alpha | 16.26 | $[10^{-1},10^{2}]$ | dimensionless |
| $dK_{D1}$ | 1.5 | $[10^{-4},10^{2}]$ | µM |
| $dK_{D2}$ | 96.5 | $[10^{-4},10^{2}]$ | µM |
| j | 5.14 | [2,10] | dimensionless |
| $k_{syn}$ | 0.004 | $[10^{-4},10]$ | 1/h |
| beta | 1.3 | $[10^{-1},10^{2}]$ | dimensionless |
| $K_{E1}$ | $5.2x10^{-4}$ | $[10^{-1},10^{2}]$ | µM |
| $K_{E2}$ | 0.11 | $[10^{-1},10^{2}]$ | µM |
| l | 4.46 | [2,10] | dimensionless |
| $k_{deg}$ | 0.006 | $[10^{-4},10^{-1}]$ | 1/h |
| $k_r$ | $7.4x10^{-6}$ | $[10^{-8},10^{-3}]$ | 1/h |

# Figures

# Bibliography


[1] M. Orth *et al.*, "Pancreatic ductal adenocarcinoma: Biological hallmarks, current status, and future perspectives of combined modality treatment approaches," *Radiation Oncology*, vol. 14, no. 1. BioMed Central Ltd., Aug. 08, 2019, doi: 10.1186/s13014-019-1345-6.

[2] T. Kamisawa, L. D. Wood, T. Itoi, and K. Takaori, "Pancreatic cancer," *The Lancet*, vol. 388, no. 10039. Lancet Publishing Group, pp. 73–85, Jul. 02, 2016, doi: 10.1016/S0140-6736(16)00141-0.

[3] S. N. Kalimuthu *et al.*, "Morphological classification of pancreatic ductal adenocarcinoma that predicts molecular subtypes and correlates with clinical outcome," *Gut*, vol. 69, no. 2, pp. 317–328, Feb. 2020, doi: 10.1136/gutjnl-2019-318217.

[4] M. Hidalgo, "Pancreatic Cancer," *New England Journal of Medicine*, vol. 362, no. 17, pp. 1605–1617, Apr. 2010, doi: 10.1056/NEJMra0901557.

[5] L. T. H. Phi *et al.*, "Cancer Stem Cells (CSCs) in Drug Resistance and their Therapeutic Implications in Cancer Treatment," *Stem Cells International*, vol. 2018, 2018, doi: 10.1155/2018/5416923.

[6] A. Maitra *et al.*, "Multicomponent analysis of the pancreatic adenocarcinoma progression model using a pancreatic intraepithelial neoplasia tissue microarray," *Modern Pathology*, vol. 16, no. 9, pp. 902–912, Sep. 2003, doi: 10.1097/01.MP.0000086072.56290.FB.

[7] M. Kanda *et al.*, "Presence of somatic mutations in most early-stage pancreatic intraepithelial neoplasia," *Gastroenterology*, vol. 142, no. 4, pp. 730-733.e9, Apr. 2012, doi: 10.1053/j.gastro.2011.12.042.

[8] A. A. Connor *et al.*, "Association of distinct mutational signatures with correlates of increased immune activity in pancreatic ductal adenocarcinoma," *JAMA Oncology*, vol. 3, no. 6, pp. 774–783, Jun. 2017, doi: 10.1001/jamaoncol.2016.3916.

[9] E. A. Collisson *et al.*, "Subtypes of pancreatic ductal adenocarcinoma and their differing responses to therapy," *Nature Medicine*, vol. 17, no. 4, pp. 500–503, Apr. 2011, doi: 10.1038/nm.2344.

[10] R. A. Moffitt *et al.*, "Virtual microdissection identifies distinct tumor- and stroma-specific subtypes of pancreatic ductal adenocarcinoma," *Nature Genetics*, vol. 47, no. 10, pp. 1168–1178, Sep. 2015, doi: 10.1038/ng.3398.

[11] P. Bailey *et al.*, "Genomic analyses identify molecular subtypes of pancreatic cancer," *Nature*, vol. 531, no. 7592, pp. 47–52, Mar. 2016, doi: 10.1038/nature16965.

[12] A. Muckenhuber *et al.*, "Pancreatic ductal adenocarcinoma subtyping using the biomarkers hepatocyte nuclear factor-1A and cytokeratin-81 correlates with outcome and treatment response," *Clinical Cancer Research*, vol. 24, no. 2, pp. 351–359, Jan. 2018, doi: 10.1158/1078-0432.CCR-17-2180.

[13] A. Kleger, L. Perkhofer, and T. Seufferlein, “Smarter drugs emerging in pancreatic cancer therapy.,” *Annals of oncology : official journal of the European Society for Medical Oncology*, vol. 25, no. 7, pp. 1260–70, Jul. 2014, doi: 10.1093/annonc/mdu013.

[14] T. Seufferlein and T. J. Ettrich, “Treatment of pancreatic cancer—neoadjuvant treatment in resectable pancreatic cancer (PDAC),” *Translational Gastroenterology and Hepatology*, vol. 4, no. March, Mar. 2019, doi: 10.21037/tgh.2019.03.05.

[15] H. A. Burris *et al.*, “Improvements in survival and clinical benefit with gemcitabine as first-line therapy for patients with advanced pancreas cancer: A randomized trial,” *Journal of Clinical Oncology*, vol. 15, no. 6, pp. 2403–2413, 1997, doi: 10.1200/JCO.1997.15.6.2403.

[16] M. J. Moore *et al.*, “Erlotinib plus gemcitabine compared with gemcitabine alone in patients with advanced pancreatic cancer: A phase III trial of the National Cancer Institute of Canada Clinical Trials Group,” *Journal of Clinical Oncology*, vol. 25, no. 15, pp. 1960–1966, May 2007, doi: 10.1200/JCO.2006.07.9525.

[17] B. A. Weaver, “How Taxol/paclitaxel kills cancer cells,” *Molecular Biology of the Cell*, vol. 25, no. 18. American Society for Cell Biology, pp. 2677–2681, Sep. 15, 2014, doi: 10.1091/mbc.E14-04-0916.

[18] R. M. Hoffman and M. Bouvet, “Nanoparticle albumin-bound-paclitaxel: A limited improvement under the current therapeutic paradigm of pancreatic cancer,” *Expert Opinion on Pharmacotherapy*, vol. 16, no. 7. Informa Healthcare, pp. 943–947, May 01, 2015, doi: 10.1517/14656566.2015.1016912.

[19] D. D. von Hoff *et al.*, “Gemcitabine plus nab-paclitaxel is an active regimen in patients with advanced pancreatic cancer: A phase I/II trial,” *Journal of Clinical Oncology*, vol. 29, no. 34, pp. 4548–4554, Dec. 2011, doi: 10.1200/JCO.2011.36.5742.

[20] D. A. Fruman, H. Chiu, B. D. Hopkins, S. Bagrodia, L. C. Cantley, and R. T. Abraham, “The PI3K Pathway in Human Disease,” *Cell*, vol. 170, no. 4. Cell Press, pp. 605–635, Aug. 10, 2017, doi: 10.1016/j.cell.2017.07.029.

[21] F. Quiñonero *et al.*, “The challenge of drug resistance in pancreatic ductal adenocarcinoma: a current overview,” *Cancer Biology and Medicine*, vol. 16, no. 4. Cancer Biology and Medicine, pp. 688–699, Nov. 01, 2019, doi: 10.20892/j.issn.2095-3941.2019.0252.

[22] C. Holohan, S. van Schaeybroeck, D. B. Longley, and P. G. Johnston, “Cancer drug resistance: An evolving paradigm,” *Nature Reviews Cancer*, vol. 13, no. 10. Nature Publishing Group, pp. 714–726, Oct. 24, 2013, doi: 10.1038/nrc3599.

[23] E. M. Noll *et al.*, “CYP3A5 mediates basal and acquired therapy resistance in different subtypes of pancreatic ductal adenocarcinoma,” *Nature Medicine*, vol. 22, no. 3, pp. 278–287, Mar. 2016, doi: 10.1038/nm.4038.

[24] J. Rautio, N. A. Meanwell, L. Di, and M. J. Hageman, "The expanding role of prodrugs in contemporary drug design and development," *Nature Reviews Drug Discovery*, vol. 17, no. 8. Nature Publishing Group, pp. 559–587, Apr. 27, 2018, doi: 10.1038/nrd.2018.46.

[25] R. Hamacher, R. M. Schmid, D. Saur, and G. Schneider, "Apoptotic pathways in pancreatic ductal adenocarcinoma," *Molecular Cancer*, vol. 7. BioMed Central, p. 64, Jul. 24, 2008, doi: 10.1186/1476-4598-7-64.

[26] S. Sigismund, D. Avanzato, and L. Lanzetti, "Emerging functions of the EGFR in cancer," *Molecular Oncology*, vol. 12, no. 1. John Wiley and Sons Ltd., pp. 3–20, Jan. 01, 2018, doi: 10.1002/1878-0261.12155.

[27] M. A. Lemmon and J. Schlessinger, "Cell signaling by receptor tyrosine kinases," *Cell*, vol. 141, no. 7. pp. 1117–1134, Jun. 2010, doi: 10.1016/j.cell.2010.06.011.

[28] S. Sigismund *et al.*, "Threshold-controlled ubiquitination of the EGFR directs receptor fate," *The EMBO journal*, vol. 32, no. 15, pp. 2140–2157, 2013, doi: 10.1038/emboj.2013.149.

[29] K. Miyabayashi *et al.*, "Erlotinib prolongs survival in pancreatic cancer by blocking gemcitabine-induced MAPK signals," *Cancer Research*, vol. 73, no. 7, pp. 2221–2234, Apr. 2013, doi: 10.1158/0008-5472.CAN-12-1453.

[30] B. E. Kadera *et al.*, "Low expression of the E3 ubiquitin ligase CBL confers chemoresistance in human pancreatic cancer and is targeted by epidermal growth factor receptor inhibition," *Clinical Cancer Research: An Official Journal of the American Association for Cancer Research*, vol. 21, no. 1, pp. 157–165, 2015, doi: 10.1158/1078-0432.CCR-14-0610.

[31] B. Mohapatra *et al.*, "Protein tyrosine kinase regulation by ubiquitination: Critical roles of Cbl-family ubiquitin ligases," *Biochimica et Biophysica Acta - Molecular Cell Research*, vol. 1833, no. 1. Elsevier, pp. 122–139, Jan. 01, 2013, doi: 10.1016/j.bbamcr.2012.10.010.

[32] F. Huang and A. Sorkin, "Growth factor receptor binding protein 2-mediated recruitment of the RING domain of Cbl to the epidermal growth factor receptor is essential and sufficient to support receptor endocytosis," *Molecular Biology of the Cell*, vol. 16, no. 3, pp. 1268–1281, 2005, doi: 10.1091/mbc.e04-09-0832.

[33] I. Dikic, "Mechanisms controlling EGF receptor endocytosis and degradation," *Biochemical Society Transactions*, vol. 31, no. Pt 6, pp. 1178–1181, 2003, doi: 10.1042/.

[34] M. H. H. Schmidt and I. Dikic, "The Cbl interactome and its functions," *Nature Reviews. Molecular Cell Biology*, vol. 6, no. 12, pp. 907–918, 2005, doi: 10.1038/nrm1762.

[35] M. Kim, T. Tezuka, K. Tanaka, and T. Yamamoto, "Cbl-c suppresses v-Src-induced transformation through ubiquitin-dependent protein degradation," *Oncogene*, vol. 23, no. 9, pp. 1645–1655, 2004, doi: 10.1038/sj.onc.1207298.

[36] S.-Y. Hong, Y.-R. Kao, T.-C. Lee, and C.-W. Wu, "Upregulation of E3 Ubiquitin Ligase CBLC Enhances EGFR Signaling in Lung Adenocarcinoma," *Cancer Research*, vol. 78, no. 17, pp. 4984–4996, 2018, doi: 10.1158/0008-5472.CAN-17-3858.

[37] T. Yamazaki, K. Zaal, D. Hailey, J. Presley, J. Lippincott-Schwartz, and L. E. Samelson, "Role of Grb2 in EGF-stimulated EGFR internalization," *Journal of Cell Science*, vol. 115, no. 9, 2002, Accessed: Mar. 02, 2020. [Online].

[38] C. Braicu *et al.*, "A comprehensive review on MAPK: A promising therapeutic target in cancer," *Cancers*, vol. 11, no. 10. MDPI AG, Oct. 01, 2019, doi: 10.3390/cancers11101618.

[39] M. C. Mendoza, E. E. Er, and J. Blenis, "The Ras-ERK and PI3K-mTOR pathways: cross-talk and compensation," *Trends in Biochemical Sciences*, vol. 36, no. 6, pp. 320–328, 2011, doi: 10.1016/j.tibs.2011.03.006.

[40] E. A. Collisson *et al.*, "A Central role for RAF→MEK→ERK signaling in the genesis of pancreatic ductal adenocarcinoma," *Cancer Discovery*, vol. 2, no. 8, pp. 685–693, Aug. 2012, doi: 10.1158/2159-8290.CD-11-0347.

[41] H. Ying *et al.*, "PTEN is a major tumor suppressor in pancreatic ductal adenocarcinoma and regulates an NF-κB-cytokine network," *Cancer Discovery*, vol. 1, no. 2, pp. 158–169, May 2011, doi: 10.1158/2159-8290.CD-11-0031.

[42] B. D. Manning and A. Toker, "AKT/PKB Signaling: Navigating the Network," *Cell*, vol. 169, no. 3. Cell Press, pp. 381–405, Apr. 20, 2017, doi: 10.1016/j.cell.2017.04.001.

[43] S. Faes and O. Dormond, "PI3K and AKT: Unfaithful partners in cancer," *International Journal of Molecular Sciences*, vol. 16, no. 9. MDPI AG, pp. 21138–21152, Sep. 03, 2015, doi: 10.3390/ijms160921138.

[44] D. R. Nelson, "The cytochrome P450 homepage," *Human Genomics*, vol. 4, no. 1, pp. 59–65, Oct. 2009, doi: 10.1186/1479-7364-4-1-59.

[45] L. J. Yu *et al.*, "P450 enzyme expression patterns in the NCI human tumor cell line panel.," *Drug metabolism and disposition: the biological fate of chemicals*, vol. 29, no. 3, pp. 304–12, Mar. 2001, Accessed: Apr. 13, 2020. [Online]. Available: http://www.ncbi.nlm.nih.gov/pubmed/11181500.

[46] P. Manikandan and S. Nagini, "Cytochrome P450 Structure, Function and Clinical Significance: A Review," *Current Drug Targets*, vol. 19, no. 1, pp. 38–54, Feb. 2017, doi: 10.2174/1389450118666170125144557.

[47] B. Rochat, "Role of cytochrome P450 activity in the fate of anticancer agents and in drug resistance: Focus on tamoxifen, paclitaxel and imatinib metabolism," *Clinical Pharmacokinetics*, vol. 44, no. 4. pp. 349–366, 2005, doi: 10.2165/00003088-200544040-00002.

[48] C. Handschin, "Induction of Drug Metabolism: The Role of Nuclear Receptors," *Pharmacological Reviews*, vol. 55, no. 4, pp. 649–673, 2003, doi: 10.1124/pr.55.4.2.

[49] O. Lolodi, Y.-M. Wang, W. C. Wright, and T. Chen, "Differential Regulation of CYP3A4 and CYP3A5 and its Implication in Drug Discovery.," *Current drug metabolism*, vol. 18, no. 12, pp. 1095–1105, May 2017, doi: 10.2174/1389200218666170531112038.

[50] S. A. Langhans, “Three-dimensional in vitro cell culture models in drug discovery and drug repositioning,” *Frontiers in Pharmacology*, vol. 9, no. JAN. Frontiers Media S.A., p. 6, Jan. 23, 2018, doi: 10.3389/fphar.2018.00006.

[51] V. Magno, A. Meinhardt, and C. Werner, “Polymer Hydrogels to Guide Organotypic and Organoid Cultures,” *Advanced Functional Materials*, vol. 30, no. 48, p. 2000097, Nov. 2020, doi: 10.1002/adfm.202000097.

[52] Y. Imamura *et al.*, “Comparison of 2D- and 3D-culture models as drug-testing platforms in breast cancer,” *Oncology Reports*, vol. 33, no. 4, pp. 1837–1843, Apr. 2015, doi: 10.3892/or.2015.3767.

[53] M. A. Lancaster and J. A. Knoblich, “Organogenesis in a dish: Modeling development and disease using organoid technologies,” *Science*, vol. 345, no. 6194, pp. 1247125–1247125, Jul. 2014, doi: 10.1126/science.1247125.

[54] M. M. Gottesman, O. Lavi, M. D. Hall, and J.-P. Gillet, “Toward a Better Understanding of the Complexity of Cancer Drug Resistance,” *Annual Review of Pharmacology and Toxicology*, vol. 56, no. 1, pp. 85–102, Jan. 2016, doi: 10.1146/annurev-pharmtox-010715-103111.

[55] J. Gómez Tejeda Zañudo, M. Scaltriti, and R. Albert, “A network modeling approach to elucidate drug resistance mechanisms and predict combinatorial drug treatments in breast cancer,” *Cancer Convergence*, vol. 1, no. 1, p. 5, Dec. 2017, doi: 10.1186/s41236-017-0007-6.

[56] N. le Novere, “Quantitative and logic modelling of molecular and gene networks,” *Nature Reviews Genetics*, vol. 16, no. 3. Nature Publishing Group, pp. 146–158, Mar. 26, 2015, doi: 10.1038/nrg3885.

[57] K. A. Janes and M. B. Yaffe, “Data-driven modelling of signal-transduction networks,” *Nature Reviews Molecular Cell Biology*, vol. 7, no. 11. Nature Publishing Group, pp. 820–828, Nov. 2006, doi: 10.1038/nrm2041.

[58] N. Jagiella, D. Rickert, F. J. Theis, and J. Hasenauer, “Parallelization and High-Performance Computing Enables Automated Statistical Inference of Multi-scale Models,” *Cell Systems*, vol. 4, no. 2, pp. 194-206.e9, 2017, doi: 10.1016/j.cels.2016.12.002.

[59] J. Metzcar, Y. Wang, R. Heiland, and P. Macklin, “A Review of Cell-Based Computational Modeling in Cancer Biology,” *JCO Clinical Cancer Informatics*, no. 3, pp. 1–13, Nov. 2019, doi: 10.1200/cci.18.00069.

[60] S. Abar, G. K. Theodoropoulos, P. Lemarinier, and G. M. P. O’Hare, “Agent Based Modelling and Simulation tools: A review of the state-of-art software,” *Computer Science Review*, vol. 24. Elsevier Ireland Ltd, pp. 13–33, May 01, 2017, doi: 10.1016/j.cosrev.2017.03.001.

[61] C. Weber, “Modelling PDAC-niche adaption,” *Nature Cell Biology*, vol. 20, no. 6, p. 1, May 2018, doi: 10.1038/s41556-018-0115-2.

[62] G. Schaller and M. Meyer-Hermann, “Continuum versus discrete model: a comparison for multicellular tumour spheroids,” *Philosophical Transactions of the Royal Society of London A:*

*Mathematical, Physical and Engineering Sciences*, vol. 364, no. 1843, pp. 1443–1464, 2006, doi: 10.1098/rsta.2006.1780.

[63] S. Polo, P. P. di Fiore, and S. Sigismund, "Keeping EGFR signaling in check: Ubiquitin is the guardian," *Cell Cycle*, vol. 13, no. 5. Taylor and Francis Inc., pp. 681–682, Mar. 01, 2014, doi: 10.4161/cc.27855.

[64] H. Schmidt-Glenewinkel, E. Reinz, R. Eils, and N. R. Brady, "Systems biological analysis of epidermal growth factor receptor internalization dynamics for altered receptor levels," *Journal of Biological Chemistry*, vol. 284, no. 25, pp. 17243–17252, Jun. 2009, doi: 10.1074/jbc.M809586200.

[65] F. Capuani *et al.*, "Quantitative analysis reveals how EGFR activation and downregulation are coupled in normal but not in cancer cells," *Nature Communications*, vol. 6, no. 1, pp. 1–14, Aug. 2015, doi: 10.1038/ncomms8999.

[66] A. Kiyatkin, E. Aksamitiene, N. I. Markevich, N. M. Borisov, J. B. Hoek, and B. N. Kholodenko, "Scaffolding protein Grb2-associated binder 1 sustains epidermal growth factor-induced mitogenic and survival signaling by multiple positive feedback loops," *Journal of Biological Chemistry*, vol. 281, no. 29, pp. 19925–19938, Jul. 2006, doi: 10.1074/jbc.M600482200.

[67] B. N. Kholodenko, O. v Demin, G. Moehren, and J. B. Hoek, "Quantification of short term signaling by the epidermal growth factor receptor," *The Journal of Biological Chemistry*, vol. 274, no. 42, pp. 30169–30181, 1999.

[68] B. Schoeberl, C. Eichler-Jonsson, E. D. Gilles, and G. Muüller, "Computational modeling of the dynamics of the MAP kinase cascade activated by surface and internalized EGF receptors," *Nature Biotechnology*, vol. 20, no. 4, pp. 370–375, Apr. 2002, doi: 10.1038/nbt0402-370.

[69] R. J. Orton, M. E. Adriaens, A. Gormand, O. E. Sturm, W. Kolch, and D. R. Gilbert, "Computational modelling of cancerous mutations in the EGFR/ERK signalling pathway," *BMC Systems Biology*, vol. 3, p. 100, Oct. 2009, doi: 10.1186/1752-0509-3-100.

[70] E. C. Stites, P. C. Trampont, L. B. Haney, S. F. Walk, and K. S. Ravichandran, "Cooperation between Noncanonical Ras Network Mutations," *Cell Reports*, vol. 10, no. 3, pp. 307–316, Jan. 2015, doi: 10.1016/j.celrep.2014.12.035.

[71] O. E. Sturm *et al.*, "The mammalian MAPK/ERK pathway exhibits properties of a negative feedback amplifier," *Science Signaling*, vol. 3, no. 153, p. ra90, Dec. 2010, doi: 10.1126/scisignal.2001212.

[72] W. W. Chen *et al.*, "Input-output behavior of ErbB signaling pathways as revealed by a mass action model trained against dynamic data," *Molecular Systems Biology*, vol. 5, p. 239, Jan. 2009, doi: 10.1038/msb.2008.74.

[73] B. Schoeberl *et al.*, "Therapeutically targeting ErbB3: A key node in ligand-induced activation of the ErbB receptor-PI3K axis," *Science Signaling*, vol. 2, no. 77, Jun. 2009, doi: 10.1126/scisignal.2000352.

[74] B. Schoeberl *et al.*, "Systems biology driving drug development: From design to the clinical testing of the anti-ErbB3 antibody seribantumab (MM-121)," *npj Systems Biology and Applications*, vol. 3. Nature Publishing Group, p. 16034, 2017, doi: 10.1038/npjsba.2016.34.

[75] C. v. Suresh Babu, S. M. E. Babar, E. J. Song, E. Oh, and Y. S. Yoo, "Kinetic analysis of the MAPK and PI3K/Akt signaling pathways," *Molecules and Cells*, vol. 25, no. 3, pp. 397–406, May 2008, Accessed: Apr. 01, 2020. [Online].

[76] P. Mendes, "Gepasi: A software package for modelling the dynamics, steady states and control of biochemical and other systems," *Bioinformatics*, vol. 9, no. 5, pp. 563–571, 1993, doi: 10.1093/bioinformatics/9.5.563.

[77] Y. Arkun, "Dynamic Modeling and Analysis of the Cross-Talk between Insulin/AKT and MAPK/ERK Signaling Pathways," *PLOS ONE*, vol. 11, no. 3, p. e0149684, Mar. 2016, doi: 10.1371/journal.pone.0149684.

[78] W. Kolch, M. Halasz, M. Granovskaya, and B. N. Kholodenko, "The dynamic control of signal transduction networks in cancer cells," *Nature Reviews. Cancer*, vol. 15, no. 9, pp. 515–527, 2015, doi: 10.1038/nrc3983.

[79] F. Michor and K. Beal, "Improving Cancer Treatment via Mathematical Modeling: Surmounting the Challenges Is Worth the Effort," *Cell*, vol. 163, no. 5. Cell Press, pp. 1059–1063, Nov. 19, 2015, doi: 10.1016/j.cell.2015.11.002.

[80] J. Chmielecki *et al.*, "Optimization of dosing for EGFR-mutant non-small cell lung cancer with evolutionary cancer modeling," *Science Translational Medicine*, vol. 3, no. 90, Jul. 2011, doi: 10.1126/scitranslmed.3002356.

[81] F. Pappalardo *et al.*, "Computational modeling of PI3K/AKT and MAPK signaling pathways in melanoma cancer," *PLoS ONE*, vol. 11, no. 3, Mar. 2016, doi: 10.1371/journal.pone.0152104.

[82] S. Hoops *et al.*, "COPASI--a COmplex PAthway SImulator\r10.1093/bioinformatics/btl485," *Bioinformatics*, vol. 22, no. 24, pp. 3067–3074, 2006, doi: 10.1093/bioinformatics/btl485.

[83] E. Kim, J. Y. Kim, M. A. Smith, E. B. Haura, and A. R. A. Anderson, "Cell signaling heterogeneity is modulated by both cell-intrinsic and -extrinsic mechanisms: An integrated approach to understanding targeted therapy," *PLoS Biology*, vol. 16, no. 3, p. e2002930, Mar. 2018, doi: 10.1371/journal.pbio.2002930.

[84] T. Shi *et al.*, "Conservation of protein abundance patterns reveals the regulatory architecture of the EGFR-MAPK pathway," *Science Signaling*, vol. 9, no. 436, p. rs6, 2016, doi: 10.1126/scisignal.aaf0891.

[85] M. Bouhaddou *et al.*, "A mechanistic pan-cancer pathway model informed by multi-omics data interprets stochastic cell fate responses to drugs and mitogens," *PLoS Computational Biology*, vol. 14, no. 3, Mar. 2018, doi: 10.1371/journal.pcbi.1005985.

[86] P. Dogra *et al.*, "Mathematical Modeling to Address Challenges in Pancreatic Cancer," *Current Topics in Medicinal Chemistry*, vol. 20, no. 5, pp. 367–376, Mar. 2020, doi: 10.2174/1568026620666200101095641.

[87] J. Chen, D. Weihs, and F. J. Vermolen, "Computational modeling of therapy on pancreatic cancer in its early stages," *Biomechanics and Modeling in Mechanobiology*, vol. 19, no. 2, pp. 427–444, Apr. 2020, doi: 10.1007/s10237-019-01219-0.

[88] H. Haeno, M. Gonen, M. B. Davis, J. M. Herman, C. A. Iacobuzio-Donahue, and F. Michor, "Computational modeling of pancreatic cancer reveals kinetics of metastasis suggesting optimum treatment strategies," *Cell*, vol. 148, no. 1–2, pp. 362–375, Jan. 2012, doi: 10.1016/j.cell.2011.11.060.

[89] A. S. Dhillon, S. Hagan, O. Rath, and W. Kolch, "MAP kinase signalling pathways in cancer," *Oncogene*, vol. 26, no. 22. pp. 3279–3290, May 14, 2007, doi: 10.1038/sj.onc.1210421.

[90] A. A. Samatar and P. I. Poulikakos, "Targeting RAS-ERK signalling in cancer: Promises and challenges," *Nature Reviews Drug Discovery*, vol. 13, no. 12. Nature Publishing Group, pp. 928–942, Dec. 11, 2014, doi: 10.1038/nrd4281.

[91] T. Maiwald and J. Timmer, "Dynamical modeling and multi-experiment fitting with PottersWheel," *Bioinformatics (Oxford, England)*, vol. 24, no. 18, pp. 2037–2043, 2008, doi: 10.1093/bioinformatics/btn350.

[92] M. M. Keane *et al.*, "cbl-3: A new mammalian cbl family protein," *Oncogene*, vol. 18, no. 22, pp. 3365–3375, Jun. 1999, doi: 10.1038/sj.onc.1202753.

[93] A. M. Weissman, N. Shabek, and A. Ciechanover, "The predator becomes the prey: Regulating the ubiquitin system by ubiquitylation and degradation," *Nature Reviews Molecular Cell Biology*, vol. 12, no. 9. Nat Rev Mol Cell Biol, pp. 605–620, Sep. 2011, doi: 10.1038/nrm3173.

[94] J. G. Albeck, G. B. Mills, and J. S. Brugge, "Frequency-Modulated Pulses of ERK Activity Transmit Quantitative Proliferation Signals," *Molecular Cell*, vol. 49, no. 2, pp. 249–261, Jan. 2013, doi: 10.1016/j.molcel.2012.11.002.

[95] J. Basbous, D. Chalbos, R. Hipskind, I. Jariel-Encontre, and M. Piechaczyk, "Ubiquitin-Independent Proteasomal Degradation of Fra-1 Is Antagonized by Erk1/2 Pathway-Mediated Phosphorylation of a Unique C-Terminal Destabilizer," *Molecular and Cellular Biology*, vol. 27, no. 11, pp. 3936–3950, Jun. 2007, doi: 10.1128/mcb.01776-06.

[96] S. J. Cohen *et al.*, "A phase 1b study of erlotinib in combination with gemcitabine and nab-paclitaxel in patients with previously untreated advanced pancreatic cancer: An Academic Oncology GI Cancer Consortium study," *Cancer Chemotherapy and Pharmacology*, vol. 77, no. 4, pp. 693–701, Apr. 2016, doi: 10.1007/s00280-016-2981-2.

[97] S. M. Kallenberger, T. Treis, C. di Ponzio, and R. Eils, "Method and system for closed-loop live-cell imaging," EP19204932.8, 2019.

[98] A. Gruber *et al.*, "Monitoring of erlotinib in pancreatic cancer patients during long-time administration and comparison to a physiologically based pharmacokinetic model," *Cancer Chemotherapy and Pharmacology*, vol. 81, no. 4, pp. 763–771, Apr. 2018, doi: 10.1007/s00280-018-3545-4.

[99] C. Jensen and Y. Teng, "Is It Time to Start Transitioning From 2D to 3D Cell Culture?," *Frontiers in Molecular Biosciences*, vol. 7. Frontiers Media S.A., p. 33, Mar. 06, 2020, doi: 10.3389/fmolb.2020.00033.

[100] N. E. Buchler, U. Gerland, and T. Hwa, "Nonlinear protein degradation and the function of genetic circuits," *Proceedings of the National Academy of Sciences*, vol. 102, no. 27, pp. 9559–9564, 2005, doi: 10.1073/pnas.0409553102.

[101] R. J. Mcmurtrey and R. J. Mcmurtrey, "Analytic and Numerical Models of Oxygen and Nutrient Diffusion, Metabolism Dynamics, and Architecture Optimization in Three-Dimensional Tissue Constructs with Applications and Insights in Cerebral Organoids," doi: 10.1089/ten.TEC.2015.0375.

[102] T. M. Achilli, S. McCalla, J. Meyer, A. Tripathi, and J. R. Morgan, "Multilayer spheroids to quantify drug uptake and diffusion in 3D," *Molecular Pharmaceutics*, vol. 11, no. 7, pp. 2071–2081, 2014, doi: 10.1021/mp500002y.

[103] J. F. Lu *et al.*, "Clinical pharmacokinetics of erlotinib in patients with solid tumors and exposure-safety relationship in patients with non-small cell lung cancer," *Clinical Pharmacology and Therapeutics*, vol. 80, no. 2, pp. 136–145, Aug. 2006, doi: 10.1016/j.clpt.2006.04.007.

[104] A. K. Dash, "Editorial: The dark side of paclitaxel," *Oncology Reviews*, vol. 4, no. 2. Springer, pp. 71–72, Jun. 27, 2010, doi: 10.1007/s12156-010-0052-1.

[105] R. Mcfadden and C. S. Kwok2, "Mathematical Model of Simultaneous Diffusion and Binding of Antitumor Antibodies in Multicellular Human Tumor Spheroids," 1988. Accessed: May 04, 2021. [Online].

[106] J. A. Leedale *et al.*, "Multiscale modelling of drug transport and metabolism in liver spheroids," *Interface Focus*, vol. 10, no. 2, Apr. 2020, doi: 10.1098/rsfs.2019.0041.

[107] A. Y. Tsygankov, A. M. Teckchandani, E. A. Feshchenko, and G. Swaminathan, "Beyond the RING: CBL proteins as multivalent adapters," *Oncogene*, vol. 20, no. 44 REV. ISS. 5. Nature Publishing Group, pp. 6382–6402, Oct. 01, 2001, doi: 10.1038/sj.onc.1204781.

[108] J. M. Kang *et al.*, "CBL enhances breast tumor formation by inhibiting tumor suppressive activity of TGF-β signaling," *Oncogene*, vol. 31, no. 50, pp. 5123–5131, Dec. 2012, doi: 10.1038/onc.2012.18.

[109] D. Bai, L. Ueno, and P. K. Vogt, "Akt-mediated regulation of NFκB and the essentialness of NFκB for the oncogenicity of PI3K and Akt," *International Journal of Cancer*, vol. 125, no. 12, pp. 2863–2870, Dec. 2009, doi: 10.1002/ijc.24748.

[110] G. Kaur, S. K. Gupta, P. Singh, V. Ali, V. Kumar, and M. Verma, “Drug-metabolizing enzymes: role in drug resistance in cancer,” *Clinical and Translational Oncology*, vol. 22, no. 10. Springer, pp. 1667–1680, Oct. 01, 2020, doi: 10.1007/s12094-020-02325-7.